國立臺灣大學生物資源暨農學院生物科技所

博士論文

Institute of Biotechnology
College of Bioresources and Agriculture
National Taiwan University
Doctoral Dissertation

蟾螈肢體再生：神經介導表現之組蛋白去乙醯化酶之角色

與雙螢光嵌合體肢體再生模式之建立

Axolotl limb regeneration:

The roles of nerve-mediated expression of histone

deacetylases and establishment of a double fluorescence

chimeric limb regeneration model

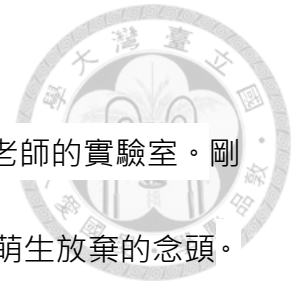王睦惠

Mu-Hui Wang

指導教授：李宣書 博士

Advisor: Hsuan-Shu Lee, Ph.D.

共同指導教授：林劭品 博士

Co-Advisor: Shau-Ping Lin, Ph.D.

中華民國 112 年 7 月

July 2023

致謝

　　最初憑著對蠑螈的一面之緣與一股衝動，就決定加入宣書老師的實驗室。剛進實驗室的時候，覺得老師很嚴格，做什麼都達不到要求，幾度萌生放棄的念頭。卻也是在最低潮的時候，才驚覺老師始終沒有放棄我。這些年，老師教會我「如何把基本功練好」，唯有把每件基本的事情做到好，才有實力站得住腳。記得最初我連神經跟肌肉都會分錯，甚至因為截錯組織，導致蠑螈的整肢手臂爛掉。每一次的犯錯與修正，累積的經驗多了，反而蠑螈相關的手術操作成為我最擅長的項目。老師總把後悔選擇投入蠑螈研究的話掛在嘴上，但我卻很感謝老師的一時錯誤，台灣才能有我這麼個稀有的蠑螈博士。也很感謝實驗室的玲玲學姊、小巫學長、小白學長、柏松學長、育文學姊、宏威學長與阿峰這幾年的幫忙。尤其踏入實驗室的時候，程度如同一張白紙，但學長姐是無限的包容，又很願意傾囊相授。時至今日能夠很驕傲地說，所有結果，除了資訊分析的部分，全憑著自己的雙手與青春，不假他人之手。

　　另一位感謝的恩師是劭品老師。其實我本身的個性內向且被動，腦子也不是很靈活，但老師身上源源不絕的正能量總能鼓勵我嘗試做一些平常不會去做，或者是不太願意去做的事情。跳脫舒適圈對我來說其實是很大的壓迫，每當我有想要退縮的念頭，看到老師這麼努力，就會覺得很慚愧，硬著頭皮也是堅持下去。可是也因為這樣，才發覺自己原來有潛力做到那些原以為我不會或做不到的事。「苦盡甘來」這四個字是老師教會我的。

求學的路上因為有家勳跟歐陽兩位好同學相互勉勵，一起同甘共苦，時不時就要約出來吐一吐實驗辛酸事，研究撞牆期的崩潰心理有人可以宣洩跟理解，也就不至於太崩潰。

　　在口試後這兩年休學與一年復學的時間裡，非常感激官振翔醫師與鄭乃禎醫師的提攜，讓我尚未畢業就已經就業，沒有後顧之憂，安心的把手上尚未結束的事項完成，以及延續蟎蟓相關研究。這三年在鄭醫師實驗室與台大醫院第八共研認識的好同事們，小琹、巧怡、育妏、徐禾、茄愷、玥蓁、琪芬、狐狸、芳宇、詠心、曉梅學姊與南哥，在工作上的各種幫忙與照顧，讓我覺得自己超級幸運能夠在一個充滿溫暖且歡樂的環境工作。

　　謝謝凱軍這三年的包容與照顧，時時叮囑我這個叮囑我那個，雖然我仍像個小朋友，任性地做自己，老是讓他擔心又無奈。生活中，喜怒哀樂總少不了他。一起通宵工作之餘，也一同享受生活，一齊朝著成為更好的我們邁進。

　　感謝自己的爸媽，在家裡最困難的時候，還願意讓孩子追一個不著邊際的夢想。看似一股腦熱的衝動，卻也是一個孩子在當時認為自己能力可及，能讓父母感到驕傲的一個選擇。中間的過程雖然不是很順遂，也曾經讓家人擔心，但現在終於夠能夠讓家人安心也放心。

中文摘要
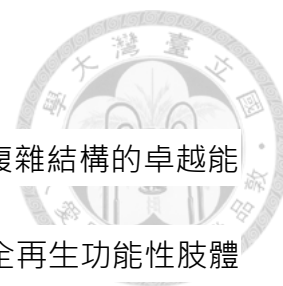
　　蠑螈以其在受傷後能夠重新生長大部分身體組織並恢復複雜結構的卓越能力而在脊椎動物中備受矚目。其中一個著名的例子就是牠們完全再生功能性肢體的能力。儘管在這個領域取得了重要進展，但對於控制肢體再生的分子信號的理解仍然有限。組蛋白去乙醯化酶（HDACs）在肢體再生過程中扮演著關鍵角色。本論文旨在研究 HDAC1 在蠑螈肢體再生中的參與情況。研究發現，在再生的早期分化階段之前，HDAC1 表現呈雙相上調。使用 MS-275 等抑制 HDAC 活性的化合物會延遲幼體的肢體再生，而局部注射 HDAC 抑制劑則會阻礙 HDAC 活性、芽基組織的形成和隨後的肢體再生。HDAC1 的表現在傷口表皮中更為明顯，且截肢前的去神經會阻止其表達上升和肢體再生。此外，補充神經因子有助於促進 HDAC1 的上調表達並增強肢體再生過程。這些發現顯示 HDAC1 在蠑螈肢體再生中的參與情況，並強調了神經因子在調節這一過程中的重要性。

　　此外，本研究探討了 HDAC 抑制對肢體再生轉錄反應的影響。轉錄組學分析揭示了表皮和軟組織中複雜的功能途徑。HDAC 活性對阻止與組織發育和分化相關的基因過早表達至關重要。抑制 HDAC1 導致再生相關基因和 WNT 通路相關基因的過早活化。使用 WNT 抑制劑處理後，部分恢復 HDAC1 的抑制作用，改善芽基組織形成。

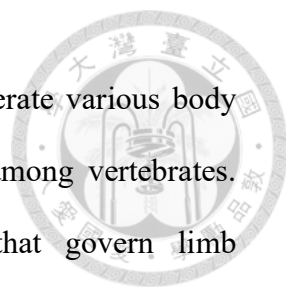　　此外，本論文還建立紅色與綠色的轉基因蠑螈，並延續先前實驗室在肌肉接合方面的研究結果，旨在透過雙螢光移植的方式，觀察再生肢體的橫截面來檢

測肌肉纖維的重新接合情況。結果顯示，不同肌肉之間的肌肉纖維接合速度不同，其中 gracilis 肌表現出外圍的重連特徵。此外，在遠端再生部位，RFP+的肌肉纖維對肌肉再生起到了貢獻作用，尤其是在小腿的腹肌表面。這個雙螢光嵌合體為瞭解蠑螈肢體再生的後期肌肉接合模式提供了新的視角。

本研究凸顯了 HDAC1 在蠑螈肢體再生中的重要作用。神經調控的 HDAC1 表達對於芽基組織的形成和成功再生至關重要。研究結果強調了在這一過程中涉及的基因表達模式和表觀遺傳修飾的複雜性。此外，肌肉纖維的重連動態為肢體再生的後期階段提供了深入的洞察。本論文推進了人們對於蠑螈肢體再生機制的理解。這些發現對於再生醫學研究具有重要意義，並可能對未來的治療方法做出貢獻。

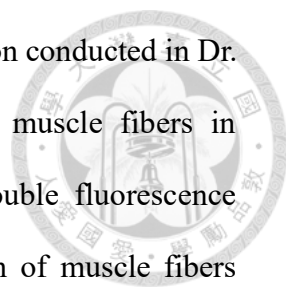**關鍵字**：蠑螈、肢體再生、組蛋白去乙醯化酶、神經因子、雙螢光嵌合體、肌肉接合

Abstract

Axolotls are renowned for their remarkable ability to regenerate various body parts, including fully functional limbs, making them stand out among vertebrates. However, our understanding of the molecular mechanisms that govern limb regeneration in axolotls remains limited. Histone deacetylases (HDACs) have been identified as crucial players in this process. This thesis aimed to investigate the role of HDAC1 in axolotl limb regeneration. The study revealed a biphasic up-regulation of HDAC1 prior to the early differentiation stage of regeneration. Inhibition of HDAC activity using the compound MS-275 caused a delay in limb regeneration in larvae, while localized injection of HDAC inhibitors hindered HDAC activity, blastema formation, and subsequent limb regeneration. Notably, HDAC1 expression was more pronounced in the wound epidermis (WE), and denervation prior to amputation prevented its elevation and subsequent limb regeneration. Furthermore, supplementation of nerve factors promoted the up-regulation of HDAC1 expression and enhanced the process of limb regeneration. These findings shed light on the involvement of HDAC1 in axolotl limb regeneration and emphasize the significance of nerve factors in regulating this process.

Furthermore, this thesis delved into the transcriptional changes occurring during limb regeneration under HDAC inhibition. Transcriptome sequencing uncovered intricate functional pathways in both the epidermis and soft tissue (ST). The activity of HDACs was crucial in suppressing the premature expression of genes associated with tissue development and differentiation. Inhibiting HDAC1 resulted in premature activation of genes linked to regeneration and the WNT pathway. Interestingly, administering a WNT inhibitor partially reversed the effects of HDAC1 inhibition and enhanced blastema formation.

In addition, this study established transgenic axolotls with red and green

fluorescence, building upon previous research in muscle reconnection conducted in Dr. Lee's laboratory. The aim was to observe the reconnection of muscle fibers in regenerative limbs through cross-sectional analysis using the double fluorescence transplantation method. The results revealed that the reconnection of muscle fibers varied in speed among different muscles, with the gracilis muscle exhibiting peripheral reconnection characteristics. Furthermore, in the distal regenerative regions, the RFP+ muscle fibers contributed to muscle regeneration, particularly on the ventral surface of the calf. This double fluorescence chimeric model provides a new perspective on the late-stage muscle reconnection patterns in axolotl limb regeneration.

Overall, this thesis highlights the essential role of HDAC1 in axolotl limb regeneration. Nerve-mediated HDAC1 expression is crucial for blastema formation and successful regeneration. The findings underscore the intricate gene expression patterns and epigenetic modifications involved in the process. Furthermore, muscle fiber reconnection dynamics provide insights into the late stages of limb regeneration. In conclusion, this comprehensive study advances our understanding of the mechanisms underlying axolotl limb regeneration. The findings have implications for regenerative medicine research and may contribute to future therapeutic approaches.

Keywords: axolotl, limb regeneration, histone deacetylases (HDACs), nerve factors, double fluorescence chimeric, muscle fiber reconnection

Contents

List of Figures

List of Tables

List of Abbreviations

AEC	apical epithelial cap
ALM	accessory limb model
nAG	newt anterior gradient
ECM	extracellular matrix
iPSC	induced pluripotent stem cell
HDACs	histone deacetylases
WE	wound epithelium/epidermis
HATs	histone acetyltransferases
ESTs	expressed sequence tags
ISH	*in situ* hybridization
aPBS	amphibian phosphate buffered saline
DMSO	dimethyl sulfoxide
PBS	phosphate buffered saline
cDNA	complementary DNA
DNA	deoxyribonucleic acid
RNA	ribonucleic acid
Q-PCR	Quantitative polymerase chain reaction
EdU	5-ethynyl-2′-deoxyuridine
PFA	paraformaldehyde
EB	early bud
MB	mid bud
LB	late bud
ED	early differentiation
NCR	near complete regeneration

dpa	days post-amputation
hpa	hours post-amputation
LD	late differentiation
TSA	trichostatin A
EdU	5-ethynyl-2′-deoxyuridine
BFF	BMP7, FGF2, and FGF8
ST	soft tissue
NGS	next generation sequencing
GO	gene ontology
DEGs	differentially expressed genes
RQN	RNA quality number
PE	paired-end
ORFs	open read frames
ORA	over-representation analysis
GSEA	gene-set enrichment analysis
GEO	gene expression omnibus
MRI	magnetic resonance imaging
EGFP-Tg	enhanced green fluorescent protein-transgenic
RFP	red fluorescent protein
IVF	*in vitro* fertilization
hCG	human chorionic gonadotrophin
MMR	Marc's modified Ringer's solution
dpt	days-post transplantation
LED	light-emitting diode
ISF	ischioflexorius

FDC	flexor digitorum communis
FMFB	femorofibularis
IOC	interosseus cruris
ECT	extensor cruris tibialis
ETT	extensor tarsi tibialis
EDL	extensor digitorum longus
ECTF	extensor cruris et tarsi fibularis
T	tenuissimus
PTB	pubotibialis
GRA	gracilis
D	dorsal
V	ventral
A	anterior
P	posterior

CHAPTER 1:

Literature Review

1.1 Introduction

Regeneration is a remarkable phenomenon observed throughout the animal kingdom. Regeneration involves the intrinsic ability to replace or revitalize damaged or missing cells, tissues, organs, and even complete body parts, leading to the restoration of their original functionality. The exploration of regeneration entails crucial inquiries concerning the understanding and control of regenerative potential, the identification of cellular sources and lineage-switching for generating diverse cell types, the discovery of initiating factors, and the unraveling of signals governing proliferation and patterning during the regenerative process. While certain forms of regeneration, such as bone marrow transplantation (1), are well-established and applied in clinical settings, many aspects of regeneration remain subjects of ongoing investigation.

Regeneration research encompasses various model systems, each offering unique experimental advantages and regenerative capabilities. From flatworms and hydras to salamanders and zebrafish, different organisms have revealed the fundamental principles of regeneration. While certain animals, including mammals, have limited regenerative abilities (2), advancements in current genetic tools and resources provide opportunities to fill, and even enhance, the regenerative potential in mammals. Therefore, regeneration research strives to unravel the mysteries of regenerative potential, cellular sources, initiating factors, proliferation control, and tissue morphogenesis during the regeneration process. By comparing knowledge from different model systems and uncovering common principles, it paves the way for future advancements in the field of tissue regeneration.

This thesis covers the regenerative abilities and their cellular aspects in invertebrates, vertebrates, and mammals, focusing on classic cases from previous scientific research to understand cellular origins and explore factors influencing variations in regenerative capacity. The final emphasis of the study will be on the

regenerative abilities of salamanders. Salamanders possess remarkable regenerative capabilities, particularly in limb regeneration, which encompasses a wide range of tissue structures and functionalities, making them an excellent research model.
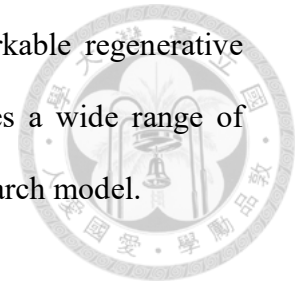
1.2 The Basic Cellular and Molecular Mechanisms of Tissue Repair and Regeneration

When tissue is injured, the body responds by initiating a series of processes to restore its structure and function. Various cell types, such as tissue resident cells, immune cells, vascular cells, fibroblasts, and tissue progenitor/stem cells, actively participate in the complex process of wound healing. However, the precise cellular and molecular mechanisms that govern wound healing are still not fully elucidated.

Interestingly, scientists have noticed that the cellular and signaling responses triggered by wounds share striking similarities with processes observed during development. Here are some key resemblances: **(1) Cell proliferation and differentiation:** In both development and wound repair or regeneration, there is an increase in cell proliferation. The newly generated cells then differentiate into specific cell types to restore the structure and function of the tissue (3). **(2) Common signaling pathways:** Signaling pathways such as the transforming growth factor-beta (TGF-β) (4-6) and Wnt (7-9) play important roles in both development and wound healing. These pathways regulate various cellular behaviors including proliferation, differentiation, migration, and tissue patterning. **(3) Remodeling of the extracellular matrix (ECM):** The ECM, which provides structural support and influences cellular behavior, undergoes dynamic changes during development to shape tissues and organs. Similarly, in wound repair or regeneration, the ECM is modified to facilitate cell migration, tissue growth, and tissue remodeling (10). Despite these notable similarities, it's crucial to recognize that development and wound healing have distinct characteristics and goals.

Development encompasses the overall growth and formation of an organism, starting from a single cell, while regeneration typically focuses on repairing or replacing specific structures or tissues within an already developed organism (11).

During the proliferative phase of the healing process, the formation of granulation tissue occurs due to the deposition of ECM and the growth of new blood vessels (10). This crucial step enables appropriate regenerative responses, including the re-epithelialization of the wound (12, 13). All animals have ability to completely re-epithelialize the wound surface. However, delayed re-epithelialization contributes to scarring and lead to non-healing wounds (14), wherein factors such as growth factors, inflammation, and mechanical forces contribute to the worsening of the healing process. The consensus is that faster wound healing is advantageous, and researchers have observed this phenomenon in specific species, such as amphibians. Different organisms exhibit varying cellular and molecular changes in response to injury. The regenerative abilities and mechanisms can differ among species, and understanding these variations is important for advancing our knowledge of tissue repair and regeneration.

1.3 Model Organisms in Regeneration Research

The physiological regeneration encompasses a diverse array of processes that lack a unified mechanism (15). For instance, the replacement of blood cells and the continuous turnover of epidermal cells differ significantly from the repair of a damaged bone in terms of their underlying mechanisms and cellular behaviors. Similarly, the cellular sources involved in regenerating a head or tail in a planarian are distinct from those required to reconstitute a missing tail in a salamander. However, despite these differences, there are important shared factors, signaling pathways, and the integration of environmental cues that contribute to the regenerative process. By conducting extensive comparative analyses, researchers can identify common genetic networks in

4

regenerative organisms or organs, while also highlighting the differences from non-regenerative tissues. This knowledge plays a vital role in addressing fundamental questions in the field of regenerative medicine.

While numerous remarkable examples of animal regeneration exist, this chapter will provide a concise overview of six species, focusing on their regenerative abilities. Two invertebrates, namely the hydra and planarian, have the extraordinary capability to fully regenerate from small fragments. Among vertebrates, the zebrafish, *Xenopus*, and salamander demonstrate impressive regenerative capacities. Additionally, the chapter will touch upon mammalian regeneration, particularly in mice, and shed light on the challenges faced in the field of regenerative medicine.

1.3.1 Regeneration Models in Invertebrates and the Cellular Basis

(1) Planarians

Planarians are small flatworms that possess the extraordinary ability to regenerate entire organisms from small fragments, including complex structures such as the central nervous system, eyes, and major organs. This ability is attributed to their abundant reservoir of adult stem cells called neoblasts. In response to injury, neoblasts accumulate to form a specialized population known as the regeneration blastema. Within the blastema, neoblasts can differentiate into any required cell type for the regeneration process. This pluripotency of neoblasts is similar to that of embryonic stem cells found in mammals. Initially, neoblasts were thought to be a homogeneous population of adult pluripotent stem cells. However, further research has revealed their heterogeneity. A subpopulation of neoblasts, called clonogenic neoblasts, can form large colonies of descendant cells and give rise to any cell type within the planarian's body (16). Transplantation of a single clonogenic neoblast has been shown to rescue regeneration in irradiated planarians, indicating their potential to regenerate the entire

body.

Recent studies utilizing multidimensional single-cell transcriptional profiling have demonstrated that neoblasts are indeed heterogeneous. They consist of two distinct subpopulations: the pluripotent sigma-neoblasts and the lineage-restricted progenitor zeta-neoblasts (17). Zeta-neoblasts are committed progenitor cells that can only give rise to postmitotic lineages such as epidermal cells and do not contribute to regeneration. On the other hand, sigma-neoblasts possess the ability to differentiate into any cell type, including zeta-neoblasts, and are primarily responsible for regeneration. Additionally, the clonogenic neoblasts are likely contained within the sigma-neoblasts (17). Thus, neoblasts represent a heterogeneous population consisting of pluripotent stem cells and lineage-restricted progenitor cells. However, regeneration primarily relies on the pluripotent sigma-neoblast subpopulation.

(2) Hydra (Hydra vulgaris)
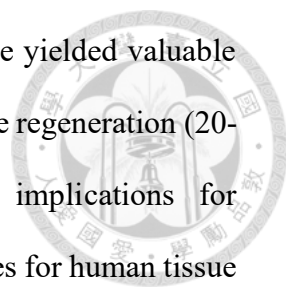
Hydra, a freshwater organism belonging to the animal phylum Cnidaria, possesses remarkable regenerative capabilities. Despite lacking pluripotent stem cells, Hydra can undergo striking regeneration. When Hydra is bisected, the upper half regenerates a foot while the lower half regenerates a head. This regenerative ability can be attributed to the presence of three types of stem cells: ectodermal and endodermal epithelial stem cells, as well as interstitial stem cells, distributed throughout its body (18). The epithelial stem cells contribute to the regeneration of the epidermal layers, while the interstitial stem cells are responsible for regenerating other tissues, including neurons, nematocytes, secretory cells, and gametes (19). Together, these three types of stem cells generate all cell types within the Hydra body, which is believed to be the primary reason for its exceptional regenerative capacity.

1.3.2 Regeneration Models in Primitive Vertebrates and the Cellular Basis

(1) Zebrafish (Danio rerio)

Zebrafish possesses remarkable regenerative abilities. It can efficiently regenerate various tissues and organs, including fins and hearts (20-22). The zebrafish fin, a complex appendage comprising bony fin rays, mesenchymal cells, nerve fibers, and blood vessels, undergoes regeneration through the formation of a specialized regenerative structure known as a blastema. Lineage-tracing studies have demonstrated that lineage-restricted progenitor cells within each fin tissue migrate to the blastema, mirroring the process observed in salamander limb regeneration (23, 24). Fin blastema formation involves a combination of dedifferentiation and activation of stem cells (25). For instance, differentiated osteoblasts undergo temporary dedifferentiation, migrate to the blastema, and then redifferentiate into osteoblasts to facilitate bone regeneration (22). On the other hand, muscle regeneration in the fin is predominantly driven by the activation of muscle stem cells without observed dedifferentiation of muscle cells (25).

Additionally, zebrafish exhibits robust natural heart regeneration capability. After the surgical removal of around 20% of the ventricle, the zebrafish heart can fully regenerate without scarring (26). Genetic-fate mapping experiments have unveiled that dedifferentiation of existing cardiomyocytes is the primary cellular mechanism driving heart regeneration in zebrafish. Following injury, cardiomyocytes near the injury site undergo dedifferentiation, characterized by decreased levels of sarcomeric contractile proteins and activation of developmental transcription factors. Dedifferentiation of these cells plays a crucial role in models of heart regeneration induced by genetic ablation of ventricular cardiomyocytes (27). In other genetic ablation models, transdifferentiation of atrial cardiomyocytes into ventricular cardiomyocytes has been observed during ventricle regeneration (28). These findings indicate that distinct types of heart injuries in zebrafish can elicit diverse cellular regenerative responses.

The regenerative capacities of zebrafish in fins and hearts have yielded valuable insights into the cellular and molecular mechanisms governing tissue regeneration (20-22). Understanding these mechanisms may have significant implications for regenerative medicine and the development of therapeutic approaches for human tissue repair. The zebrafish model continues to contribute to our understanding of regenerative processes and presents exciting possibilities for future research in the field of regeneration.

(2) *Xenopus laevis* (African clawed frog)

Xenopus laevis, an amphibian species, demonstrates tail regeneration from larval life to metamorphosis. When the tail is amputated, the regrowth occurs from the tail regeneration bud. Unlike salamanders, *Xenopus*' tail regeneration bud lacks typical features of a limb blastema, such as a notochord bud, neural ampulla, and blastema formation (29). Lineage analysis studies have revealed that lineage-restricted progenitor cells, found in the spinal cord, notochord, and muscle, become activated and migrate to form the three components of the regeneration bud. Interestingly, no myofiber fragmentation occurs during tail regeneration in *Xenopus* tadpoles (30). Hence, the activation of resident progenitor cells constitutes the primary mechanism for tail regeneration in *Xenopus laevis*.

Xenopus laevis serves as a valuable model organism for comprehending the regenerative processes involved in spinal cord regeneration and tail regrowth. Through the study of *Xenopus*, researchers have gained insights into the activation and migration of lineage-restricted progenitor cells and their role in tissue regeneration. The exploration of *Xenopus* regeneration mechanisms contributes to our broader understanding of regenerative processes and offers potential avenues for therapeutic interventions in the context of spinal cord injuries and other regenerative challenges.
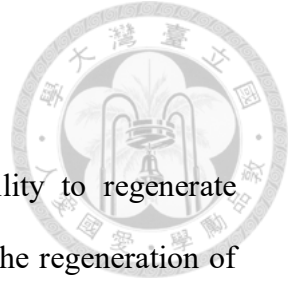
(3) Salamanders (urodele amphibians)

Salamanders, including newts and axolotls, possess the ability to regenerate significant portions of their bodies, although not the entire body. The regeneration of limbs in salamanders serves as a well-established model for studying the regeneration of complex tissues. When a limb is amputated, salamanders have the remarkable capability to completely regrow the missing segments. Lineage-tracing experiments conducted in axolotls, a specific type of salamander, have demonstrated that progenitor cells within each tissue of the limb migrate to form the blastema (31). Therefore, blastema formation does not involve the conversion of one tissue cell type into another. Instead, the blastema comprises a diverse collection of lineage-restricted progenitor cells derived from the original limb tissue.

The exact origin of these lineage-restricted progenitor cells remains a subject of debate. The dedifferentiation of mature cells is thought to contribute to blastema formation, but the activation of resident stem cells also appears to play a role, depending on the species and specific tissues involved. For example, in newts, studies have demonstrated that multinucleate myofibers undergo fragmentation and transition into proliferating mononucleate cells within the blastema. These cells, which do not express Pax7, a marker for muscle stem cells, generate new limb muscles (32). However, recent research has revealed that programmed cell death triggers the dedifferentiation of myofibers into muscle progenitor cells in newt limbs (33). The role of muscle stem cells, specifically Pax7-positive satellite cells, in the blastema is still not completely understood. Conversely, in axolotls, limb muscles predominantly regenerate through the activation of muscle satellite cells rather than muscle dedifferentiation.

Limb muscle regeneration in salamanders demonstrates evolutionary variations among different species. The involvement of muscle stem cells in muscle regeneration

9

is relatively restricted in newts, whereas in axolotls, they play a more significant role. The contribution of other limb tissues to the blastema, whether through the dedifferentiation or activation of stem cells, or a combination of both, remains unclear. Further research is required to elucidate the precise mechanisms by which different cell populations contribute to the regeneration of limb tissues in salamanders.

1.3.3 Regeneration Models in Mammals and the Cellular Basis

Mice (Mus musculus):

While mice do not possess the same extensive regenerative abilities as the organisms mentioned earlier, they serve as significant models for studying tissue repair and regeneration in mammals. Although adult mammalian hearts have limited regenerative potential, neonatal mice demonstrate a greater ability to regenerate their hearts (34). Mice have proven valuable in studying regeneration in various organs, including the digit (35, 36), skin (37, 38), liver (39, 40), and intestine (41, 42). Their utilization has led to advancements in our comprehension of stem cell populations, signaling pathways, and immune responses involved in tissue regeneration. Through genetic manipulation techniques like transgenic and knockout technologies, researchers can investigate the functions of specific genes and their contributions to the regenerative process.

1.4 Regeneration Process in Axolotl Limb Regeneration

While many cases of limb loss are related to traumatic events, the majority of limb loss is caused by diseases that affect the body's blood vessels. One such disease is diabetes, where gradual declines in blood flow to the lower extremities can eventually lead to complete limb loss. Unfortunately, prosthetic limbs remain the only replacement option currently available following amputation. However, while artificial limbs can

replicate the shape of the lost limb, their functionality is still severely lacking. Thus, what if we could regrow lost limb instead of relying on prosthetics?

Although there are no known mammals capable of fully regenerating lost appendages, many exhibit hints of regenerative potential. For instance, it has been observed that mice and human can regenerate the digit tips (43, 44). Axolotls possess an unparalleled regenerative ability, making them ideal models for studying tissue regeneration and repair. When an axolotl loses a limb, it can regrow a fully functional replacement in a matter of weeks. This process involves the activation of specialized cells known as blastema cells, which differentiate into various tissue types, including muscle, bone, and nerves. By understanding the mechanisms underlying axolotl regeneration, scientists hope to unlock the secrets of tissue regeneration in humans and potentially develop new therapies for treating injuries and diseases.
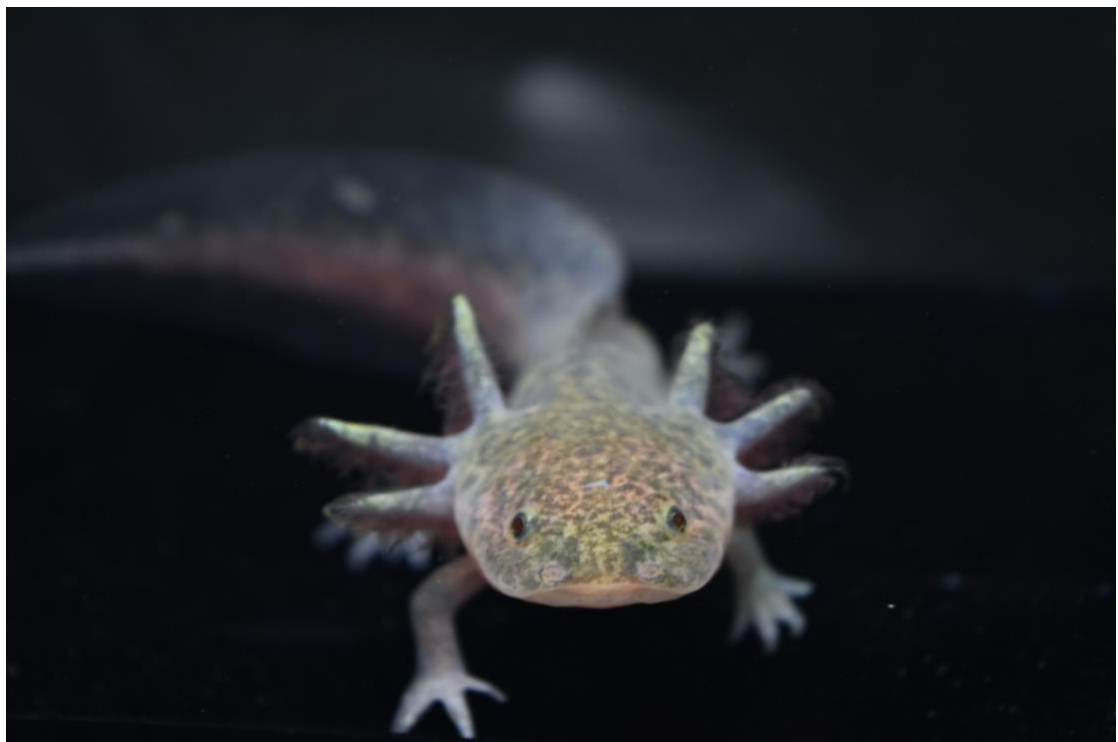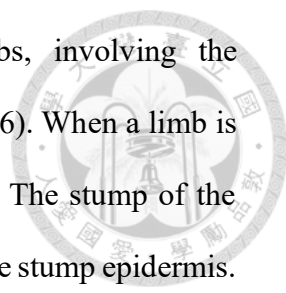
Figure 1.1 A Photograph of an Axolotl in Dr. Lee's Laboratory.

Figure 1.1 shows a photograph of a wild type axolotl in Dr. Lee's laboratory.

11

Axolotls have a complex process of regenerating entire limbs, involving the coordinated actions of surviving cells in the limb (Figure 1.2, (45, 46). When a limb is lost, a blood clot quickly forms to stop bleeding at the injury site. The stump of the wound is covered by a thin layer of migrating epidermal cells from the stump epidermis. These cells gather and multiply, forming a distinct structure called the WE, which is different in structure and molecular composition compared to the fully developed epidermis (47, 48). The WE then progresses into a thicker structure known as the apical epidermal cap (AEC), which acts as a specialized signaling center located at the distal region of the blastema.

Following re-epithelialization, progenitor cells from various tissue types such as bone, cartilage, and muscle undergo a transformation where they lose their specific characteristics and become activated within the stump tissues. The activation process involves both the re-entry of progenitor cells into the cell cycle and their accumulation beneath the WE at the tip of the stump. These activated cells, which can originate from either stem cells or through dedifferentiation, gather and form a cone-shaped structure called the blastema. The blastema cells demonstrate high rates of proliferation and are influenced by factors produced by the overlying WE, although their behavior is not solely dependent on one-way signaling. Blastema is considered autonomous unit because it can be transplanted to other receptive areas of the body, where it is capable of generating limbs (49).

The blastema carries positional information, as evidenced by the ability of transplanted blastema to produce specific limb structures even when relocated (49). Although blastema cells share similarities and morphologically resemble fibroblasts, transplantation studies suggest that they have diverse origins and potential (31, 50). As the blastema expands, pattern formation occurs, allowing the cells to organize themselves and regenerate the distinct structures of the limb, including bones, muscles,

12

nerves, and blood vessels. Signaling pathways and gradients of morphogens play crucial roles in orchestrating this pattern formation process, providing spatial information that guides cell differentiation and tissue development. The establishment of these gradients is essential for correctly positioning different cell types within the developing limb.

Differentiation represents the final stage of axolotl limb regeneration, during which blastema cells undergo specialization to form the various tissues that constitute the regenerated limb. This process involves the activation of specific genetic programs that drive the cells to adopt specific cell fates and acquire the characteristics of the original tissues. The reformation of limb structures occurs in a precise and coordinated manner, ensuring that the regenerated limb closely resembles the original limb in terms of both form and function.
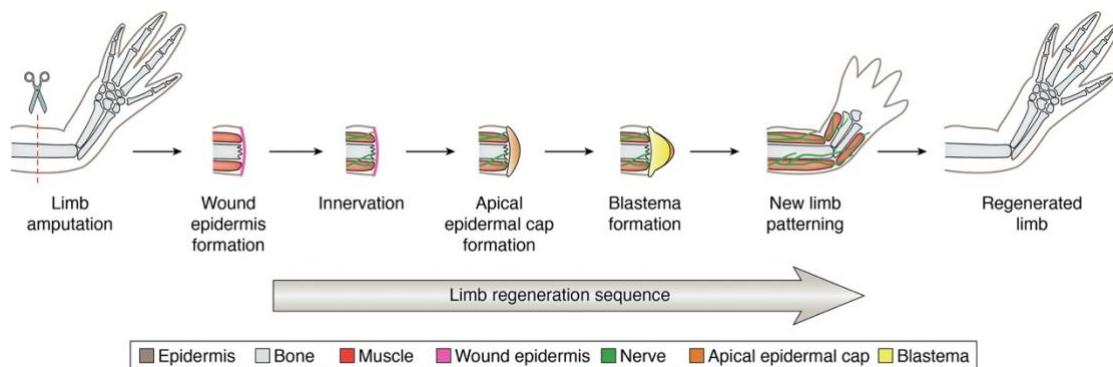
Figure 1.2 An Overview of the Cellular Processes During Limb Regeneration. Upon amputation, stump epidermal cells migrate to form a thin layer known as the WE over the cut stump. Over the course of a few days, the WE becomes innervated and transforms into the AEC. The AEC acts as an attraction point for blastema-forming cells, leading to the formation of a blastema. The blastema subsequently undergoes continuous proliferation and differentiation until a fully regenerated limb is ultimately formed. This figure is adapted from the research works of McCusker et al. 2015 and Min and Whitted. 2023 (45, 46).
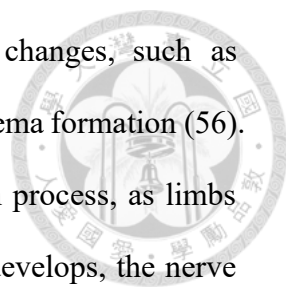
1.5 Blastema Formation is a Unique Structure as a Sign for a Successful Limb Regeneration

Although wound healing is necessary for eventual regeneration, it is not enough to initiate blastema formation. This concept is illustrated in the accessory limb model (ALM), which serves as a gain-of-function experiment to study the signaling mechanisms involved in blastema development for limb regeneration (51). In this model, a blastema similar to one induced by amputation is generated on the arm's side by creating a small full-thickness skin wound and surgically redirecting the brachial nerve to the wound site (51, 52). If the nerve is not redirected, no blastema forms (51). This suggests that blastema formation relies on a specific level of nerve signaling and the involvement of the WE.

Nerve signaling plays a crucial role in promoting cell division and repairing injured tissues, and it is necessary for both the initial formation and subsequent growth of the blastema. The ALM has provided evidence that nerves have the ability to transform the healing of skin wound into the formation of new limb. Additionally, denervation has been shown to inhibit limb regeneration, highlighting the essential role of nerves in this process. It has been proposed that nerves secrete specific factors that stimulate appendage regeneration in amputated limbs (53). One such factor is the newt anterior gradient (nAG) protein, which has been demonstrated to contribute to the nerve dependence of limb regeneration in newts (54). Studies have shown that expression of nAG after electroporation can rescue denervated limbs, allowing them to complete the proximodistal axis and form digits (54). Furthermore, the application of nerve factors such as FGF2, FGF8, BMP2, or BMP7 to wounded skin has been found to trigger limb formation in the ALM model (55).

After receiving signals from the nerves, the WE undergoes maturation and

transforms into the AEC. The AEC then undergoes additional changes, such as stratification, which occur either before or simultaneously with blastema formation (56). Innervation of the WE is a crucial step in guiding the regeneration process, as limbs that are denervated fail to regenerate. As the blastema grows and develops, the nerve itself regenerates and maintains its connection to the WE/AEC, indicating the presence of a feedback loop in the signaling pathways between the nerve and WE/AEC.

1.6 Hypothesis and Aims

During the generation of induced pluripotent stem cells (iPSCs), the chromatin structure of differentiated cells is reset to resemble that of embryonic cells (57). Various factors that can modify epigenetic control have been found to enhance iPSC generation, highlighting the significance of epigenetic reprogramming in cellular reprogramming processes (58, 59). Regeneration triggers significant changes in the transcriptional programs of cells involved in the process. To restructure the missing tissue, multiple developmental and patterning signaling pathways need to be coordinated and reactivated. Therefore, it has been widely accepted that blastema cells originating from different parts of the limb undergo dedifferentiation, returning to a pluripotent state, and then redifferentiate to restore all the lost cell types (60). However, recent studies have revealed that blastema cells do not actually revert to a pluripotent state, but instead become heterogeneous progenitor cells with distinct and mostly limited regenerative abilities (31, 61). On the other hand, certain genes involved in chromatin remodeling have been identified as upregulated during limb and lens regeneration, such as methylation states and histone demethylases, which act as regulatory components in the regeneration of *Xenopus* tadpole limbs and zebrafish fins (61-63). The underlying epigenetic mechanisms are still not fully understood, and more comprehensive genome-wide studies are needed to determine the extent and functions of epigenetic remodeling

during regeneration. In summary, blastema growth relies on permissive factors provided by nerves, the WE/AEC, as described previously. However, without proper epigenetic regulation among blastema cells from different positions, successful regeneration may not be achieved.

Based on the information, it is crucial and intriguing to investigate the molecules and signaling pathways that are instrumental in the interactions between the WE/AEC and nerves during blastema formation. Recent studies have shed light on various molecules and signaling pathways involved in this process. Moreover, there is evidence of significant changes in epigenetic modifications within the regulatory regions of tissue-specific genes (64). One crucial mechanism of epigenetic regulation involves histone acetylation and deacetylation, which are mediated by histone acetyltransferases (HATs) and histone deacetylases (HDACs), respectively. HDACs have been implicated in development and the maintenance of stem cell pluripotency (65). Notably, recent investigations have highlighted the importance of HDACs in tadpole tail regeneration, with HDAC1 expression observed in regenerating buds for up to two days following amputation (66). Therefore, it is reasonable to hypothesize that HDACs play roles in the WE/AEC-nerve axis during axolotl limb regeneration.

Based on previous observations and findings, it is postulated that the reconnection of muscles during axolotl limb regeneration is facilitated by the undifferentiated ends of both the remnant and regenerating muscles. The hypothesis is based on the understanding that these undifferentiated muscle ends lack fully organized sarcomere structures, creating a favorable environment for reconnection. During the early stages of limb regeneration, the remnant muscles undergo dedifferentiation and maintain an undifferentiated state throughout the limb differentiation (LD) stage. This undifferentiated state, coupled with the partially differentiated state of the regenerating muscles, provides conditions conducive to reconnection.

It is hypothesized that the undifferentiated muscle ends possess a higher degree of plasticity, enabling them to reposition and reconnect with the regenerating muscle fibers. The process of muscle reconnection is expected to be a coordinated and synchronized event involving multiple muscles within the limb. The timing of reconnection may be influenced by the progression of the LD stage and the degree of sarcomere organization in the regenerating muscles. The reconnection of muscles is believed to contribute to the restoration of functional muscle tissue and the successful overall regeneration of the axolotl limb.

Chapter 2:

The Role of Nerve-Mediated HDAC Expression in the Regulation of Limb Regeneration in Axolotls

2.1 Summary
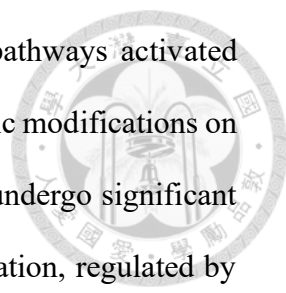
Axolotls exhibit extraordinary limb regeneration capabilities, and this intricate process is profoundly influenced by both the nerve and WE. Recent investigations have shed light on the significant role of histone deacetylases (HDACs) in amphibian limb and tail regeneration. Particularly, a biphasic increase in HDAC1 expression has been observed during the initial stages of axolotl limb regeneration. Intriguingly, larvae treated with an HDAC inhibitor, MS-275, displayed delayed limb regeneration. Similarly, local injections of MS-275 or another HDAC inhibitor, TSA, into the amputation sites of juvenile axolotls did not affect wound healing but impeded blastema formation and subsequent limb regeneration by inhibiting local HDAC activity. Notably, HDAC1 expression was found to be more prominent in the WE compared to the mesenchyme. Denervation prior to limb amputation prevented the up-regulation of HDAC1 expression and hindered limb regeneration. However, supplementation of nerve factors BMP7, FGF2, and FGF8 in denervated limb stumps after amputation not only facilitated HDAC1 up-regulation but also resulted in more extensive limb regeneration. In conclusion, nerve-mediated HDAC1 expression is an indispensable requirement for blastema formation and successful limb regeneration in axolotls.

2.2 Introduction

Regeneration is a remarkable phenomenon observed in many animal species, although its complexity tends to decrease as animals evolve. While planarians can regenerate entire bodies, organisms like *Xenopus* and mammals are only capable of regenerating specific structures during early life stages (67, 68). Among these, axolotl limb regeneration serves as a well-studied model for the regeneration of complex vertebrate structures. Following limb amputation, the initial response involves rapid migration of epidermal cells from the stump edge to cover the wound. This results in the formation of a thickened WE, which later develops into an apical epithelial cap (AEC). Dedifferentiation of cells beneath the AEC gives rise to a blastema, consisting of undifferentiated and proliferating cells. In non-regenerative animals, blastema formation fails to occur after limb amputation (55, 69, 70). The differentiated blastema cells then undergo further differentiation into various cell types and contribute to limb growth. Ultimately, a fully functional limb is regenerated. Therefore, blastema formation stands as a critical event in successful limb regeneration.

The successful formation of the blastema relies on both the WE/AEC and nerve signaling (45, 71). It has been demonstrated that both the WE and AEC serve as information centers that influence the underlying mesenchymal tissues to initiate blastema formation during regeneration (69, 72, 73). During the early stages of limb regeneration, nerve signaling regulates the WE to generate keratinocytes and promotes the transformation of the WE into the AEC (74). Failure in WE formation or denervation of limbs results in the inability to form a blastema (75-79). Collectively, this evidence highlights the critical roles played by both the WE/AEC and nerve signals in blastema formation.

Investigating the molecules and signals that influence the WE/AEC and nerve-mediated blastema formation represents a crucial and intriguing area of research.
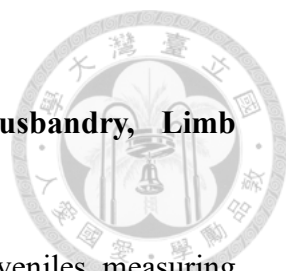
Recent studies have indicated that several molecules and signal pathways activated during development are also involved in regeneration (80). Epigenetic modifications on the regulatory regions of tissue-specific genes have been found to undergo significant changes during regeneration (64). Histone acetylation and deacetylation, regulated by histone acetyltransferases (HATs) and HDACs, respectively, are vital epigenetic mechanisms. HDACs, a group of enzymes that remove acetyl groups from lysine residues, play important roles in chromatin structure and gene silencing (81, 82). Among the four classes of HDACs, class I and class II have been identified as essential for tissue regeneration (83). Class I HDACs (HDAC1, 2, 3, and 8) primarily target chromatin, while class II HDACs (HDAC4, 5, 6, 7, 9, and 10) shuttle between the cytoplasm and nucleus. HDACs are involved in regulating various cellular functions, including microtubule dynamics, aging, and differentiation (84, 85). They have been implicated in development and stem cell pluripotency (86), and recent studies have demonstrated the significance of HDACs in tadpole tail regeneration, with HDAC1 expression observed in regenerating buds up to two days after amputation (66). Thus, it is reasonable to hypothesize that HDACs play a role in the WE/AEC-nerve axis during axolotl limb regeneration.

The present study unveils a two-phase up-regulation of HDACs during axolotl limb regeneration. Inhibition of HDAC activity impedes the process of limb regeneration. Denervation of axolotl limbs halts the up-regulation of HDAC1, resulting in the inhibition of limb regeneration. The addition of BMP7, FGF2, and FGF8 to the stumps partially rescues the denervation-induced lack of regeneration. These findings provide evidence for the crucial involvement of nerve-mediated HDACs in axolotl limb regeneration.

2.3 Materials and methods

2.3.1 Care and Experimental Procedures for Axolotl Husbandry, Limb Amputation, and Denervation

The axolotls utilized in this study were reared as larvae and juveniles, measuring 3-4 cm and 8-16 cm in snout-to-tail-tip length, respectively. Juvenile axolotls were fed fish pellets three times a week, while larvae received a daily diet of brine shrimp. The axolotls were housed in a modified Holtfreter's solution composed of 118.4 mM NaCl, 1.3 mM KCl, 1.8 mM $CaCl_2$, 1.6 mM $MgSO_4.7H_2O$. Prior to any manipulations or imaging, the axolotls were anesthetized using a 0.1% MS-222 solution (Sigma-Aldrich, St. Louis, MO, USA). Limb amputation was performed on the middle upper arms of both larvae and juveniles, while denervation of the brachial plexus was carried out in juveniles following previously described methods (87). For short-term follow-up experiments lasting less than 6 days, a single round of denervation was performed. For longer follow-up observations exceeding 20 days, a second round of denervation was conducted, spaced 7 days apart to ensure a fully denervated state (88, 89). All animal care and experimental procedures adhered to approved guidelines and were approved by the Institutional Animal Care and Use Committee of the National Taiwan University College of Medicine.

2.3.2 Q-PCR for Evaluating HDAC Expression in Axolotl Stump Ends

For analysis purposes, stump ends were collected from larvae at specific time points: 0, 12, 24, 36, 48, 72, 120, and 168 hours post-amputation (hpa). Similarly, stump ends were harvested from 8-12 cm juveniles at the following time points: 0, 1, 2, 3, 4, 5, 6, 10, 20, 28, and 33 days post-amputation (dpa). The utilization of juvenile axolotls for analysis was preferred due to the ease of denervation and the separation of the WE from the underlying mesenchyme. Stump ends from juvenile axolotls were collected at
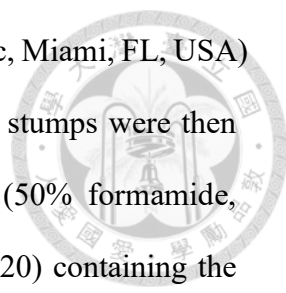
0, 24, 48, 72, 96, and 120 hpa, and the WE and underlying mesenchyme were separated for subsequent quantitative polymerase chain reaction (Q-PCR) analysis.

Total RNA was extracted from the collected tissues using Trizol reagent (Invitrogen, Carlsbad, CA, USA), and reverse transcription was performed at 50°C using Superscript III reverse transcriptase (Invitrogen). The resulting first-strand cDNAs were diluted 1:9 and utilized as templates for Q-PCR. Q-PCR reactions were carried out in a total volume of 10 μl using the SYBR Green kit (Stratagene, La Jolla, CA, USA). The gene-specific primers, designed based on next-generation transcriptome sequencing and axolotl Expressed Sequence Tags (ESTs) from Sal-Site (90), were added at a concentration of 0.8 μM following the manufacturer's instructions. Q-PCR was performed using the ABI StepOne™ Real-Time PCR System, and the resulting data were analyzed using StepOne™ software version 2.1 (Applied Biosystems, Foster City, CA, USA).

2.3.3 ISH for Localizing HDAC1 Expression

For *in situ* hybridization (ISH), 12 cm juveniles were utilized following a previously described method (87). A 230 bp cDNA fragment of HDAC1 was amplified by RT-PCR, using sense primers linked to the SP6 promoter sequence and antisense primers linked to the T7 promoter sequence. The DIG RNA-labeling kit (Roche, Indianapolis, IN, USA) was employed to synthesize sense and antisense RNA probes. The primers used for RNA probe preparation were as follows: HDAC1 (antisense), 5´ -CGTAATACGACTCACTATAGGGAGAGTGAGAGGCCTTCCAAAATG-3';   and HDAC1   (sense),   5´   - CGATTTAGGTGACACTATAGAAGAGTCTTAATGCAGGGAGGGTTG-3'.

The juveniles with post-amputation limb stumps were fixed in 4% paraformaldehyde (PFA) in $1 \times$ phosphate-buffered saline (PBS) at 4°C overnight.

Subsequently, they were embedded in Cryomatrix (Thermo Scientific, Miami, FL, USA) and frozen at -80 °C until sectioning at 10 μm thickness. The limb stumps were then subjected to overnight hybridization in a hybridization solution (50% formamide, $5 \times$ SSC, 50 μg/mL yeast RNA, 50 μg/mL heparin, and 1% Tween-20) containing the DIG-labeled RNA probe (5-10 μg/mL) at 60 °C, following prehybridization. The DIG-labeled probes were detected using anti-DIG-alkaline phosphatase antibody (Roche, Indianapolis, IN, USA) and visualized with a mixture of 5-bromo-4-chloro-3-indolyl-phosphate and 4-nitroblue tetrazolium chloride (BCIP/NBT) solution (Sigma-Aldrich) dissolved in 1 mM levamisole solution (Sigma-Aldrich).

2.3.4 Nuclear Protein Extraction and Measurement of HDAC Activity

For the extraction of nuclear proteins, regenerating tissue samples were collected at specific time points and placed in ice-cold PBS supplemented with phosphatase inhibitors. The tissues were then transferred to a hypotonic solution and incubated for 30 minutes at 4°C. Subsequently, the tissues were homogenized using a dounce homogenizer to obtain a single-cell slurry. The cytoplasmic fraction was lysed using a lysis buffer, while the resulting nuclei were isolated, and nuclear proteins were extracted and stored at -80°C until further use.

HDAC activity in the nuclear extracts was measured using the HDAC Activity Colorimetric Assay kit (BioVision, Mountain View, CA, USA) following the manufacturer's instructions. This assay utilizes a short peptide substrate containing an acetylated lysine residue, which can be deacetylated by specific HDAC enzymes. Upon deacetylation, the substrate undergoes a reaction with a lysine developer, resulting in the formation of a chromophore. The concentration of the chromophore was determined by measuring the absorbance at 405 nm using an ELISA plate reader. A series of standard deacetylated lysine concentrations was used to establish a calibration curve for

quantification.

2.3.5 Larval Axolotl Incubation in MS-275-Containing Solution

A stock solution of MS-275 was prepared using dimethyl sulfoxide (DMSO) and subsequently diluted to the desired concentrations using modified Holtfreter's solution. Limb amputation was performed on the middle upper arms of 3-4 cm larvae, followed by the placement of individual larvae in 6-well plates containing 6 mL of Holtfreter's solution supplemented with varying concentrations of MS-275 (Selleckchem, Houston, TX, USA) for specific treatment periods or different MS-275 concentrations for various treatment durations. A control group treated with 0.1% DMSO was included as a reference. Each experimental group consisted of five animals exposed to different MS-275 concentrations and treatment durations, as outlined in Figure 2.2A-D and 2.3. The MS-275-containing solution was renewed daily to maintain the stability of the inhibitor. Daily microscopic examinations were performed to monitor the progression of developmental stages in the axolotls.

2.3.6 Injection of HDAC Inhibitors into Amputated Limbs of Juvenile Axolotls

To facilitate the injections, a stock solution of MS-275 and TSA (ApexBio Technology, Houston, TX, USA) was initially prepared using DMSO. These stock solutions were then diluted with filtered 0.8× amphibian PBS (aPBS; 1× PBS diluted with dH2O) to attain the desired final treatment concentration. Glass Pasteur pipettes (Kimble Chase, Vineland, NJ, USA) with a manually sharpened external tip diameter of 40 μm were utilized for the injections. In each injection, 2 μl of 25 mM MS-275, 10 mM TSA, or a control solution of 2% DMSO in aPBS was delivered beneath the WE of the limb stumps of 15-16 cm juveniles every other day post-amputation.

2.3.7 Establishment of Morphological Criteria for Different Stages of Limb Regeneration

To accurately monitor the progression of limb regeneration, I established specific morphological criteria for different stages, namely early bud (EB), mid bud (MB), late bud (LB), early differentiation (ED), late differentiation (LD), and non-regenerative (NCR). These criteria were derived from previous studies (91, 92) with certain modifications, as detailed in Table 2.1 and Figure 2.1.

2.3.8 EdU Labeling for Identification of Dividing Cells

In order to pinpoint dividing cells in the regenerating bud, a 15–16 cm juvenile axolotl was subjected to an intraperitoneal injection of 100 μg/g body weight of 5-ethynyl-2′-deoxyuridine (EdU) (Invitrogen) 20 hours prior to tissue collection. The collected tissues were fixed with 4% PFA in $1 \times$ PBS and subsequently embedded in Cryomatrix (Thermo Scientific). For EdU labeling, the sections were processed using the reagents provided in the Click-iT EdU Alexa Fluor 594 Imaging Kit (Invitrogen), following the manufacturer's instructions. The resulting slides were mounted with fluorescence mounting medium (DakoCytomation, Carpinteria, CA, USA) and examined using a fluorescence microscope to identify EdU-positive nuclei.

2.3.9 Bead Grafting Procedure

The process of bead grafting involved the use of gelatin beads with a diameter of 200-400 μm. Initially, the beads were dried and subsequently allowed to swell in aPBS or aPBS containing mouse BMP7, FGF2, and FGF8 (BFF, R&D systems, Minneapolis, MN, USA) at a concentration of 0.1 μg/μl each (55). Denervation was carried out on 8-12 cm juvenile axolotls 7 days prior to amputation. Two days after the amputation, three beads soaked in either aPBS with or without BFF were grafted beneath the wound

epithelium, targeting locations roughly corresponding to the three major nerve ends. Subsequently, a second round of denervation was performed at 7 dpa, followed by the placement of beads specific to the experimental group. The stages of limb regeneration were documented at 35 dpa.
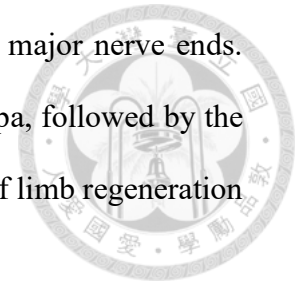
2.3.10 Microscopy and Image Processing Methods

Bright-field and fluorescence images were captured using Olympus BX51 and Olympus SZX7 microscopes (Olympus, Tokyo, Japan). To enhance the quality of the images, Photoshop software (Adobe Systems, San Jose, CA, USA) was utilized. The adjustments made in Photoshop were limited to the uniform modification of brightness and contrast functions for both experimental and control images, aiming to enhance the signal-to-noise ratio.

2.3.11 Statistical Analysis Methods

ach experiment was replicated three times per animal, and the data are reported as mean ± SEM. To compare the means across multiple groups, either two-way ANOVA with Bonferroni's post hoc test or one-way ANOVA with Dunnett's multiple comparison test was performed. Prism software (GraphPad Software, La Jolla, CA, USA) was used for all statistical analyses, and a significance level of $P < 0.05$ was considered statistically significant.

2.4 Results

2.4.1 Bi-phasic Up-regulation of HDACs during Axolotl Limb Regeneration

To gain insights into the expression dynamics of HDACs during axolotl limb regeneration, stump ends and regenerating buds from 3-4 cm larval axolotls and 10-12 cm juvenile axolotls were examined. Q-PCR analysis revealed a bi-phasic up-regulation pattern of HDAC1, 4, and 6 in both larvae and juveniles.

In larvae, a rapid and significant up-regulation of HDAC1, 4, and 6 was observed, reaching peak levels at approximately 12-24 hpa. However, this initial elevation returned to basal levels by 72 hpa, coinciding with the initiation of blastema formation. Intriguingly, a second wave of up-regulation, primarily in HDAC1, was detected from 120 hpa onwards, with significant up-regulation at 168 hpa, corresponding to the mid bud stage (Figure 2.2A).

Consistent with larval findings, the expression pattern of HDAC1 in juvenile axolotls exhibited a similar bi-phasic up-regulation. Rapid up-regulation occurred at 3 dpa, followed by a return to basal levels at 6 dpa, corresponding to the pre-blastema stage. Subsequently, a second wave of up-regulation was observed during the blastema stage, with peaks at 10 dpa (EB stage) and 20 dpa (MB stage), before returning to basal levels at 33 dpa, marking the late bud stage (Figure 2.2B).

These findings provide valuable insights into the temporal regulation of HDAC expression during axolotl limb regeneration, highlighting distinct phases that may contribute to the complex processes underlying regeneration.

2.4.2 Delayed Progression of Axolotl Larval Limb Regeneration by Incubation with HDAC Inhibitor MS-275

After observing the up-regulation of HDACs during the early phase of limb regeneration, I conducted an experiment to investigate the effects of incubating axolotl

28

larvae in Holtfreter's solution containing MS-275, a synthetic inhibitor of class I HDACs, on limb regeneration. To determine the optimal concentration of MS-275, I tested escalating concentrations (6.25, 12.5, 25, and 50 μM) in Holtfreter's solution for larval incubation. It was found that when the concentration of MS-275 was increased to 50 μM, approximately half of the larvae died. Therefore, only the concentrations of 6.25, 12.5, and 25 μM were used for the remaining experiments. The activities of HDACs in the stump ends showed a dose-dependent decrease following treatment with MS-275 at 6.25, 12.5, and 25 μM from 12 to 48 hpa (Figure 2.2A). However, the inhibition of HDAC activities at the 25 μM concentration from 12 to 48 hpa was only mildly to moderately effective, reducing HDAC activity by 14.7% to 34.8%. This suggests that the larval incubation method of MS-275 treatment was not sufficiently effective in reducing regional HDAC activity at the amputation site. Figure 2.2B illustrates the dose-dependent delay in regeneration at 15 days post-amputation (dpa) due to MS-275 treatments (6.25-25 μM). Control subjects reached the near complete regeneration (NCR) stage in approximately 21.8 ± 1.2 days, while the MS-275-treated groups took significantly longer periods in a dose-dependent manner (25.5 ± 2.2 days at 6.25 μM, 30.3 ± 1.8 days at 12.5 μM, and 38.0 ± 2.6 days at 25 μM of MS-275) to reach the NCR stage (Figure 2.2B).

To gain a better understanding of the role of HDAC at different stages of limb regeneration, we conducted MS-275 treatments at various timings and durations following amputation. Daily microscopic observations were carried out on the treated axolotl larvae, and detailed records of the corresponding limb regeneration stages for each treatment protocol were carefully documented (Figure 2.3). Treatment administered during the initial three days after amputation (0-3 days post-amputation or dpa group) did not affect the speed of regeneration compared to the vehicle control group. However, treatments given for the initial nine and thirteen days post-amputation

(0-9 dpa group and 0-13 dpa group, respectively) exhibited a duration-dependent delay in regeneration. Notably, the delay observed with treatment administered throughout the initial thirteen and seventeen days (0-13 dpa group and 0-17 dpa group) was similar to that of the group treated for the entire 37-day course (whole course group), indicating that treatment during the initial thirteen days had already achieved maximum impact. On the other hand, treatment between 0-3 days (0-3 dpa group), 3-9 days (3-9 dpa group), or 9-17 days (9-17 dpa group) did not affect the speed of regeneration compared to the vehicle control group. This suggests that treatment within the initial three days and between 3 dpa and 9 dpa was crucial for delaying the progression of regeneration. In line with the biphasic pattern of HDAC1 up-regulation observed (Figure 2.1), both the pre-blastema and blastema waves of HDAC1 expression were essential for successful regeneration.

2.4.3 Profound Inhibition of Limb Regeneration and Reduction in Cell Proliferation by Local Injection of HDAC Inhibitors MS-275 and TSA in Juvenile Axolotls

Due to the potential lethal systemic effects of incubating larval axolotls in higher concentrations of MS-275 and only mild delay in regeneration progression in lower concentrations (Figure 2.4), I explored a more effective method of MS-275 administration to further clarify the requirement of HDAC1 for limb regeneration. I injected high doses of MS-275 and TSA, another well-known pan-HDAC inhibitor (93), into the stump ends of juvenile axolotls to minimize the indirect systemic effects from high dosages of HDAC inhibitor treatments. The experimental protocol is shown in Figure 4A. The injections started immediately after amputation and repeated every other day until 34 dpa. Two microliters of 25 mM MS-275 or 10 mM TSA, along with an equal volume of 2% DMSO (as vehicle control), were injected into the stump ends.

Progression of the regeneration stages was classified as early bud (EB), mid bud (MB), late bud (LB), early differentiation (ED), late differentiation (LD), and near complete regeneration (NCR). The definition of regeneration stages is presented in Figure 2.1 and Table 2.1. In the control group, 3 of the regenerating limbs reached the ED stage, and 7 reached the LD stage of regeneration at 34 dpa (Figure 2.5B and E). In contrast, injection of MS-275 or TSA completely inhibited blastema formation and limb regeneration (Figure 2.5C–E). The juveniles receiving injections of these two kinds of HDAC inhibitors were healthy and did not show any abnormalities in activities or feeding. HDAC inhibition by this local injection model in juveniles was more profound, with 58.5% and 67.2% reduction of HDAC activities by MS-275 and TSA treatment, respectively (Figure 2.5F), in contrast to only milder reduction (14.7–34.8%, Figure 2.3A) for the larvae incubated in $25\,\mu M$ MS-275-containing solution. The results showed that both MS-275 and TSA profoundly reduced HDAC activities and completely inhibited limb regeneration, indicating that their effects were through specific HDAC inhibition instead of other off-target functions.

Local injection of a 25 mM MS-275 into juveniles did not impair wound healing but profoundly inhibited blastema formation leading to the failure of regeneration, as observed at 13 dpa (Figure 2.6A and B). The percentage of cell proliferation in the mesenchyme was significantly reduced in the stumps of MS-275-treated axolotls, as revealed by EdU labeling (Figure 2.6C, D, C', D', and E). These data indicated that the local injection of HDAC inhibitor in juvenile axolotls resulted in a significant reduction of cell proliferation and profound inhibition of limb regeneration.

2.4.4 Preferential Expression of HDAC1 in the WE Mediated by Nerves during Limb Regeneration in Juvenile Axolotls

I focused on investigating the expression of HDAC1 in axolotl limb regeneration, specifically targeting the inhibition of class I HDACs by MS-275. To examine HDAC1

expression in different tissues, I isolated the wound epidermis and underlying mesenchyme from juvenile axolotl limbs. In control juveniles, I observed a significant increase in HDAC1 expression in the WE between 3 and 4 dpa, while the increase in the underlying mesenchyme was not statistically significant (Figure 2.7A). However, denervated limbs did not show any up-regulation of HDAC1 in either the wound epidermis or underlying mesenchyme. These findings were further confirmed through ISH analysis, which demonstrated higher levels of HDAC1 expression in the wound epidermis and neighboring skin, with lower expression in the underlying mesenchyme (Figure 2.7B). As a control, ISH using a sense probe did not show significant HDAC1 expression (Figure 2.7C). In conclusion, these results indicate that the up-regulation of HDAC1 expression in both the wound epidermis and underlying mesenchyme relies on the presence of nerves.

2.4.5 Partial Restoration of HDAC1 Expression and Limb Regeneration in Denervated Limbs by BMP7, FGF2, and FGF8 Treatment

Nerve factors released from the stump ends play a crucial role in blastema formation and limb regeneration (94, 95). Previous studies using the ALM have demonstrated that nerves can induce ectopic limb formation (51). In ALM experiments, grafting gelatin beads soaked in a mixture of BFF has been shown to substitute for nerve ends and induce accessory limb formation (55). These findings suggest that these three nerve factors may be key in inducing blastema formation and limb regeneration.

Based on this, I hypothesized that BMP7, FGF2, and FGF8 might rescue limb regeneration by reactivating HDAC1 expression in denervated limbs. The experimental protocol is depicted in Figure 2.8A. At 35 dpa, representative photos revealed limb regeneration up to the LD stage in the control non-denervated axolotl (Figure 2.8B), to the ED stage in a denervated limb treated with BFF (Figure 2.8C), and no regeneration

32
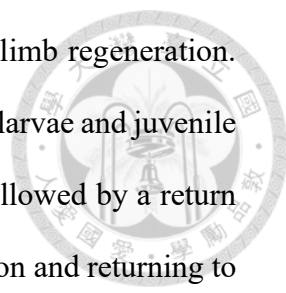
at all in a denervated limb treated with the vehicle control aPBS (Figure 2.8D). The number of limbs reaching various regeneration stages at 35 dpa is shown in Figure 2.8E. All non-denervated control limbs reached the LD stage. In the denervation + BFF group, 2 limbs failed to regenerate, 1 regenerated into MB, 4 into LB, 1 into ED, and 2 into LD stage. In contrast, all denervation + aPBS limbs failed to regenerate.

Additionally, I examined the expression of HDAC1 in the WE from 1 to 6 dpa. The data revealed a significant increase in HDAC1 expression at 4 dpa in the denervation + BFF group, while no such increase was observed in the denervation + aPBS group (Figure 2.8F). These findings support our hypothesis that BFF can partially substitute for nerve factors, inducing HDAC1 expression and promoting limb regeneration in denervated limbs.

2.5 Discussion

Axolotl limb regeneration is initiated by the amputation process, which triggers wound healing. Subsequently, cells surrounding the wound edge are mobilized to form a blastema in response to signals that promote regeneration (51, 96). The formation of the blastema is mediated by interactions between nerves and the WE (94). While denervation prior to amputation does not affect wound healing, it impedes blastema formation and subsequent limb regeneration (97). Research on ALM has also demonstrated that nerves can induce successful ectopic limb formation (51, 52).

HDACs have essential functions in various biological processes, such as cellular growth and proliferation. (98). The use of HDAC inhibitors in clinical cancer therapy is based on their ability to inhibit cell growth and proliferation (99). However, their effects on tissue regeneration remain poorly understood and subject to ongoing debate. Some studies suggest that HDACs may inhibit regeneration, while others report that they improve regeneration. For example, treatment with HDAC inhibitors has been shown to enhance digital regeneration in mice by increasing proliferation, collagen deposition, and stem cell numbers at the amputation site (100). Similarly, HDAC inhibitors have been demonstrated to reduce cell apoptosis and improve functional recovery in spinal cord injury regeneration (101). In contrast, HDACs have also been reported to impair regeneration. Pharmacological blockade of HDACs has been shown to inhibit tail regeneration in tadpoles (66, 102), delay liver regeneration and hepatocyte proliferation (103), and impede keratinocyte proliferation and terminal differentiation (104, 105). Furthermore, HDAC1-null mice have exhibited disrupted hair follicle regeneration (106). Additionally, blocking the activities of class I HDACs with MS-275 has been shown to impair renal regeneration by increasing tubular injury and apoptosis (107).

These findings suggest a positive role for HDACs in axolotl limb regeneration. Interestingly, I observed a biphasic up-regulation of HDAC1 in both larvae and juvenile axolotls, with the first phase occurring in the pre-blastema stage, followed by a return to baseline levels, and a second phase beginning at blastema formation and returning to baseline levels prior to early differentiation. This biphasic pattern may explain why incubation with the HDAC inhibitor MS-275 during specific time periods had no inhibitory effect on regeneration, suggesting that each wave of HDAC1 up-regulation is essential for successful regeneration. However, the biological significance of this biphasic up-regulation of HDAC1 instead of persistent up-regulation remains unknown. To further investigate the role of HDACs, I conducted loss-of-function studies using the HDAC inhibitor MS-275. Our results showed that while incubation with MS-275 delayed regeneration, limb regeneration eventually reached the normal completion rate after a longer period. Local injection of either MS-275 or TSA at a high dose completely inhibited limb regeneration, indicating that the regeneration-inhibitory effects of these HDAC inhibitors were indeed due to HDAC inhibition rather than non-specific functions.

The local injection method is a superior approach for delivering HDAC inhibitors compared to the incubation method. By injecting a higher dose of inhibitors directly into the local region, the concentration of the inhibitors remains elevated while minimizing the possibility of systemic detrimental effects that may arise from incubating the entire larvae. This strategy allowed the juveniles to maintain normal feeding activities, resulting in more potent HDAC1 inhibition and more significant impairment of limb regeneration. Furthermore, treatment with MS-275 strongly suppressed cell proliferation in the mesenchyme (Figure 2.6E), suggesting that HDACs may stimulate cell proliferation and promote blastema formation. These findings align

35

with recent studies indicating that class I HDACs play a crucial role in cell proliferation (83, 108, 109).

To explore the potential link between nerve stimulation and HDAC up-regulation, I conducted a study comparing the expression of HDAC1 in the WE and underlying mesenchyme of normal innervated limbs versus post-denervation limbs. I focused on juvenile axolotls as denervation of the brachial plexus and separation of the WE and mesenchyme tissues could be more easily performed on juveniles. Our results showed that HDAC1 up-regulation was preferentially observed in the WE and to a lesser extent in the mesenchyme. This is in contrast to a previous study on *Xenopus* tail regenerating buds, where HDAC1 expression was mainly found in the mesenchyme (66), but the reason for this difference is unknown. Interestingly, HDAC1 expression in both the WE and mesenchyme was not elevated in denervated limbs, strongly suggesting that HDAC1 up-regulation is indeed mediated by nerve stimulation.

For nearly 250 years, it has been recognized that the regeneration of salamander limbs depends on nerves (97). Consequently, identifying nerve-secreted factors that stimulate blastema formation and limb regeneration has been a major research focus (75, 94). Several candidate factors, such as transferrin (110, 111), anterior gradient protein (54), FGFs (112), and neuregulin-1 (88), have been identified. In axolotl limb models, grafting of gelatin beads soaked in a mixture of these factors has been used as an alternative to nerves to promote accessory limb formation (55). Following this approach, supplementation of these factors was used in the following experiments.

It is intriguing to determine if applying nerve factors corresponding to the denervated limb stumps could rescue HDAC1 up-regulation and promote regeneration. These findings demonstrate that applying nerve-derived factors, such as BMP7, FGF2, and FGF8, soaked in beads could transiently increase HDAC1 expression and lead to partial regeneration improvement. However, there are potential reasons why complete

36

effects on HDAC1 up-regulation and regeneration induction were not observed in this experiment. First, additional nerve factors may be required in conjunction with BFF. Second, the natural spatiotemporal concentrations of these factors in the tissues may not have been accurately replicated by bead grafting.

The precise molecular mechanisms through which HDACs regulate tissue regeneration are not well comprehended. It is believed that HDACs modify the structure of chromatin and gene expression through epigenetic regulation. Moreover, HDACs can interact with other transcriptional regulators and become part of large transcriptional complexes (113, 114). Further research is necessary to gain a deeper understanding of these mechanisms and their significance in axolotl limb regeneration. Such knowledge has the potential to pave the way for exciting biomedical therapies that promote regenerative repair of intricate structures.

To summarize, the increased expression of HDACs in the WE and mesenchyme after amputation is facilitated by factors like BMP7, FGF2, and FGF8, which are mediated by nerves. HDACs might serve as intermediaries between these nerve factors and cell proliferation during the pre-blastema and blastema stages, initiating and coordinating blastema formation and limb regeneration (refer to Figure 2.9).

2.6 Tables and Figures

Figure 2.1. Stages of Axolotl Limb Regeneration on Dorsal and Ventral Sites. This figure illustrates the distinct stages of axolotl limb regeneration on both the dorsal and ventral sides. The stages depicted are as follows: amputation, early bud (EB), mid bud (MB), late bud (LB), early differentiation (ED), late differentiation (LD), and near complete regeneration (NCR).
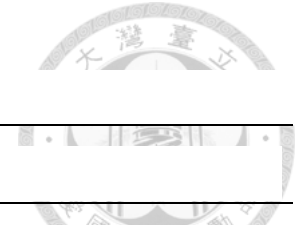
Table 2.1 Major Gross Observations Defining the Different Stages of Limb Regeneration

Stage	Description
Early bud (EB)	Begins with the outgrowth of the blastema, forming a symmetric cone.
Mid bud (MB)	Characterized by the presence of a symmetric cone.
Late bud (LB)	Begins with the flattening of the dorsally curved blastema cone.
Early differentiation (ED)	Begins with the appearance of the first digital primordium.
Late differentiation (LD)	Begins with the appearance of the fourth digital primordium.
Near complete regeneration (NCR)	Begins when the four digits are completely separated.

Table 2.2 Primers.

Gene	Forward	Reverse
HDAC1	CCTCGCCAACATTGAACCTCT	CTATGAAACCGCACCGGATTC
HDAC3	TGAGAGATGCCATTGCGTTTG	TGAAGGCCCGGATATGGTTT
HDAC4	GTTTCATGGCGAGCATCTCCT	AGTCCCAATGGATCTCCGCTT
HDAC6	TGAGGAGCTTCAGATGTGCCA	CCACTGCATTTTGCACTTTGC
S21 ribosomal RNA*	ACTTGAAGTTTGTTGCCAGGAC	TGGCATCTTCTATGATCCCATC

* serve as an internal control.
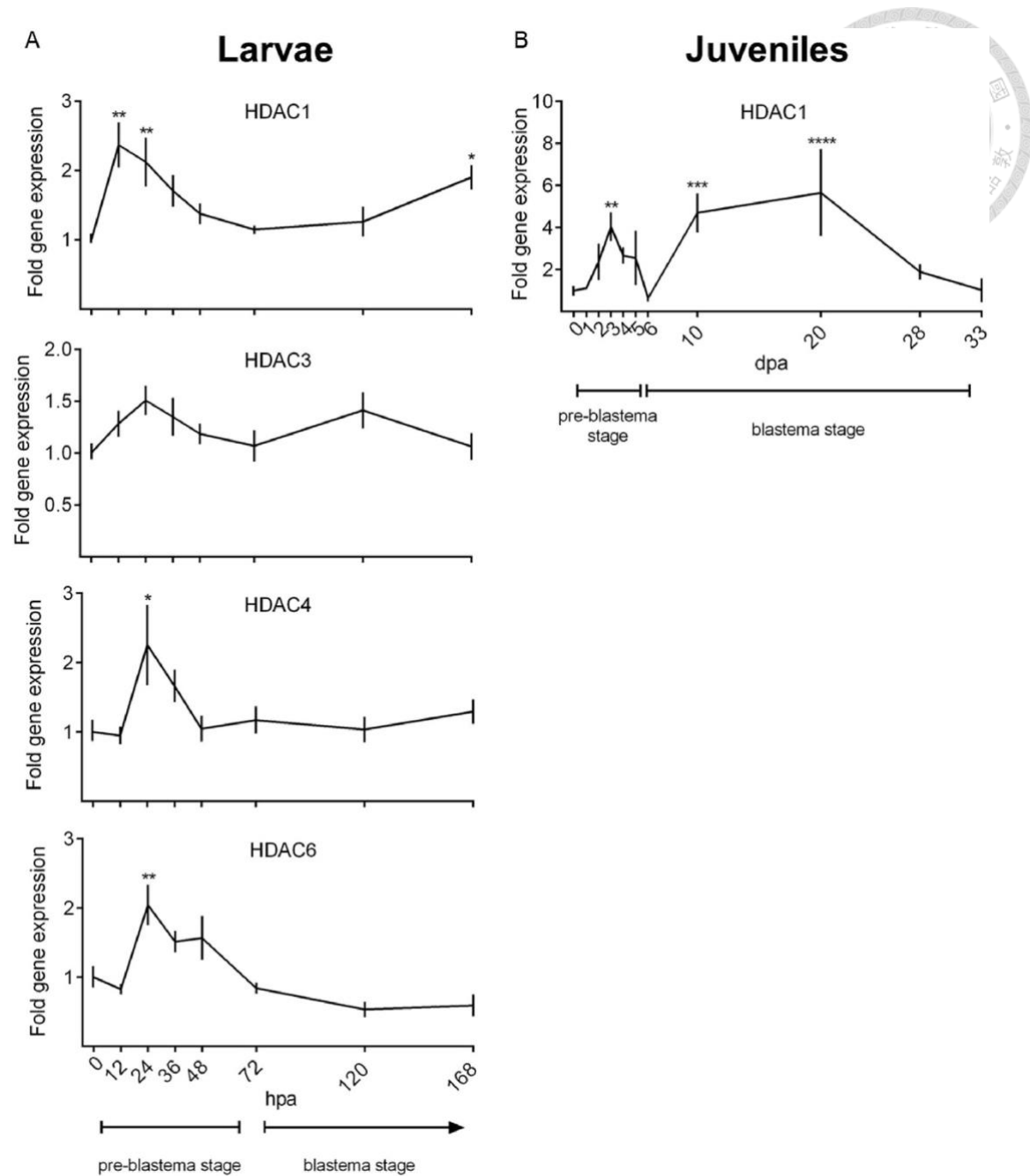
Figure 2.2 Bi-Phasic Up-Regulation of HDAC Expression during Axolotl Limb Regeneration. (A) The expression patterns of HDACs during axolotl limb regeneration are depicted in this figure. In larvae, HDAC1 expression in the stump ends and regenerating buds exhibits two significant peaks at 24 and 168 hpa. Additionally, HDAC4 and HDAC6 expression shows a notable increase only at 24 hpa. (B) In juveniles, a clear bi-phasic up-regulation of HDAC1 is observed during both the pre-

blastema and blastema stages. Statistical significance is denoted as follows: *p < 0.05,

**p < 0.01, ***p < 0.001, ****p < 0.0001.
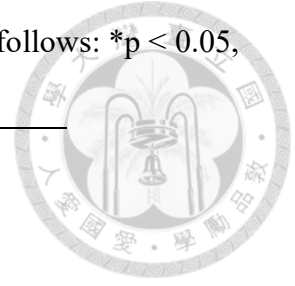
Figure 2.3 Dose-Dependent Effects of MS-275 on HDAC Activities and Limb Regeneration in Larval Axolotls. (A) Larval axolotls were incubated in Holtfreter's solution containing different concentrations of MS-275 (6.25, 12.5, or 25 μM) after amputation un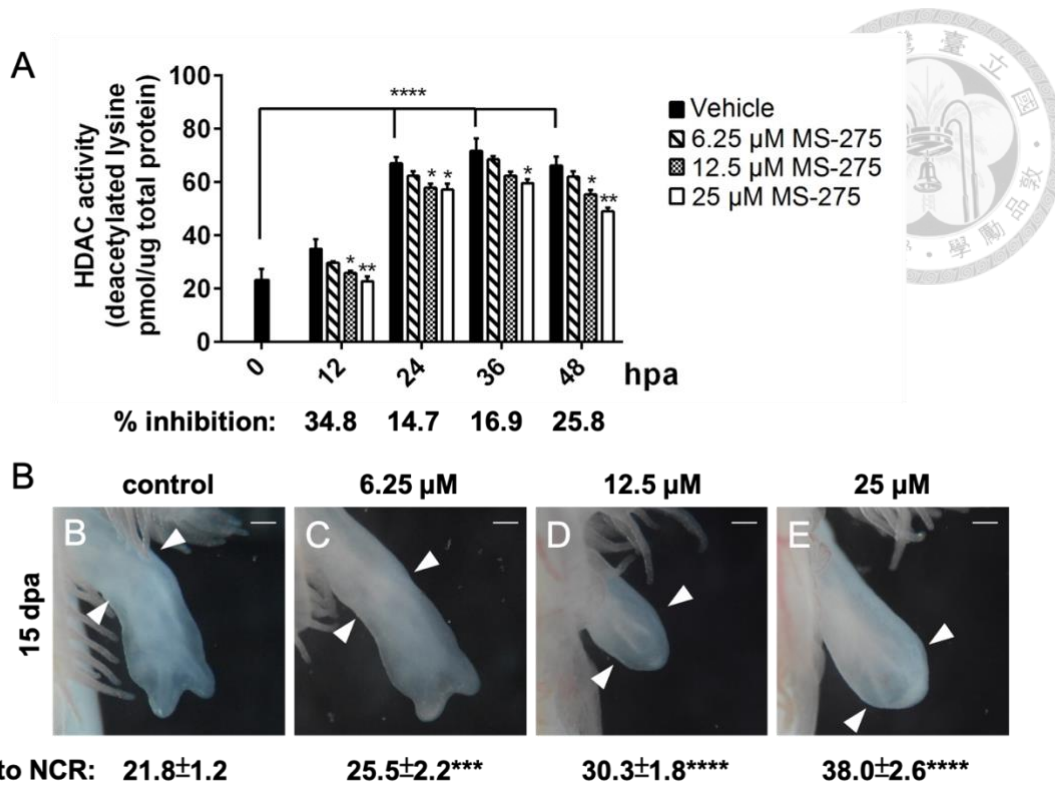til 48 hpa. HDAC activities in the stump ends were significantly and dose-dependently reduced at all time points. However, even at the highest concentration of 25 μM, the percentage of inhibition ranged from 14.7% to 34.8%. (B) Photos of regenerating limbs at 15 dpa under various concentrations of MS-275 (0, 6.25, 12.5, or 25 μM) demonstrate the dose-dependent inhibition of regeneration. The plane of amputation is indicated by white arrowheads. The duration to reach the NCR stage was also prolonged in a dose-dependent manner. The percentage of inhibition was calculated as: % inhibition = (activity in control - activity in 25 μM MS-275) / activity in control × 100%. Scale bars = 1 mm. Statistical significance is indicated as follows: $p < 0.05$, $p < 0.01$, $p < 0.001$, $p < 0.0001$.
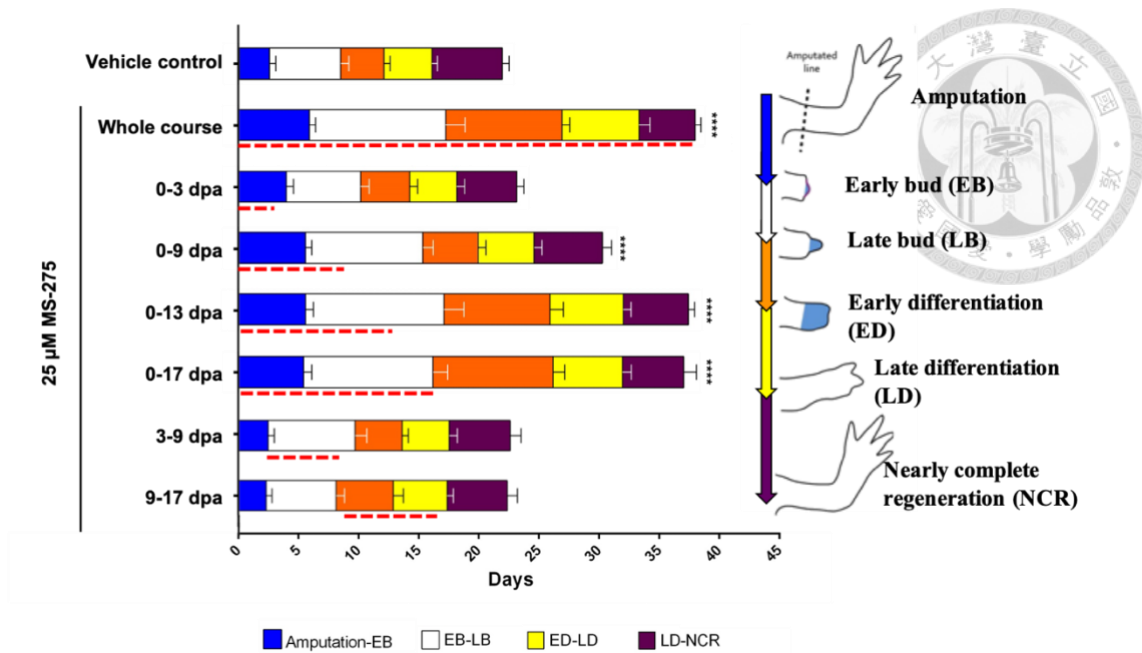
Figure 2.4 Effects of 25 μM MS-275 Treatment on the Progression of Limb Regeneration Stages in Larval Axolotls. The progression of limb regeneration stages in larvae axolotls treated with 25 μM MS-275 was observed. The red dashed line indicates the period of MS-275 treatment. When treated for the entire course (0-37 dpa), there was a significant delay in the progression of regeneration stages. The longer the treatment period, the greater the delay in progression, with the maximum delay observed when treatment was extended up to 13 dpa. The progression of the 0-13 dpa and 0-17 dpa groups was similar to that of the whole course group. Notably, the 3-9 dpa and 9-17 dpa groups showed similar progression to the vehicle control, indicating that treatment during the initial 3 days was critical for delaying the progression of regeneration. Statistical significance is indicated as ****$p < 0.0001$.
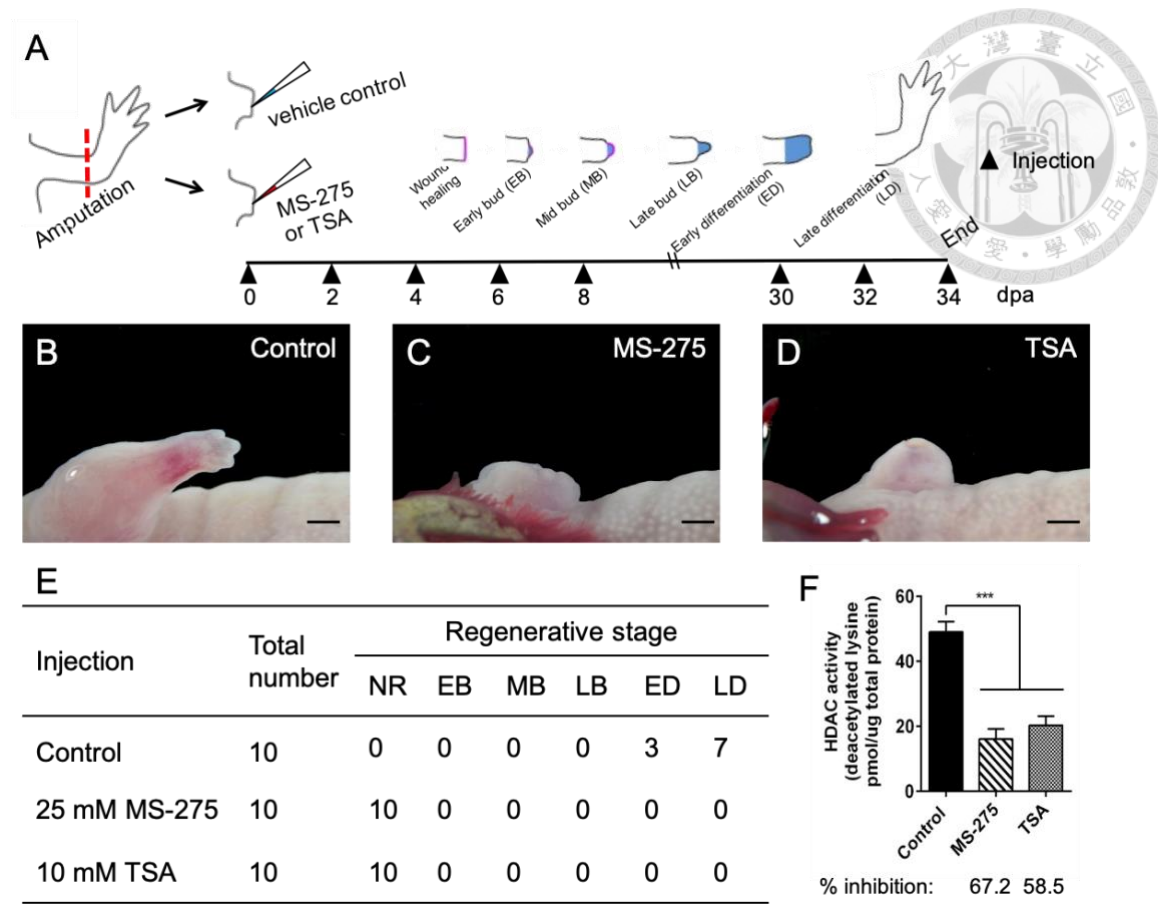
Figure 2.5 Inhibition of Regeneration Induced by MS-275 and TSA in Juvenile Axolotls is Associated with Reduced HDAC Activities. (A) Experimental protocol involved the injection of MS-275 or TSA into the stump every other day from amputation until 34 dpa, with three groups: 2% DMSO (control), 25 mM MS-275, and 10 mM TSA. Representative photos at 34 dpa showed limb regeneration reaching the LD stage in the control group (B), while no regeneration was observed in the MS-275 (C) and TSA (D) groups. (E) Summary table of the outcomes in the three groups at 34 dpa. (F) HDAC activities were significantly reduced after MS-275 or TSA treatment in the stump ends. Percentage of inhibition calculated as: % inhibition = (activity in control - activity in treatment) / activity in control × 100%. Scale bars = 1 mm. Statistical significance indicated as ***$p < 0.001$.
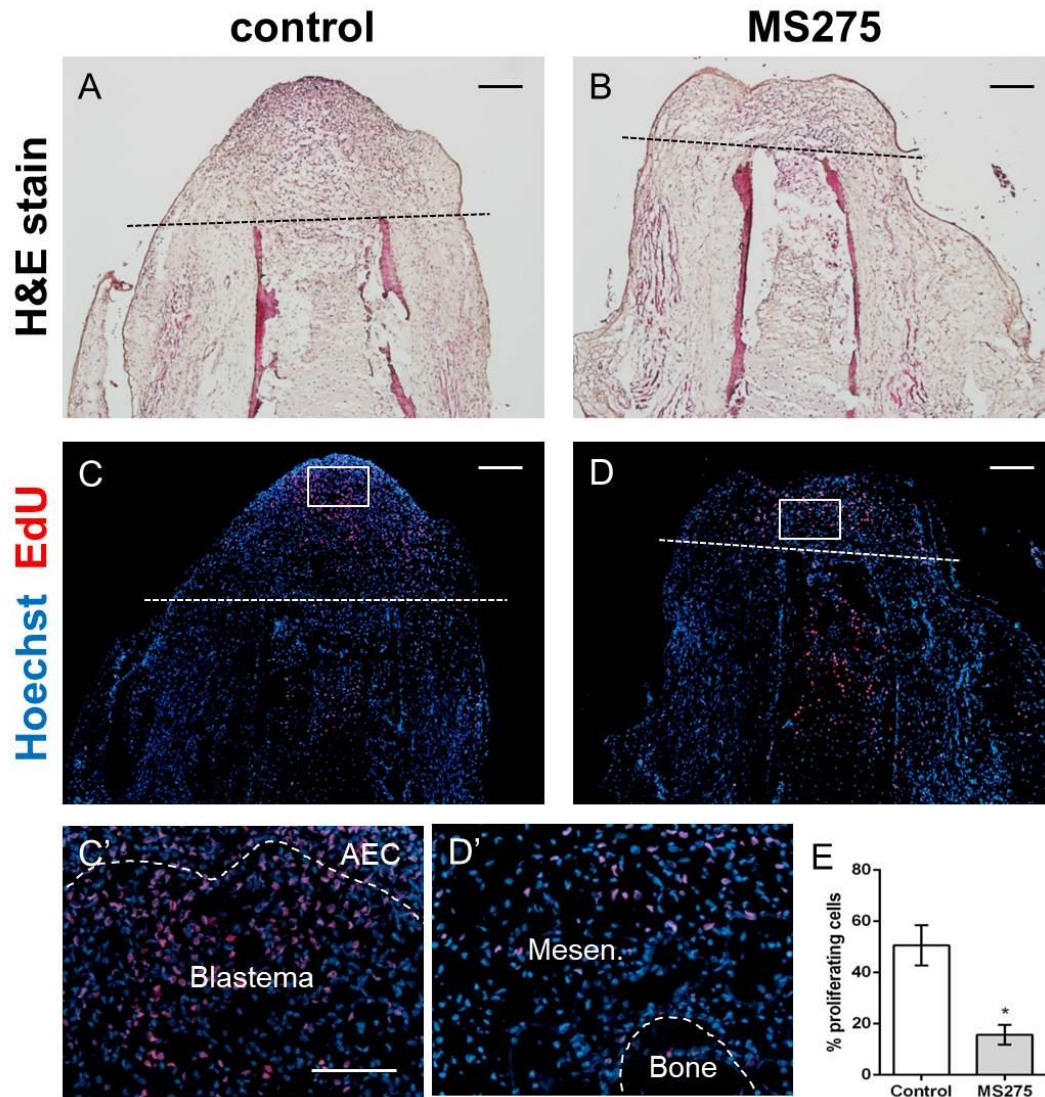
Figure 2.6 Inhibition of Limb Regeneration by MS-275 through Decreased Cell Proliferation in Juvenile Axolotls. (A-B) Hematoxylin and Eosin (H&E) staining of control and MS-275-treated specimens at 13 dpa revealed the inhibition of blastema formation in the MS-275-treated group. The black dashed lines indicate the plane of amputation. (C-D) EdU incorporation (red) and Hoechst counterstaining (blue) demonstrated the blocking of cell proliferation by MS-275. The dotted lines in (C' and D') indicate the boundary between the basal keratinocytes of the AEC and the blastema cells or the bone, respectively. Mesen. refers to the mesenchyme. (E) The percentage of proliferating cells in the mesenchyme was significantly reduced in the MS-275-treated

group (n = 3) compared to the control group (n = 3). Scale bars = 500 μm (A, B, C, D) and 100 μm (C', D'). Statistical significance indicated as $*p < 0.05$.
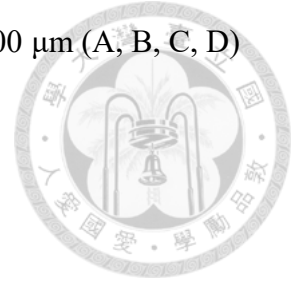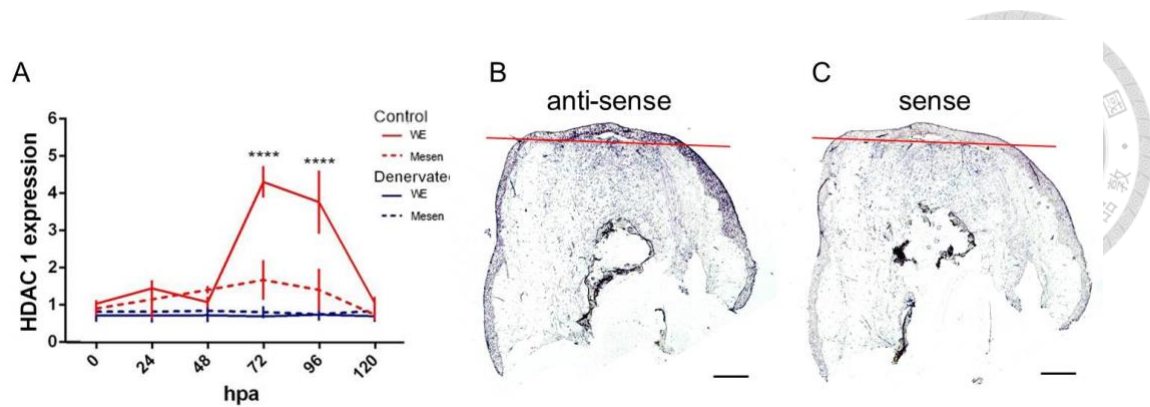
Figure 2.7 Nerve-Mediated HDAC1 Expression Preferentially in the WE of Juvenile Axolotls. (A) Q-PCR analysis revealed the expression level of HDAC1 in the WE and mesenchyme of control (innervated) juvenile axolotls. In the control group, HDAC1 expression was significantly elevated in the WE between 3 and 4 dpa, while no significant increase was observed in the mesenchyme. Denervation prior to amputation abolished the upregulation of HDAC1 expression in both the WE and mesenchyme. (B) ISH was performed to visualize the expression pattern of HDAC1. The results showed that HDAC1 was expressed in a majority of the WE and neighboring skin at 3 dpa. The red lines indicate the amputation line. (C) A sense probe control was used, which displayed a faint signal compared to the antisense probe. However, the signal was much weaker, confirming the specificity of HDAC1 expression. Scale bars = 500 μm (B, C). Statistical significance indicated as ****$p < 0.0001$.
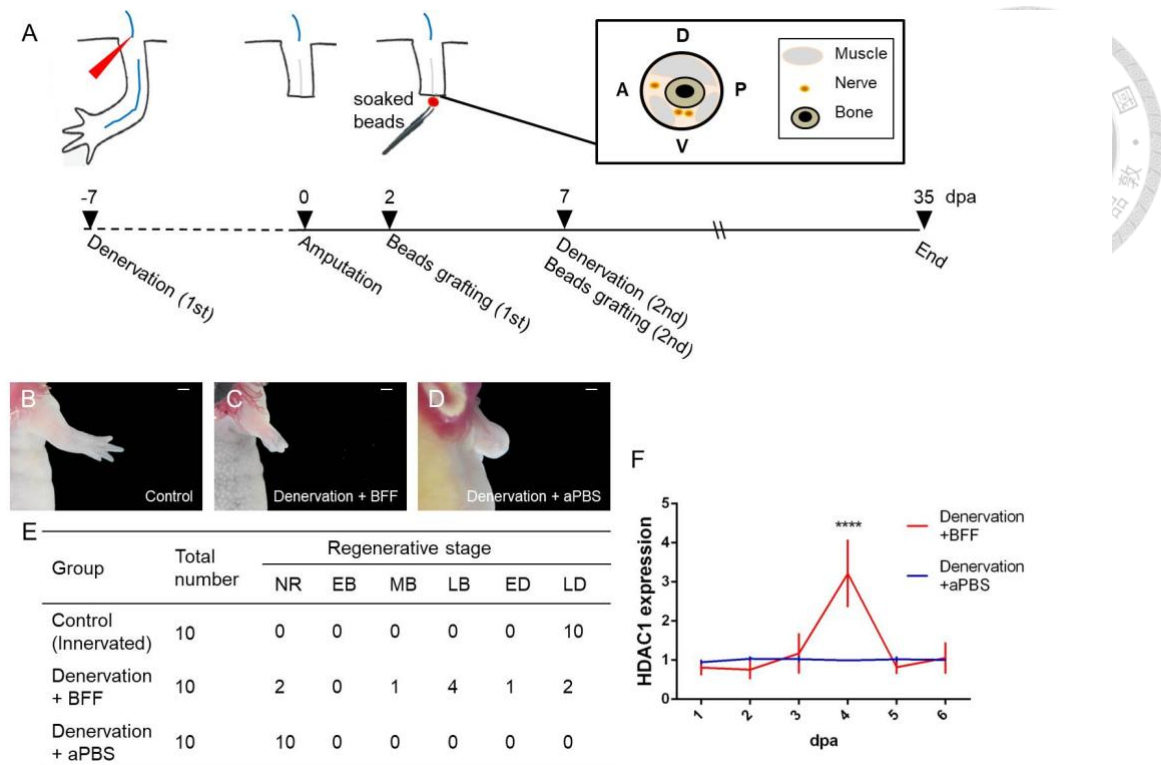
Figure 2.8 Nerve Factors Regulate HDAC1 Expression during Limb Regeneration in Juvenile Axolotls. (A) Experimental protocol involving amputation performed 7 days following the first denervation. Beads soaked in aPBS containing BMP7, FGF2, and FGF8 (BFF) or aPBS alone were grafted under the WE at 2 dpa. Second denervation was performed at 7 dpa to prevent nerve reconnection, followed by the second bead grafting. Regeneration progress was monitored until 35 dpa. The inset shows the orientation of the axolotl limb with A = anterior, P = posterior, D = dorsal, and V = ventral. (B-D) Representative photos at 35 dpa illustrate the limb regeneration stages: control group (B) reaching the late differentiation stage, denervation + BFF group (C) regenerating into the early regeneration stage, and denervation + aPBS group (D) showing no regeneration. (E) Summary table presenting the outcomes of the three experimental groups at 35 dpa. (F) Q-PCR analysis of HDAC1 expression in the WE indicates a transient increase at 4 dpa in the Denervation + BFF group (2 days after BFF bead grafting), while no significant increase is observed in the Denervation + aPBS group. These results suggest that HDAC1 expression during axolotl limb regeneration

49

is dependent on nerve factors, specifically BMP7, FGF2, and FGF8. Scale bars = 1 mm

(B, C, D). Statistical significance indicated as ****$p < 0.0001$.
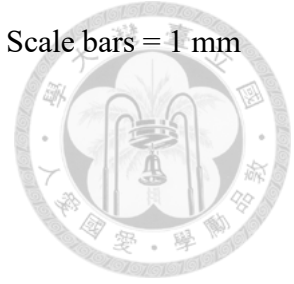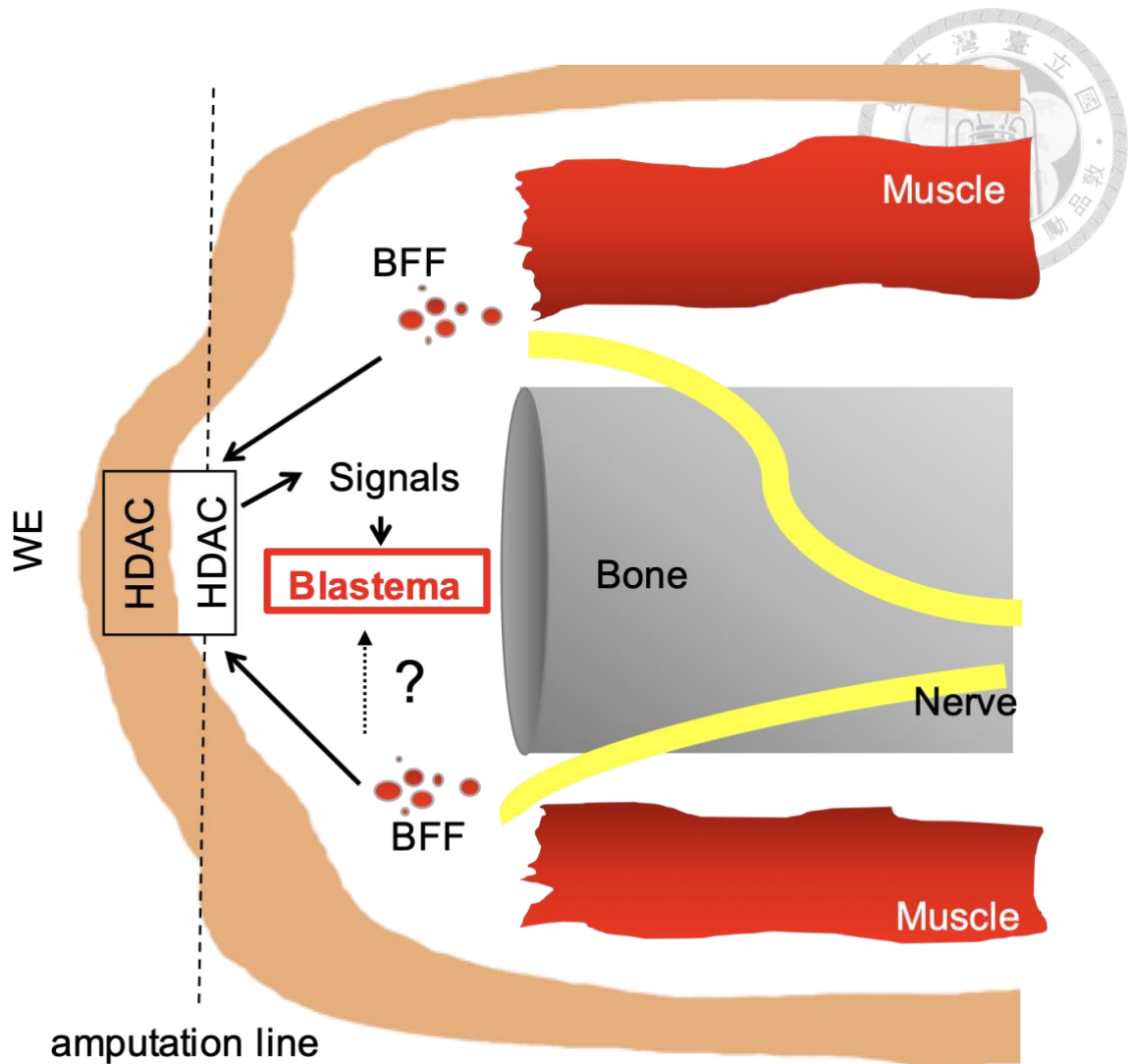
Figure 2.9 The Schematic Diagrams Depict the Key Findings of the Study. After amputation, nerve-derived factors including BFF are released from the nerve ends, leading to the up-regulation of HDACs, particularly HDAC1, in the WE and to a lesser extent in the underlying mesenchyme. HDACs are believed to play a crucial role in promoting cell proliferation and activating signaling pathways that facilitate limb regeneration. Overall, the study highlights the dependence of axolotl limb regeneration on HDAC activity and demonstrates that the up-regulation of HDACs following amputation is influenced by nerve-derived factors.

Chapter 3:

The Importance of Timing: Nerve-Mediated HDAC1 Regulates the Sequential Expression of Morphogenic Genes in Axolotl Limb Regeneration

3.1 Summary
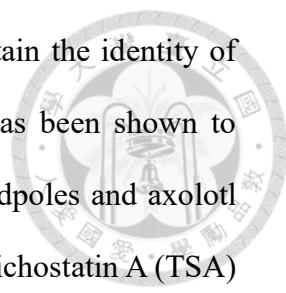
The process of axolotl limb regeneration is a highly organized and complex process that relies on precise gene expression and epigenetic modifications at specific positions and time intervals. Previously, we observed two distinct phases of HDAC1 expression, a repressive epigenetic regulator mediated by nerves, during the wound healing (3 dpa) and blastema formation (8 dpa onwards) stages in young axolotls. The inhibition of HDAC1 through local administration of an HDAC inhibitor called MS-275 significantly impeded limb regeneration. To investigate the transcriptional response of axolotl limb regeneration after MS-275 treatment in a tissue-specific and time-dependent manner, I conducted transcriptome sequencing of the epidermis and soft tissue (ST) at 0, 3, and 8 dpa with and without MS-275 treatment. Gene Ontology (GO) enrichment analysis of each group of co-regulated genes revealed a complex range of functional pathways in both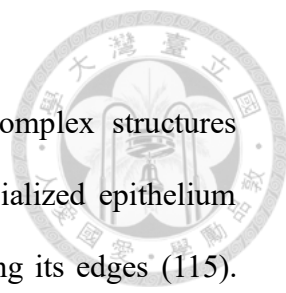 the epidermis and ST. Specifically, HDAC activity was necessary to prevent the premature activation of genes involved in tissue development, differentiation, and morphogenesis. Independent validation using Q-PCR in separate specimens demonstrated that when HDAC1 activity was inhibited, the expression of five out of six genes crucial for development and regeneration, which should only be upregulated during the blastema stage, was prematurely elevated during the wound healing stage. Genes associated with the WNT pathway were also prematurely activated under HDAC1 inhibition. Applying a WNT inhibitor to MS-275-treated amputated limbs partially mitigated the effects of HDAC1 inhibition, leading to defects in blastema formation. Based on these findings, I propose that post-amputation HDAC1 expression is partially responsible for regulating the timing of expression of morphogenic genes, ensuring appropriate limb regeneration.

3.2 Introduction

Axolotls possess an exceptional capability to regenerate complex structures composed of multiple tissues. Following limb amputation, a specialized epithelium derived from keratinocytes rapidly covers the exposed wound along its edges (115). Instead of migrating across the wound surface, this sheet of epithelial tissue is propelled forward through the absorption of water and expansion of peripheral cells (116). Underneath the wound epidermis, progenitor cells gather, leading to the formation of a distinct structure called the blastema. The blastema consists of both lineage-restricted and multipotent progenitors that regenerate the internal components of the newly formed limb (31, 80, 117, 118). The interaction between the epidermis and the underlying ST is critical for promoting blastema cell proliferation (72), tissue degradation in the stump (119), and guiding blastema outgrowth (120). Changes in cellular behavior during regeneration coincide with alterations in gene transcription (121). Precise expression patterns of various genes involved in morphogenesis, specific to cell lineage and regeneration stage, are crucial for successful limb regrowth (87, 122-127). These findings underscore the highly coordinated and sequential nature of axolotl regeneration, necessitating precise control of gene expression.

During the process of injury, there are numerous changes that involve the regulation of epigenetic mechanisms, which are responsible for modifying the structure of chromatin and the properties of proteins involved in transcriptional regulation and cell signaling (128). One such mechanism is the deacetylation of histone proteins by HDACs, which leads to the compaction of chromatin structure and plays a significant role in the regeneration of amphibians. HDACs have also been associated with promoting growth and proliferation (98). However, the study of epigenetic mechanisms during axolotl regeneration has been limited by the scarcity of detailed genomic data until recently (129). A study on *Xenopus* limb bud regeneration highlighted the

importance of histone modifications in regulating genes that maintain the identity of limb cells (130). Pharmacological inhibition of HDAC activity has been shown to reduce HDAC activity and impede tail regeneration in *Xenopus* tadpoles and axolotl larvae (102). In another study, the use of valproic acid (VPA) and trichostatin A (TSA) to inhibit *Xenopus* tadpole tail regeneration resulted in abnormal expression of notch1 and bmp2, two genes crucial for *Xenopus* tail regeneration (66). This supports the notion that HDAC activity is required for proper gene expression during regeneration. In my previous study, I discovered biphasic expression patterns of nerve-mediated HDACs during the wound healing and blastema formation stages of axolotl limb regeneration (131). Moreover, the use of two HDAC inhibitors, namely MS-275 and TSA, resulted in a substantial decrease in cell proliferation and a distinct lack of limb regeneration. These findings indicate the essential role of HDACs in the successful regrowth of limbs following amputation.

To gain a better understanding of the mechanisms underlying the roles of HDACs in the regeneration of amphibian appendages, I employed our axolotl limb regeneration model to investigate the changes in the transcriptome during the wound healing and blastema formation stages when HDAC activity was suppressed using MS-275. I conducted a clustering analysis of genes with similar expression patterns during the early stages of limb regeneration in both the epidermis and soft tissue, comparing samples treated with and without MS-275. By employing gene set enrichment analysis (GSEA), I found that the upregulation of HDAC expression following amputation is necessary for the appropriate timing of gene expression. Interestingly, I observed premature enrichment of genes involved in tissue development, differentiation, and morphogenesis during the wound healing stage when exposed to MS-275. To further confirm the requirement of HDAC1 activity in preventing the premature activation of

gene expression specific to the regeneration stage, I performed Q-PCR and functional

analysis of candidate genes and pathways using independent animals.
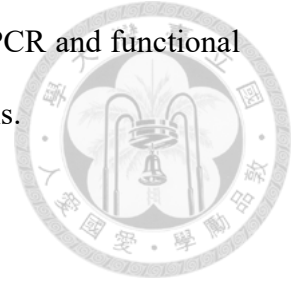
3.3 Materials and Methods

3.3.1 Animal Handling

To conduct the experiments involving axolotls, I raised them until they reached the juvenile stage, typically measuring between 12 and 16 cm in length from snout to tail tip. The axolotls were housed in a modified Holtfreter's solution consisting of 118.4 mM NaCl, 1.3 mM KCl, 1.8 mM CaCl$_2$, 1.6 mM MgSO$_4$.7H$_2$O. Before any experimental procedures, the axolotls were anesthetized using a 0.1% solution of MS-222 (Sigma-Aldrich, St. Louis, MO, United States). For limb amputation, we surgically removed the middle upper forelimbs on both the right and left sides. Tissue samples were collected at 0, 3, and 8 dpa as depicted in Figure 3.1A. To inhibit HDAC activity in the amputated limbs of juvenile axolotls, I followed the previously described method (131). Specifically, I injected 2 μl of a 25 mM solution of MS-275 (Selleckchem, Houston, TX, United States) into the stumps just below the wound epidermis every other day after amputation. All animal care and experimental procedures were approved by the Institutional Animal Care and Use Committee of the National Taiwan University College of Medicine and were conducted in accordance with the approved guidelines.

3.3.2 cDNA Library Preparation and Illumina Sequencing

To obtain total RNA from axolotl tissues, I followed the manufacturer's instructions and utilized TRIzol reagent (Invitrogen, CA, United States). The extracted RNA samples were then purified using the RNeasy Mini Kit (Qiagen, Hilden, Germany) and quantified using the Qubit 4 fluorometer (Invitrogen, CA, United States) and Qsep100 capillary gel electrophoresis (BiOptic, New Taipei City, Taiwan). All samples had an RNA quality number (RQN) exceeding 9.0, ensuring high RNA quality. To minimize variability between individuals, I pooled tissues from both the right and left limbs of two animals at each time point to create a single replicate. This resulted in two

replicates for each condition at each time point after amputation, involving 4 animals (8 forelimbs) in total. Thus, there were two biological replicates for each of the five conditions (3 dpa and 8 dpa with and without MS-275 treatment, along with the homeostatic control at 0 dpa), comprising tissues from 40 limbs of 20 axolotls. From these pooled tissue samples, ten RNA samples from both the ST and epidermis were selected for subsequent construction of cDNA libraries and Illumina deep sequencing.

For library preparation, the TruSeq Stranded mRNA Preparation Kit (Illumina, CA, United States) according to the provided instructions was employed. In brief, 10 µg of total RNA from each sample underwent poly-A selection using oligo(dT) magnetic beads, followed by fragmentation of the resulting mRNA molecules. First-strand cDNA synthesis was then carried out through reverse transcription using random primers. Subsequently, DNA polymerase I and RNase H (Invitrogen) were used for the synthesis of second-strand cDNA. The cDNA fragments obtained were ligated with paired-end (PE) oligoadapters (Illumina) using T4 ligase. The resulting cDNA fragments were purified and enriched via PCR. Finally, the cDNA libraries were subjected to sequencing using the Illumina HiSeq2000 platform, which generated paired-end (PE) raw reads of approximately 150 bp in length.

3.3.3 Transcriptome Re-annotation

To re-annotate the axolotl transcriptome, I obtained the transcriptome data from the website https://axolotl-omics.org and employed two annotation methods. Firstly, I conducted a BLAST search (132) of the nucleotide sequences against the UniProt database using the BLASTx algorithm, with an e-value threshold of 1e-5. Secondly, I extracted amino acid sequences based on predicted open reading frames (ORFs) using TransDecoder and performed a BLAST search of these sequences against the UniProt database using the BLASTp algorithm, also with an e-value threshold of 1e-5. To

establish associations with human gene symbols, I utilized the R package biomaRt (133) to map protein names from various organisms to human gene symbols.
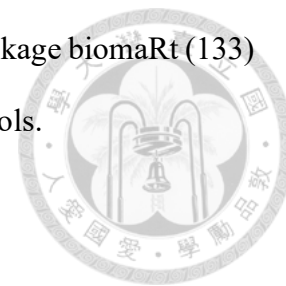
3.3.4 Processing and Analysis of RNA-seq Data

The raw FASTQ files obtained from RNA-seq underwent quality assessments using FastQC (v0.11.7) and were subjected to trimming using cutadapt (v2.10). The resulting high-quality reads were aligned to the axolotl transcriptome using bowtie2 (v2.3.4) (134). Expression levels for each transcript were quantified using RSEM (135) and reported as log2TPM (transcripts per million) for subsequent analyses. To ensure normalization across all samples, I employed the trimmed mean of M-values (TMM) method implemented in the edgeR package (136). Differential expression analysis was conducted using the limma package (137). First, linear models were constructed based on gene expression profiles and the experimental conditions (time point and MS-275 treatment) using the lmFit function. Next, the contrasts.fit function was used to calculate estimated coefficients and standard errors for specific experimental comparisons. Finally, an empirical Bayes framework implemented in the eBayes function was employed to compute statistics for differential expression of all genes. To identify temporal clusters, I applied the fuzzy c-means algorithm generated with the Mfuzz package (138). For each tissue, genes with a p-value less than 0.05 in at least one of the comparisons (3 dpa vs. 0 dpa, 8 dpa vs. 0 dpa, dpa8 vs. dpa 3, 3 dpa with MS-275 vs. 0 dpa, 8 dpa with MS-275 vs. 0 dpa, and 8 dpa with MS-275 vs. 3 dpa with MS-275) were included in the clustering analysis. Time-series profiles with and without MS-275 treatment ([0 dap, 3 dpa, and 8dpa] and [0 dpa, 3 dpa with MS-275, and 8 dpa with MS-275]) were merged into a single matrix for the clustering analysis. To determine the optimal number of clusters, I performed repeated soft clustering with

cluster numbers ranging from 4 to 27 and calculated the minimum centroid distance between two cluster centers produced by c-means clustering (139).

3.3.5 Function Analysis

The gene sets of GO biological processes were obtained from MSigDB (v7.0), and genes that were not present in the axolotl transcriptome were excluded from the analysis. Overrepresentation analysis (ORA) and GSEA were conducted using functions implemented in the clusterProfiler package (140). For GSEA, genes were ranked based on log-transformed p-values derived from the limma test, with signs set to positive/negative for fold changes greater than 1 or less than 1, respectively. An enrichment map was constructed using custom R scripts in the R statistical environment version 3.5.2 and visualized using Cytoscape.

3.3.6 Cell Abundance Estimation

Transcriptomic markers of different cell types were defined based on previous studies (141, 142). The potential abundance of each specific cell type was estimated by calculating the arithmetic mean of normalized read counts from all signature genes.

3.3.7 RT-Q-PCR for Validation

RNA was extracted using TRIzol Reagent (Invitrogen) from epidermis and ST samples collected at 0, 3, and 8 dpa for Q-PCR analysis. At 0 dpa, the proximal 2 mm of the amputated parts were harvested immediately after amputation. The epidermis and underlying soft tissue were collected separately. Total RNA from the collected tissues was extracted using TRIzol reagent (Invitrogen). Reverse transcription was performed at 50°C using Superscript III reverse transcriptase (Invitrogen). The first-strand cDNAs were diluted 10 times and used as templates for Q-PCR. Reactions were carried out in

a total volume of 10 µl using the SYBR Green kit (Stratagene, La Jolla, CA, United States) with 0.8 µM of each primer according to the manufacturer's instructions. The gene-specific primers' sequences were determined based on our next-generation transcriptome sequencing data (Table 3.1). Q-PCR was performed and analyzed using the ABI StepOne Real-Time PCR System with StepOne software version 2.1 (Applied Biosystems, Foster City, CA, United States).

3.3.8 Local Injection of MS-275 and a Wnt inhibitor

Among the biological/signaling pathways affected by the increased HDAC1 activity after amputation, the Wnt signaling pathway was found to be prematurely activated during the healing stage when amputated limbs were treated with MS-275. To investigate whether the alteration in Wnt signaling-associated gene expression from 8 to 3 dpa contributed to blastema formation defects upon HDAC1 inhibition, rescue experiments with Wnt inhibitors were performed. Two microliters of 1 µM Wnt inhibitor (Calbiochem, Billerica, MA, United States) were co-injected with MS-275, while 25 mM MS-275 only or vehicle only was administered. The timing of the inhibitor injection into the amputated limbs of juvenile axolotls followed the protocol as described (131)(Figure 3.1 and 3.3).

3.4 Results

### 3.4.1 Transcriptome Profiling of the Epidermis and ST During Early Limb Regeneration with HDAC1 Inhibition

Following my previous study, I observed two distinct waves of HDAC1 expression after amputation, corresponding to the wound healing stage and the period of blastema formation. Inhibiting HDAC activity using the HDAC inhibitor MS-275 or TSA disrupted blastema formation and hindered subsequent limb regeneration (131). To delve deeper into the transcriptional changes underlying the inhibitory mechanism of MS-275 on regeneration, I performed comprehensive RNA sequencing during the early stages of axolotl limb regeneration using the Illumina sequencing platform. I profiled gene expression in two types of tissues, the epidermis and the underlying ST, treated with either DMSO (as a control) or MS-275 at three different time points: 0 dpa as the homeostatic control, 3 dpa representing the wound healing stage, and 8 dpa corresponding to the blastema formation stage of regeneration (Figure 3.1A). Tissue samples from four limbs of two animals were pooled as one biological replicate for each time point and treatment condition. Overall, a total of 40 limbs from 20 animals were utilized for the transcriptome analysis.

Due to the incomplete axolotl genome, I aligned the sequencing reads to the axolotl transcriptome (Figure 3.4A)(129). On average, approximately 78% of the sequencing reads from each sample were successfully mapped to known axolotl transcripts (Table 3.2). To gain additional functional information for each gene, I reannotated the axolotl transcripts by conducting a basic local alignment search tool (BLAST) search against the UniProt database (Figure 3.4A). In total, 127,858 expressed transcripts in the epidermis and 128,513 expressed transcripts in the ST were identified. Hierarchical clustering and principal component analysis (PCA) of the gene expression profiles across all samples revealed that the expression patterns primarily

depended on the regeneration status and the treatment with MS-275 (Figures 3.1B, C, and Figure 3.3B). These findings indicate that HDAC1 inhibitor treatment can be distinguished based on the gene expression profiles during limb regeneration.
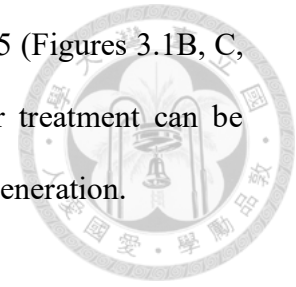
3.4.2 The Requirement of HDAC Activity for Proper Timing of Gene Expression in ST during Limb Regeneration

In order to identify the biological pathways crucial for key stages of limb regeneration and those affected by HDAC inhibition, I conducted GSEA by grouping genes from each GO term. The comparisons included the wound healing stage (3 dpa) with or without MS-275 treatment, as well as the blastema formation stage (8 dpa) with or without MS-275 treatment, against the homeostatic control (0 dpa). I found that a total of 1,133 GO terms were significantly enriched (FDR < 0.05) in at least one of the comparisons for each regeneration stage and treatment relative to homeostasis. Heatmaps were generated to depict the activity of pathways and biological processes at different regeneration stages (Figure 3.5A).

The analysis revealed that genes associated with transcriptional regulation and cytoskeletal organization displayed increased expression at both 3 and 8 dpa compared to 0 dpa, but this response was absent under HDAC1 inhibition (Figure 3.5A). These findings suggest that HDAC1 inhibition disrupted the active responses to amputation and signaling regulation during the early stages of normal regeneration. Conversely, the expression of genes related to lymphocyte migration was abnormally upregulated by HDAC1 inhibition (Figure 3.5A). Notably, biological functions such as developmental growth and tissue morphogenesis, which were typically observed only at 8 dpa vs. 0 dpa in normal regeneration, occurred earlier at 3 dpa with MS-275 treatment vs. 0 dpa in the ST (Figure 3.5A). Thus, it appears that inhibiting HDAC activity during limb regeneration may lead to the occurrence of the correct processes at the wrong time.

63

Moreover, numerous pathways associated with regeneration, including developmental cell growth, mesenchymal cell differentiation, embryonic morphogenesis, and neuron differentiation, were enriched at both 8 dpa and 8 dpa with MS-275 treatment compared to 0 dpa, but were observed earlier at 3 dpa with MS-275 treatment compared to 0 dpa (Figures 3.5A and B). In summary, the surge in HDAC activity following amputation is essential for maintaining the proper timing of gene expression involved in tissue development, differentiation, and morphogenesis in the ST.

3.4.3 Cluster Transition in the ST in Response to HDAC1 Inhibition

To provide further evidence that significant changes initially observed at 8 dpa occurred earlier at 3 dpa with MS-275 treatment, genes were categorized into clusters based on their expression patterns from 0 to 3-8 dpa. I conducted differential expression analysis at different time points, focusing on genes that displayed significant differential expression (p-value < 0.05) in at least one of the pairwise comparisons between time points (0 vs. 3 dpa, 0 vs. 8 dpa, and 3 vs. 8 dpa) with either DMSO or MS-275 treatment (Table 3.3). A total of 37,798 genes were subjected to unsupervised clustering analysis using Mfuzz, resulting in their assignment to eight groups based on temporal expression patterns (Figures 3.6A and B).

I summarized the proportions (Figure 3.6C), exact numbers of genes (Table 3.4), and gene identities with stage-dependent expression patterns in the ST that transitioned between defined clusters after MS-275 treatment. My focus was on the transitions from cluster 4 to 5 (C4 > 5) and cluster 4 to 6 (C4 > 6) since they represented the premature activation of pathways related to development and morphogenesis. The transition of genes from C4 > 5 was associated with various developmental processes, including organ and system development, neuron development, bone growth, and response to growth factors (Figures 3.6D and E). Similarly, the transition of genes from C4 > 6 was

linked to connective tissue development, embryo development, response to growth factors, neuron development, and cytoskeleton organization (Figures 3.6F and G). Additionally, the transition of genes from C4 > 7 was also related to development, specifically neurogenesis and ECM structure organization (Figure 3.6H).

Highlighted in Figures 3.6E and G are genes that exhibited cluster transitions from C4 > 5 and C4 > 6, respectively. Many of these genes have been identified as critical during the early stages of appendage regeneration. Typically, their expression is significantly upregulated at the blastema formation stage at 8 dpa in normal regeneration (117, 123, 143). However, under HDAC1 inhibition, these genes are expressed prematurely, specifically during the wound healing stage (mmp13, fgfr1, twist1, sox9, tg fb2, pdg frb, msx2, fn1, sall4, and tg fb3). To validate the diverse gene expression patterns, I performed Q-PCR on independent animals, which confirmed similar premature elevation patterns for five out of the six tested genes, consistent with the sequencing analysis (Figure 3.7). Overall, these results indicate that HDAC1 plays a crucial role in preventing the premature activation of developmental genes post-amputation, ensuring precise timing for successful blastema formation, a critical step in limb regeneration.
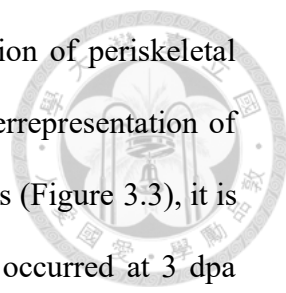
3.4.4 Inhibiting HDAC1 Activity Alters the Expression Pattern of Cell Type-Associated Signature Genes

Limb regeneration relies on the coordinated contribution of various cell types derived from the epidermis, endothelium, nerves, muscle, and connective tissue (CT) (144). The composition and ratios of these cell types are crucial for successful limb regeneration. Differences in the cellular composition of the ST may be a possible explanation for the failure of blastema formation when HDAC activity is blocked post-amputation. Since a cell tracking system was lacked, I employed a transcriptome-based

approach to estimate the cell composition based on the expression levels of cell type-enriched genes defined in a previous study (142).

I focused on examining the CT cell composition in the ST during regeneration, as CT cells are the most abundant contributors to the blastema (31, 50, 117, 145). Figure 3.8A illustrates that CT cells could be divided into two groups based on their differential abundance across regeneration time points. The first group included fCT I, II, III, and IV cells, which decreased in number at 3 dpa, while the second group consisted of cycling cells, fCT V cells, periskeletal cells, and tendon cells, which increased in number at 8 dpa. Interestingly, except for genes representing cycling cells, which showed delayed activation, the expression of genes representing various fCT cells, periskeletal cells, and tendon cells was abnormally upregulated or failed to be downregulated during the wound healing stage under MS-275 treatment (Figure 3.8B). These abnormal changes in cell composition may contribute to impaired limb regeneration. Additionally, the delayed expression of genes representing cycling cells suggests limited progress in regeneration.

Based on the cell composition analysis results, the pattern transitions of fCT I, fCT II, fCT III, and fCT IV cells were similar to clusters 2 and 8 (Figure 3.8C), while the transitions of fCT V cells, periskeletal cells, and tendon cells were similar to clusters 4 and 6 (Figure 3.6F). I focused on the transition from cluster 2 to 8 (C2 > 8). Genes enriched in this transition were involved in tissue remodeling processes, such as cellular component morphogenesis, cell junction organization, extracellular matrix (ECM) organization, and tissue migration. This indicates that tissue repair and positive matrix remodeling should have declined during the early stages of axolotl limb regeneration, but MS-275 treatment somehow caused a delay in these processes (Figure 3.8C). While it cannot be completely ruled out that the sampling of MS-275-treated regeneration-defective tissues slightly overrepresented homeostatic tissues, leading to higher
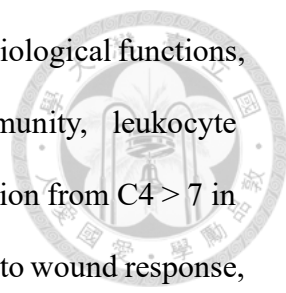
, 66

transcript quantities of CT-associated genes, the premature activation of periskeletal and tendon-associated genes cannot be explained solely by the overrepresentation of homeostatic tissues. Moreover, based on morphological observations (Figure 3.3), it is less likely that overrepresentation of homeostatic tissue sampling occurred at 3 dpa compared to 8 dpa. These observations further support the main conclusion that blastema stage-expressing genes are prematurely elevated during the wound healing stage when the repressive histone modifier HDACs are inhibited.

3.4.5 The Expression Timing of Genes in the Epidermis Requires HDAC Activity after Amputation

The formation of the epidermis is crucial for initiating blastema formation, as it involves the rapid closure of open wounds by migrating epidermal cells from the basal layer (51). While there was no significant delay in wound healing between the control and MS-275 treatment in our limb regeneration model (131), it is still possible that the ability of the epidermal layers to cover the wound edge may be affected. To investigate whether the composition of the epidermis is influenced by MS-275, I performed cell composition analysis based on gene expression profiles of the epidermis using marker genes identified in a previous single-cell study (129) Figure 3.9A). The analysis revealed that the expression of genes associated with epidermal Langerhans cells, intermediate epidermis, and small secretory cells was affected by HDAC1 inhibition, indicating a potential alteration in the priority of cell migration (Figure 3.9B).

To identify genes associated with potential changes in cell position, I conducted clustering analysis of 39,581 differentially expressed genes across pairwise time points and categorized them into eight groups (Figures 3.10A and B). Interestingly, the transition from cluster 4 to 7 (C4 > 7) coincided with the expression patterns observed in epidermal Langerhans cells, intermediate epidermis, and small secretory cells (SSCs,
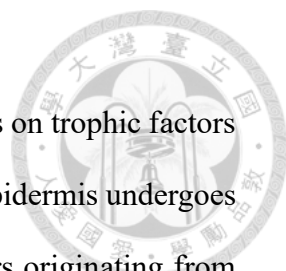
Figures 3.9B, 3.10C, Table 3.5). Genes involved in immune-related biological functions, including the inflammatory response, leukocyte-mediated immunity, leukocyte differentiation, and leukocyte migration, were enriched in the transition from C4 > 7 in the epidermis (Figure 3.10D). Similarly, gene ontology terms related to wound response, leukocyte activation, and migration were specifically enriched at 8 dpa vs. 0 dpa in normal regeneration but showed earlier enrichment during the wound healing stage in MS-275-treated wound epidermis at 3 dpa compared to homeostatic epidermis at 0 dpa (Figure 3.11). Overall, these results suggest that HDAC1 activity mediated by nerves is necessary for coordinating gene expression at the appropriate stages of regeneration in both the ST and WE.

3.4.6 Partial Rescue of Blastema Formation Defects Induced by MS-275 through Wnt Inhibition

I observed the premature expression of developmental pathway-associated genes when HDAC1 activity was inhibited after amputation. Among these genes, I focused on those associated with the Wnt signaling pathway to investigate their potential role in the impaired regeneration caused by HDAC1 inhibition. Although Wnt signaling has been implicated in vertebrate limb regeneration, it requires spatial-temporal regulation during limb development (146, 147). To determine if premature elevation of the Wnt pathway contributes to the regeneration defects observed upon HDAC1 inhibition, I conducted a functional assay using 15 juvenile axolotls and subjected their 30 limbs to three different treatments: control treatment (vehicle injection), regeneration-inhibiting treatment (25 mM MS-275 alone), and rescue treatment (25 mM MS-275 plus 1 μM Wnt inhibitor). Limb regeneration progress was monitored daily until 26 dpa. In the control group, a blastema was clearly visible at 8 dpa (Figure 3.2B), whereas the axolotls treated with MS-275 alone showed a lack of regeneration (Figure 3.2C).
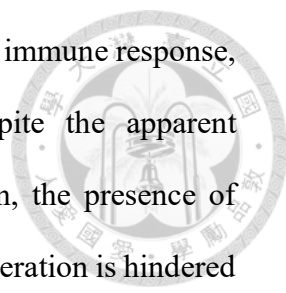
However, axolotls treated with MS-275 plus Wnt inhibitor exhibited a smaller blastema compared to the control group (Figure 3.2D). Among the control animals, all regenerated limbs developed digits. In contrast, out of the 10 limbs treated with MS-275 alone, 9 failed to regenerate, and only 1 limb progressed to the early bud blastema stage. In the MS-275 plus Wnt inhibitor group, 1 limb did not regenerate, 8 limbs developed into the blastema stage, and 1 limb further regenerated into the early differentiation stage. These results indicate that the addition of a Wnt inhibitor partially rescued the blastema formation defects induced by MS-275. Further optimization of a regeneration stage-dependent Wnt inhibition protocol in the context of HDAC1-inhibited amputated limbs would be necessary to fully evaluate the rescue effect. This experimental model provides a useful approach for functional testing of regeneration stage-sensitive pathways.

3.5 Discussion

Regeneration in axolotls is initiated following injury and relies on trophic factors derived from nerves (148). Within hours of the wound, the wound epidermis undergoes rapid migration to cover the injured area. Subsequently, nerve fibers originating from the amputation site innervate the wound epidermis, leading to the formation of the AEC, a signaling center. The AEC produces various signals that facilitate dedifferentiation and proliferation of blastema cells (149). The wound epidermis plays a crucial role in initiating blastema formation and limb regeneration as a specialized epithelium (76-78, 150, 151). However, its specific functions during the early stages of limb regeneration and the molecular mechanisms mediated by nerve-mediated HDAC in its transition are not well understood. Previous studies (47, 152) have shown that the epidermis in the proximal region to the wound site retains proliferative capacity after amputation, albeit at a reduced rate compared to the wound epidermis. Furthermore, the rapid coverage of the wound surface by the epidermis is attributed to basal epidermal cells (51, 115). In this study, I observed premature elevation of various cell type-associated signature genes when HDAC activity was inhibited (Figure 3.9). To gain further clarity on the changes in cell composition associated with HDAC1, future research should include in situ characterization of marker genes representing the basal epidermis (collagen type XVII alpha 1 chain, col17a1), proliferating epidermal cells (high levels of proliferating cell nuclear antigen, PCNA), intermediate epidermis (krt12), and SSCs (otogelin, otog). This validation would provide a clearer understanding of the alterations in cell composition induced by HDAC1 during tissue regeneration.

The loss of complete scar-free regenerative potential in various tissues in mammals and amphibians appears to coincide with the emergence of the immune system during development (153). Achieving successful transplantation from a different donor (allograft) requires minimizing rejection (31, 154, 155). A higher rate
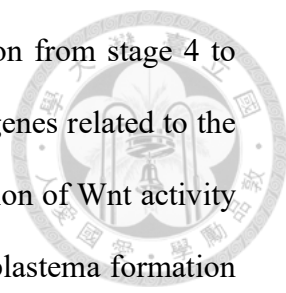
of success in axolotl allotransplantation is associated with a reduced immune response, suggesting that immune activity suppresses regeneration. Despite the apparent contradiction between a robust immune response and regeneration, the presence of immune cells is necessary for the regenerative process. In fact, regeneration is hindered when macrophage levels are low, whereas adequate macrophage numbers facilitate healthy regeneration (156, 157). Additionally, our research revealed a significant shift in the inferred population of epidermal cells (Figure 3.9B), and genes related to immune functions were expressed earlier during the wound healing stage after MS-275 treatment (Figure 3.10D). Differences in immune responses can determine the outcome between scarring and regeneration (156).

The formation of the blastema during limb regeneration requires not only a specialized WE but also the coordinated proliferation and migration of progenitor cells derived from various tissues, including muscle, bone, dermal fibroblasts, CT, and potentially other undiscovered populations (31, 50, 117, 118, 129, 158). The CT plays a crucial role in deciphering the molecular processes of regeneration, as it expresses factors that guide the regrowth of specific limb structures (31, 154). The findings indicate that the expression levels of genes associated with mature fibrous CT populations decrease after amputation (Figure 3.5A), consistent with previous research showing reduced representation of these cell types during the wound healing stage (141). In contrast, cycling cells are enriched in the early stages of regeneration, while fCT V cells, periskeletal cells, and tendon cells are enriched during blastema formation (Figure 3.8). However, the modulation of CT cell compositions within the blastema remains unclear due to challenges in isolating and analyzing blastema cells. Interestingly, upon treatment with MS-275, signature genes associated with most CT cell types, except cycling cells, show a significant enrichment (Figure 3.8). This suggests that blocking HDAC1 activities may inhibit the proliferation of blastema

progenitors, potentially impacting CT cell activities and resulting in the failure of blastema formation. Further studies employing in situ staining or single-cell analyses will be necessary to investigate the dynamic composition of each cell type throughout the regeneration process.

Numerous candidate genes have been identified through bulk transcriptome studies at different stages of axolotl limb regeneration, revealing their crucial roles in blastema initiation and maintenance (87, 122, 124-126, 141, 159). I observed that the administration of MS-275 disrupted the expression of certain genes associated with regeneration, which could directly result in a failure of limb regeneration (Figures 3.6E and G). Specifically, genes related to the deposition and remodeling of the ECM, such as spalt-like transcription factors (125, 135, 160) and collagens, showed low expression levels at the beginning of axolotl regeneration but increased during the blastema formation stage (Figures 3.6E and G). Additionally, Twist1 was identified as an early marker for the limb blastema mesenchyme (161), while Msx2 served as a marker gene for the blastema (52, 55, 95). Sox9 was found to be essential for sclerotome development and cartilage formation (162). Notably, PDGFRB, identified as a chemotactic growth factor involved in wound healing or regeneration in initial screening, was expressed in the mesenchymal blastema as confirmed by *in situ* hybridization (117, 125). Intriguingly, all these genes, which should normally exhibit upregulation at the blastema stage, showed premature elevation during the wound healing stage when HDAC1 was inhibited.

Modulating the activity of Wnt signaling during different stages of limb regeneration has distinct effects (147). Activation of Wnt signaling through chemical means during the wound-healing stage inhibits limb regeneration. Similarly, treatment administered after blastema establishment but before morphogenesis leads to disorganization of skeletal elements. In present study, Wnt signaling emerged as one of

, 72

the gene ontology terms associated with DEGs during the transition from stage 4 to stages 5 or 6 (Figures 3.6D and F), indicating earlier activation of genes related to the Wnt pathway under MS-275 treatment. Through continuous inhibition of Wnt activity alongside HDAC1 inhibition, we demonstrated a partial rescue of blastema formation (Figure 3.2), indicating that abnormal Wnt activity contributed to the regeneration defects induced by MS-275 treatment. To optimize a stage-specific and dosage-dependent protocol for rescuing HDAC1 inhibition-induced limb regeneration defects, it would be valuable to profile the expression of genes related to the Wnt pathway throughout the approximately 26-day process of limb regeneration in both control and MS-275-treated limbs. The preliminary findings demonstrate the feasibility of conducting limb regeneration rescue assays under conditions of HDAC1 inhibition to investigate the novel pathway specifically modulated by post-amputation HDAC activities.

HDACs exist in complex formations with distinct components, and they are believed to carry out various cellular functions, including the regulation of the cell cycle (163) and the maintenance of stem cell pluripotency (164). In the metamorphosis of anuran amphibians, HDACs play a role in controlling the precise timing of transcriptional programs across tissues and organs by interacting with thyroid hormone receptors (165). During the premetamorphic stage of tadpoles, unliganded thyroid hormone receptors recruit HDAC-containing corepressor complexes to repress gene expression, while during metamorphosis, liganded thyroid hormone receptors activate target gene transcription. This ligand switching behavior is crucial for orchestrating dramatic morphological development. It is possible that regeneration-specific mechanisms may involve the derepression of HDAC corepressor complexes during regeneration to temporally regulate transcription. Since HDAC1 is highly conserved in other vertebrates, it would be worth investigating whether it performs similar roles in

other models of appendage regeneration and whether it is differentially activated in

non-regenerative systems following significant limb injury.
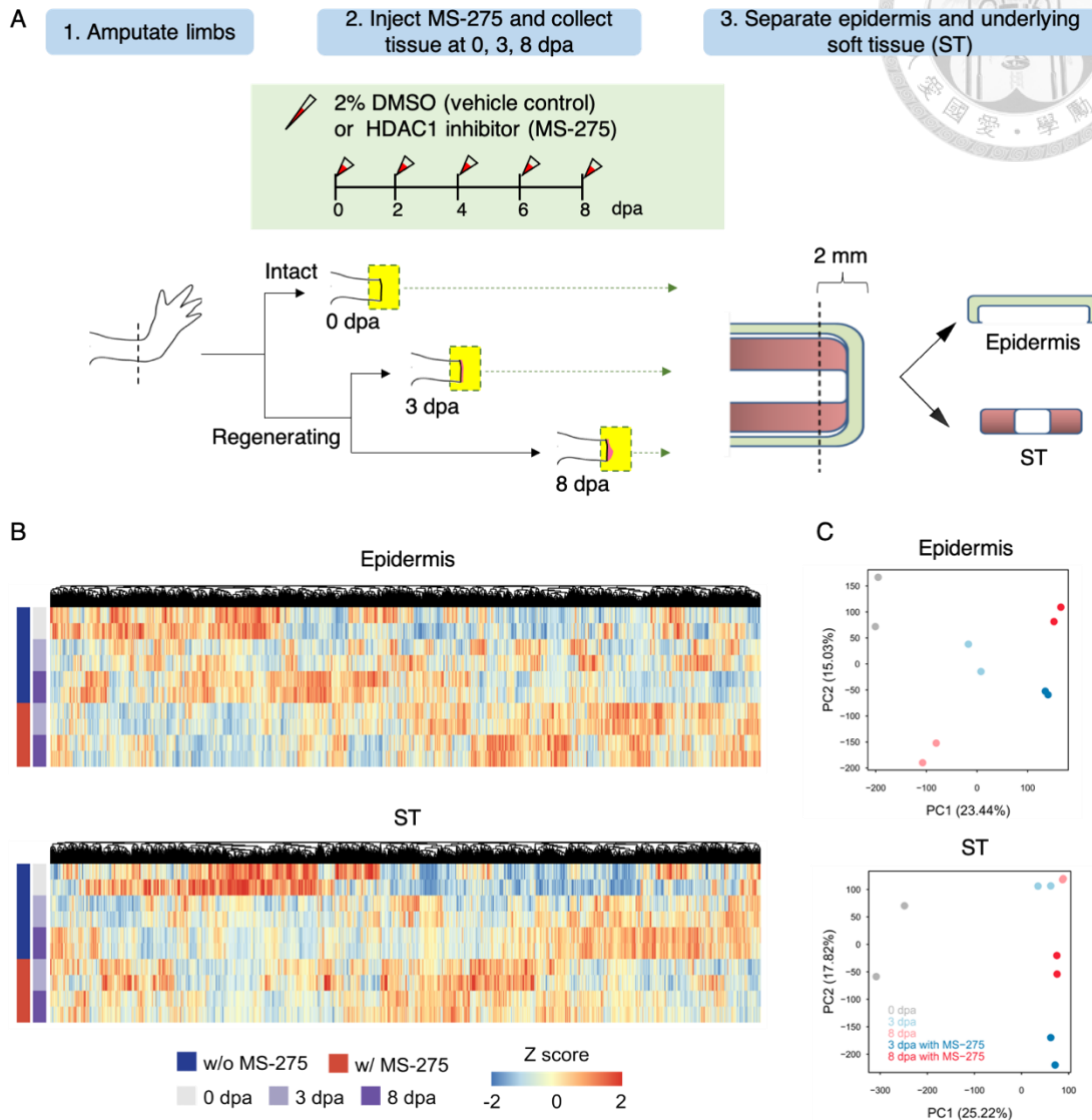
3.6 Tables and Figures

Figure 3.1 The Impact of HDAC1 Inhibition on the Global Transcriptome Profiles of the WE and ST during the Early Stage of Limb Regeneration. (A) To investigate the impact of depleting HDAC1 on the composition of the transcriptome during the early stages of limb regeneration, the HDAC1 inhibitor MS-275 was injected into the amputation site every other day after limb amputation. Two biological replicates were collected for each of the WE and ST at 0, 3, and 8 dpa from animals treated with HDAC1 inhibitor and vehicle control. The regenerates' most distal portion, measuring 2-3 mm, was isolated at 3 and 8 dpa, corresponding to the wound healing and blastema

formation stages, respectively. These samples were compared to homeostatic control samples obtained immediately after amputation. (B) The transcriptome profiles were subjected to hierarchical clustering based on the HDAC1 inhibitor MS-275 treatment and the regeneration time course in both WE and ST. The expression values of genes were transformed into z-scores, with colors reflecting the gene expression level (low: blue; high: red). (C) Principal Component Analysis (PCA) was performed to analyze the transcriptome profiles of WE (top) and ST (bottom). The values in parentheses indicate the percentage of variance explained by each Principal Component (PC) axis.
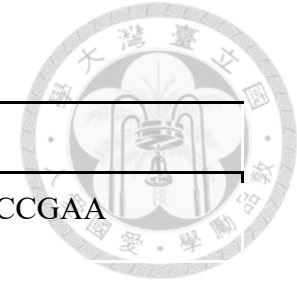
Table 3.1 Primer sequences for Q-PCR of HDACs.

| Gene	F	as
sulf1	GACGCACCAAGTTTGTCCAA	TGGTCACTTCATCTGCCGAA
atp7a	CAGCCGCTATAGGTACTCCAACTA	TTGTTGGATGTGGTGGCAAG
ptk7	GGGTCACTGTGTTTGCCAAT	CATGTCCTTGATGTCTGCGA
crabp2	AATCAGGCCAGCATTGTCCA	GCAGACTGAGTCCACATACAGGAA
gli3	CACTCTCCGATCACAGCTTTGA	TAAGTGACCGTATGACCCACTAGC
epha2	CGTAGACTATGGCACCAACTTC	CACCTCCACGTTTAGCTTCA
S21 ribosomal RNA*	ACTTGAAGTTTGTTGCCAGGAC	TGGCATCTTCTATGATCCCATC

* serve as an internal control.
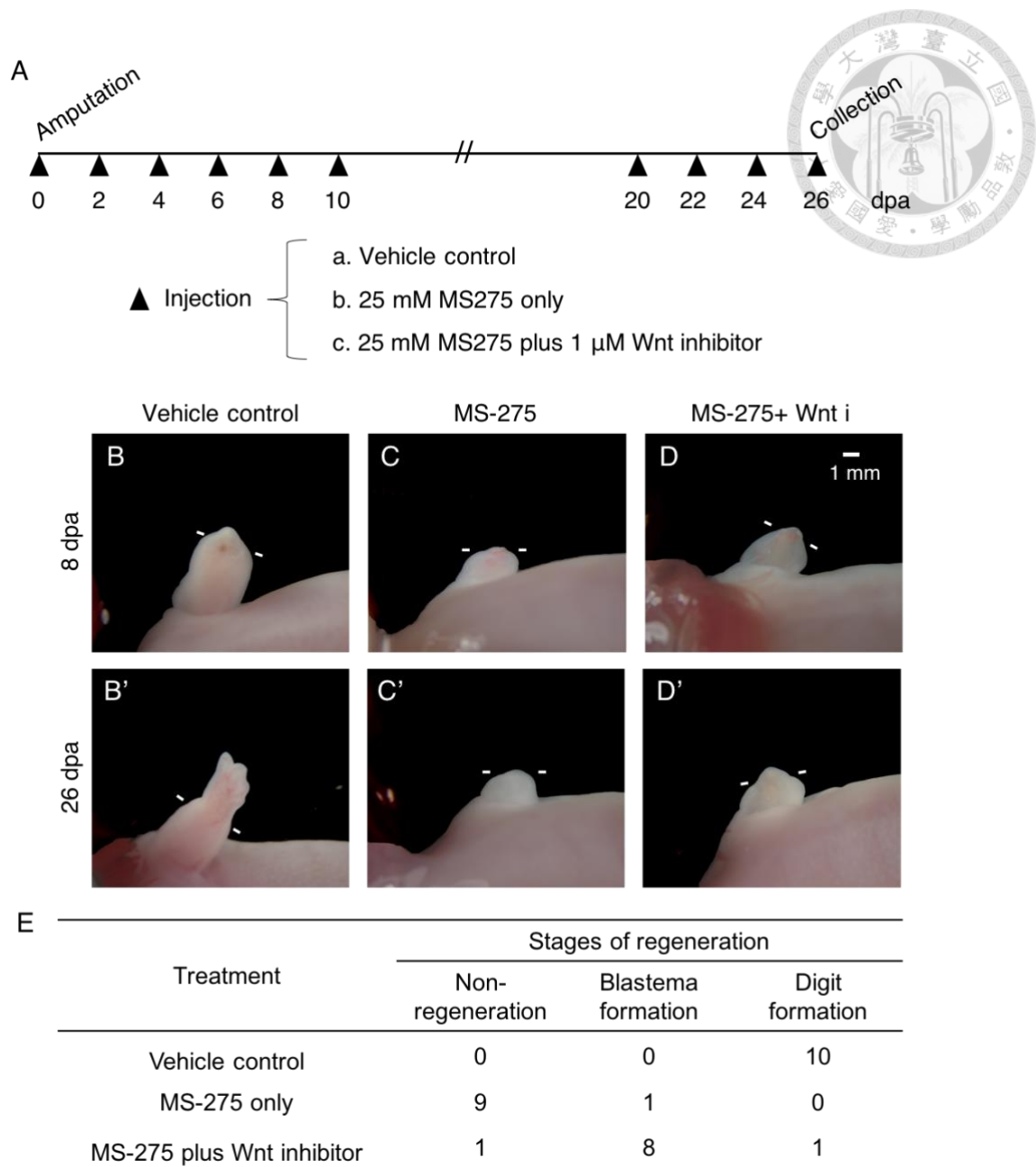
Figure 3.2 The Partial Rescue of MS-275-Induced Regeneration Inhibition through the Use of a Wnt Inhibitor. (A) The figure outlines the experimental protocol, indicating the timing of local injections (administered every other day) from the time of amputation until 26 dpa (days post-amputation). The injections were divided into three groups: (a) vehicle control, (b) 25 mM MS-275 alone, and (c) 25 mM MS-275 plus 1 μM Wnt inhibitor. Representative photos taken at 8 dpa illustrate the outcomes in each group: blastema formation in group a (B), non-regeneration in group b (C), and a smaller blastema in group c (D). By 26 dpa, the results are shown in the corresponding

,   78

photos: a new limb with four digits in group a (B'), non-regeneration in group b (C'), and a blastema in group c (D'). (E) The table summarizes the overall outcomes of these three groups at 26 dpa, with a sample size of 10 limbs in each group. The white bar indicates the amputation line, and the scale bars represent 1 mm.
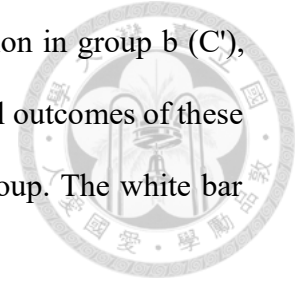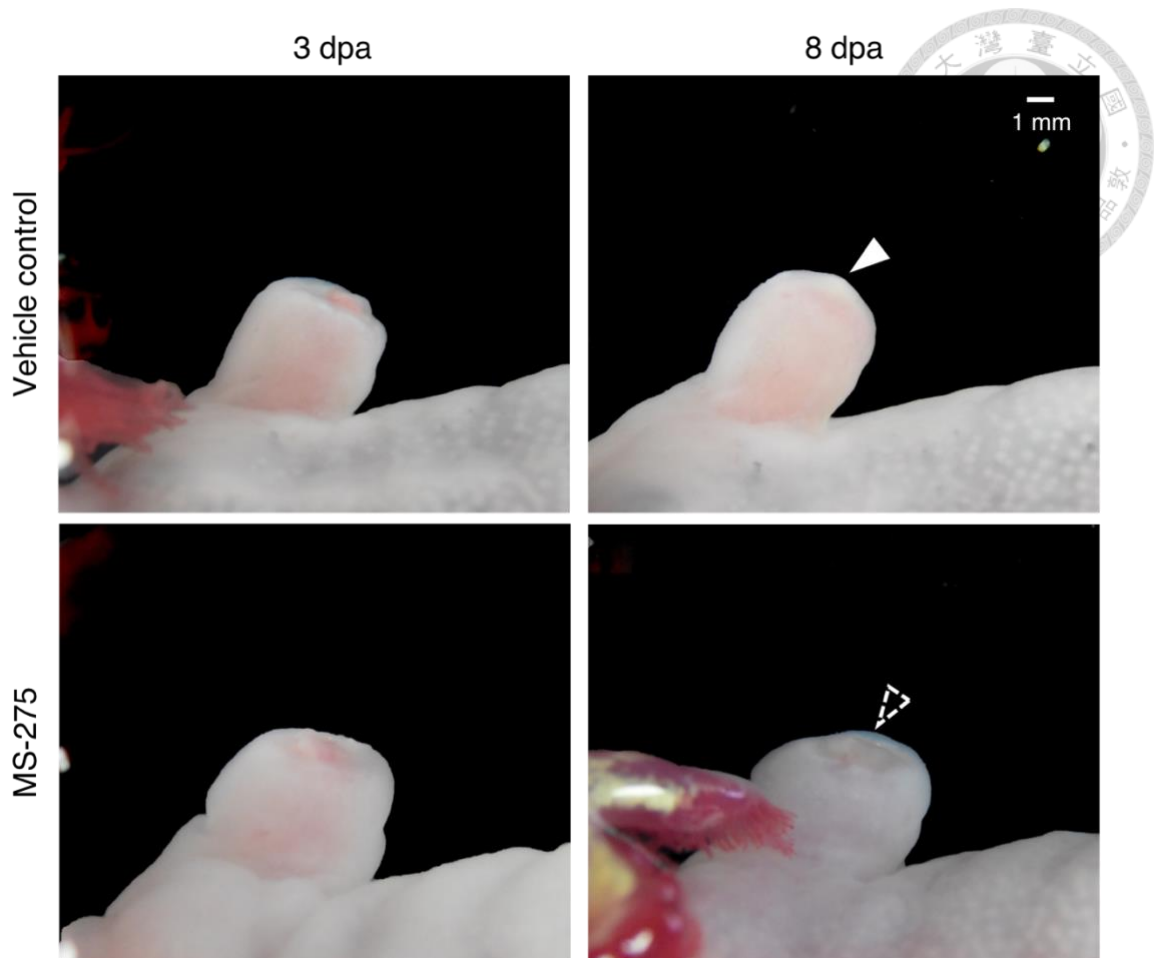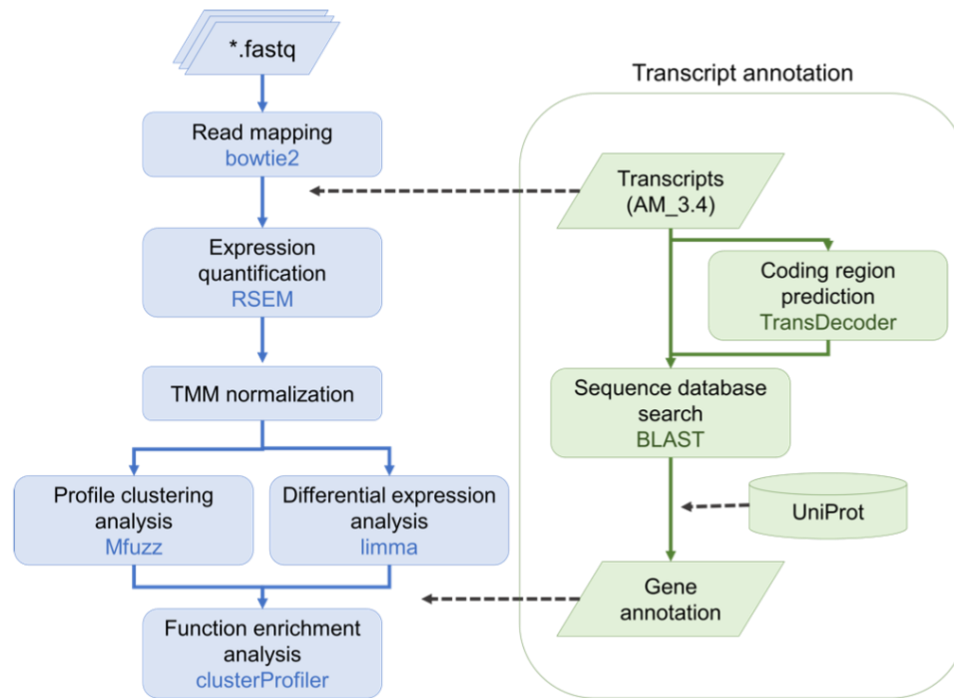
Figure 3.3 The Impact of MS-275 on the Initiation of LB Blastema. It presents visual examples captured using bright-field imaging, demonstrating the lack of outgrowth in the blastema at 8 dpa). The blastema and the amputation plane are denoted by solid and dashed arrows correspondingly. Scale bars = 1 mm.
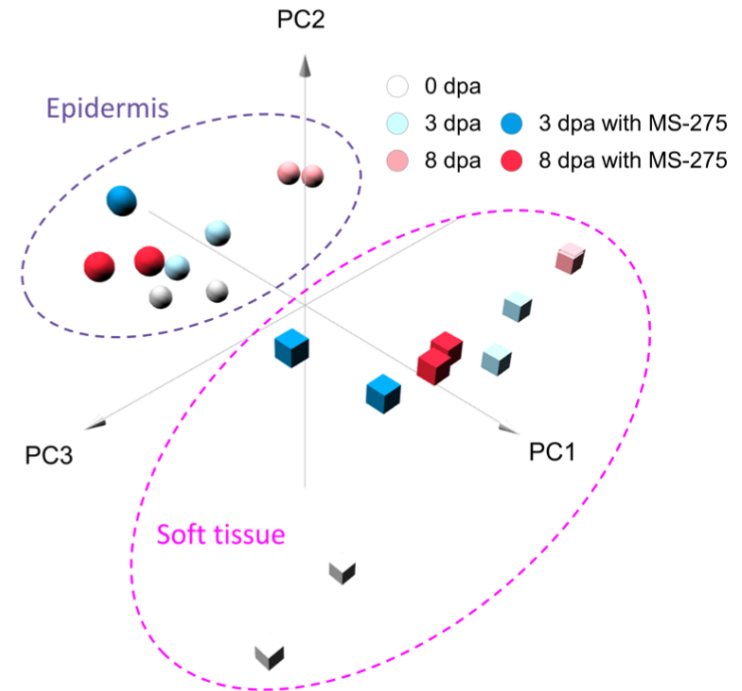
Figure 3.4 A Comparative Analysis of Transcriptome Profiles. (A) The flowchart illustrates the process of analyzing RNA-seq data and re-annotating the reference transcriptome of the axolotl based on the work by Nowoshilow et al. (129). (B) A 3D-projection plot of PCA is shown, representing the transcriptome profiles utilized in this study.

Table 3.2 A Summary of the Alignment of Sequencing Reads to the Reference Transcript in Terms of Sequencing Reads Alignment.

Sample name	# reads	Overall alignment rate
D3-ST-1	22,557,069	78.64%
D3-ST-2	36436803	80.59%
D3-ST-M1	19284219	76.49%
D3-ST-M2	28457400	77.32%
D3-WE-1	35204053	77.21%
D3-WE-2	40040745	76.47%
D3-WE-M1	38514305	77.14%
D3-WE-M2	34524802	75.96%
D8-ST-1	38603215	79.13%
D8-ST-2	30457341	79.43%
D8-ST-M1	32595534	78.19%
D8-ST-M2	42965033	80.49%
D8-WE-1	30721211	79.38%
D8-WE-2	35942941	78.26%
D8-WE-M1	46718700	77.71%
D8-WE-M2	34046014	78.87%
O-ST-1	46463921	78.69%
O-ST-2	27450973	80.87%
O-WE-1	41412254	88.23%
O-WE-2	35303186	78.49%
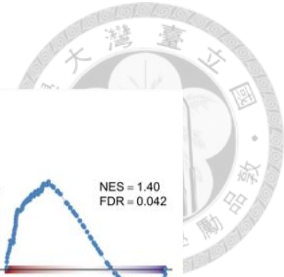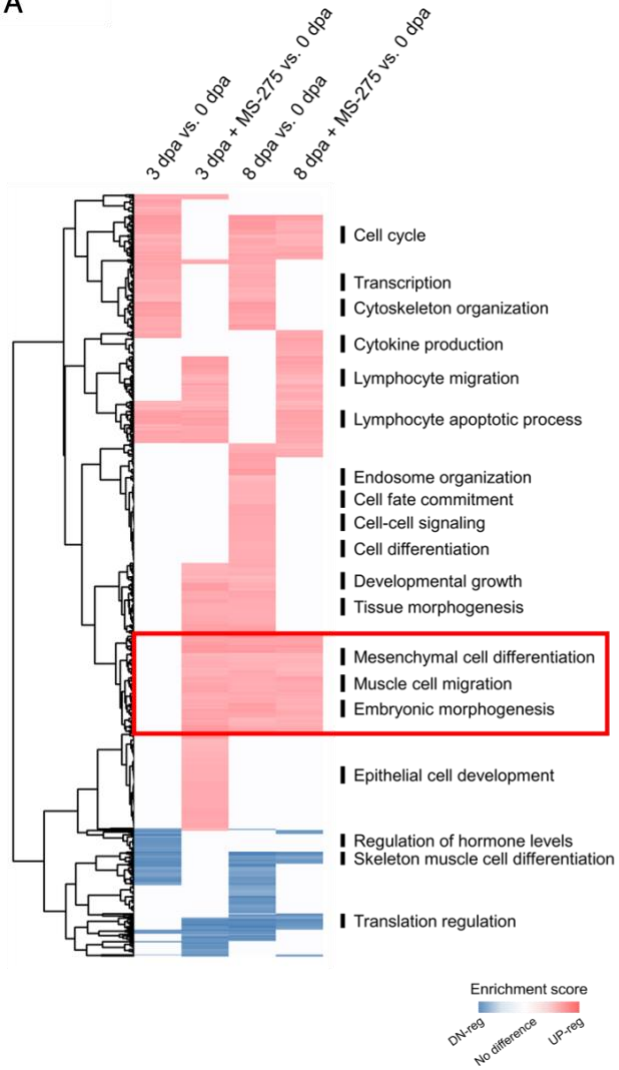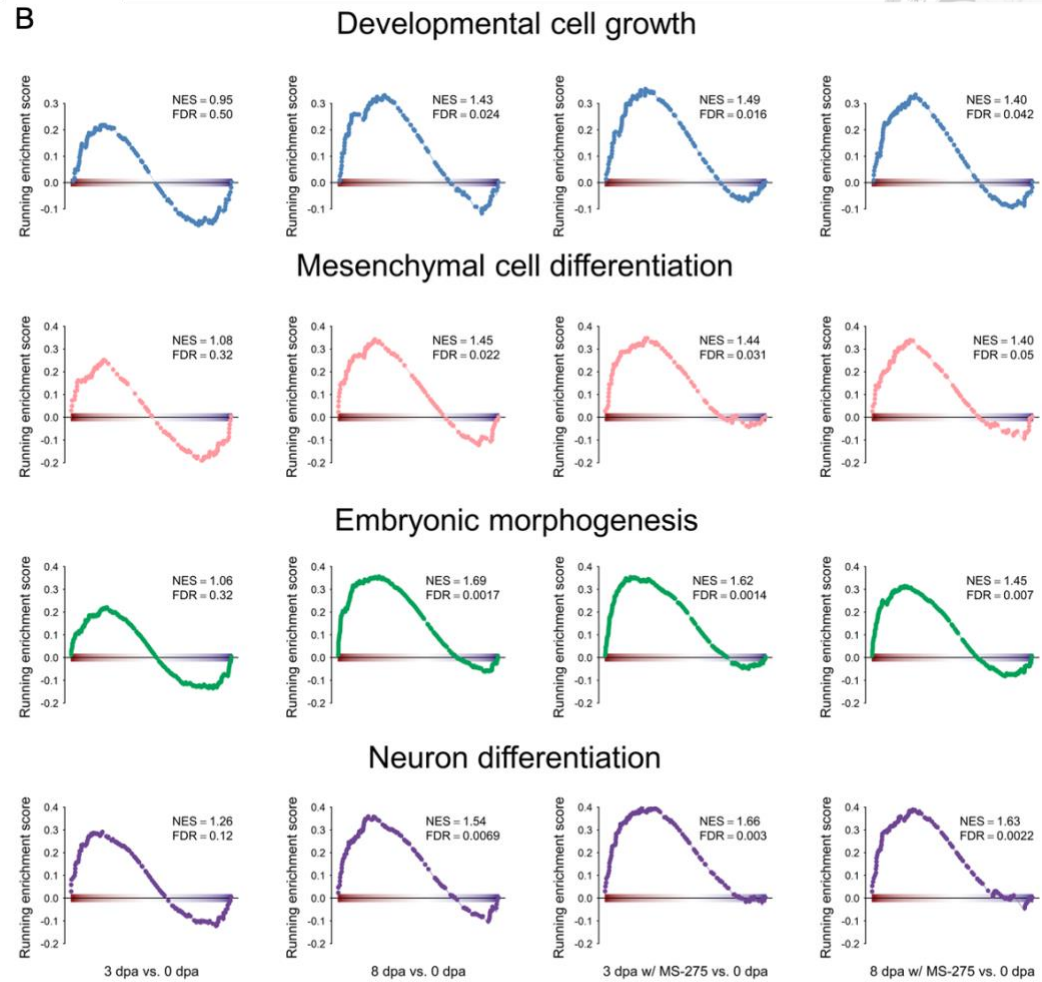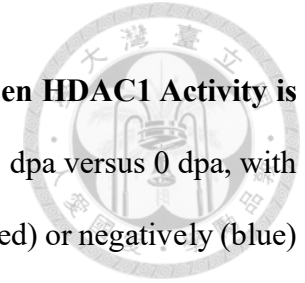
Figure 3.5 The Premature Enrichment of Genes Related to Morphogenesis in the ST of the Regenerating Limb when HDAC1 Activity is Absent. (A) The heatmap presents the results of GSEA comparing gene sets defined by GO at 3 dpa versus 0 dpa, and at 8 dpa versus 0 dpa, with and without MS-275 treatment. In the heatmap, red and blue colors indicate gene sets that are significantly and positively (red) or negatively (blue) enriched, respectively, at 3 or 8 dpa (FDR < 0.05), with intensity associated with the normalized enrichment score (NES). (B) GSEA plots illustrate the representative gene sets highlighted in (A). The abbreviations NES and FDR are included for reference.

84

Table 3.3 Counts of Genes Showing Differential Expression in each Comparison.

	Epidermis	Soft tissue
3 dpa vs. 0 dpa	16,413	22,413
8 dpa vs. 0 dpa	16,677	24,892
8 dpa vs. 3 dpa	14,074	12,255
3 dpa w/MS-275 vs. 0 dpa	23,176	23,544
8 dpa w/MS-275 vs. 0 dpa	23,053	23,981
8 dpa w/MS-275 vs. 3 dpa w/MS-275	11,087	10,855
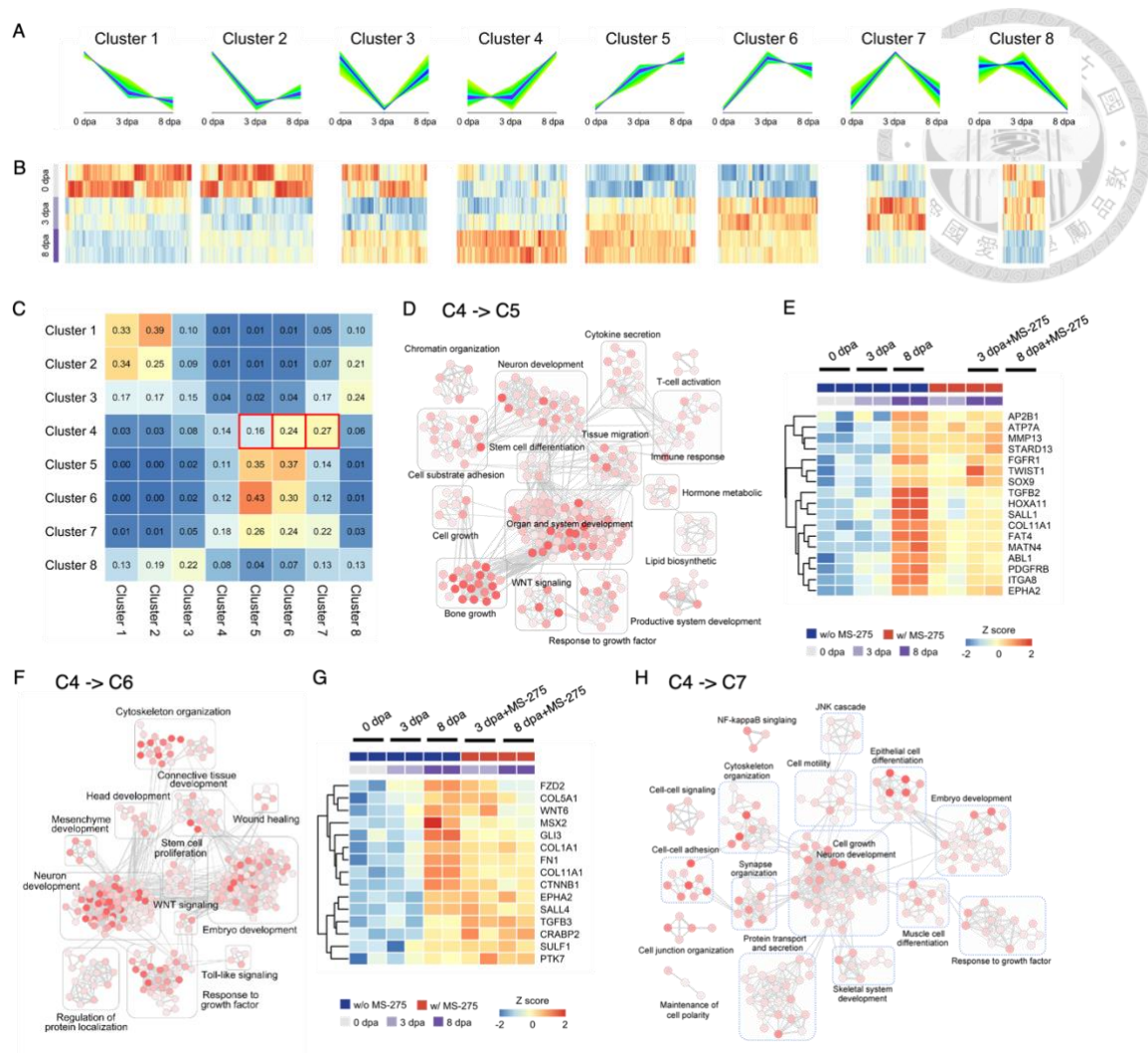
Figure 3.6 HDAC1 Inhibition-Induced Changes in Gene Expression Trends during Regeneration Stages and Associated GO Terms Based on Unsupervised Transcript Clustering. (A) Transcripts were clustered in an unsupervised manner based on their expression patterns during normal regeneration at 0, 3, and 8 dpa. (B) Heatmap displaying the relative expression levels of transcripts associated with each cluster. Transcript datasets from the corresponding stages without MS-275 treatment were included for comparison. (C) Cluster transition matrix indicating the proportion of genes in each cluster (row) that exhibited changes in their expression patterns to other clusters (column) after MS-275 treatment. (D) Enrichment maps showing gene sets significantly enriched (FDR < 0.05) by genes transitioning from cluster 4 to cluster 5 after exposure to MS-275. (E) Heatmap representing the expression values of selected

genes that transitioned from cluster 4 to cluster 5 following MS-275 exposure. (F) Enrichment maps depicting gene sets significantly enriched (FDR < 0.05) by genes transitioning from cluster 4 to cluster 6 after MS-275 treatment. (G) Heatmap displaying the expression values of selected genes that transitioned from cluster 4 to cluster 6 after MS-275 exposure. (H) Enrichment maps illustrating gene sets significantly enriched (FDR < 0.05) by genes transitioning from cluster 4 to cluster 7 after MS-275 treatment. The red to white color gradient for each GO node indicates the significance of enrichment for that specific GO term, with red indicating higher significance.
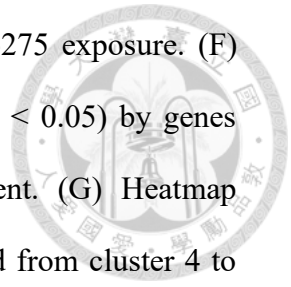
Table 3.4 Matrix Showing the Quantity of Genes Displaying Alterations in Their Gene Expression Trajectories following Treatment with MS-275 (Soft Tissue).

ST

MS-275 treatment

	Cluster 1	Cluster 2	Cluster 3	Cluster 4	Cluster 5	Cluster 6	Cluster 7	Cluster 8
Cluster 1	1977	2425	661	69	43	84	316	669
Cluster 2	1872	1399	509	78	40	70	394	1257
Cluster 3	765	751	629	169	97	188	727	1038
Cluster 4	155	159	426	717	877	1360	1463	320
Cluster 5	5	21	108	590	1955	2045	727	65
Cluster 6	14	24	102	570	2192	1540	537	49
Cluster 7	31	42	154	554	868	766	630	104
Cluster 8	296	465	543	201	107	174	293	302

Control

88
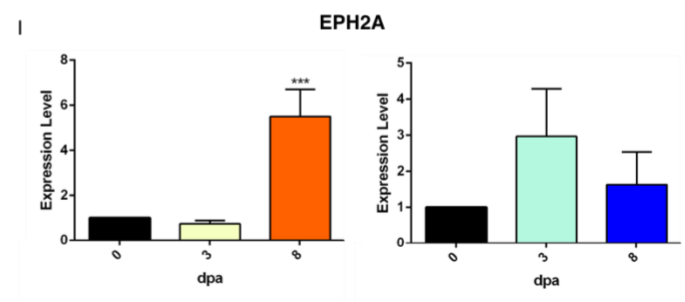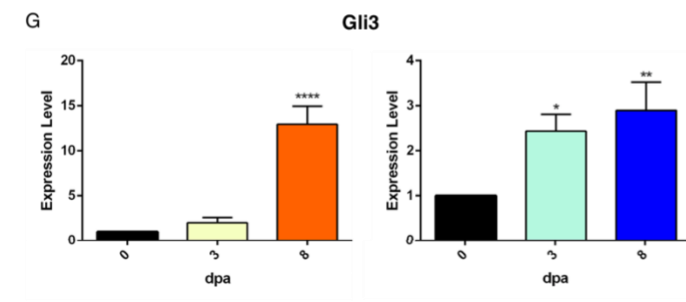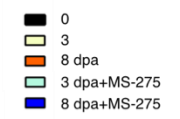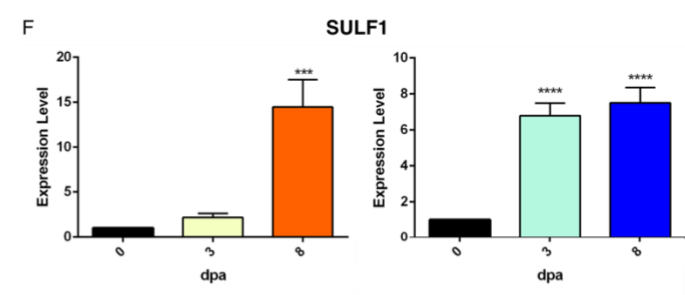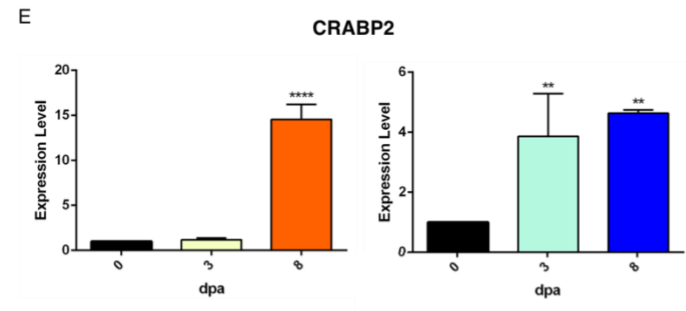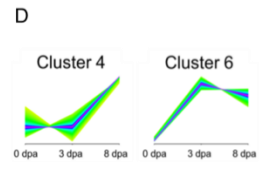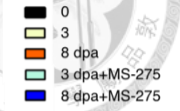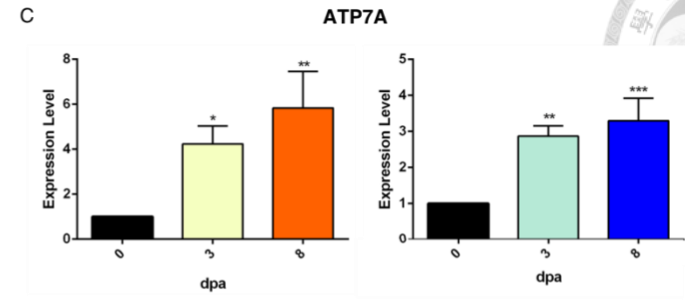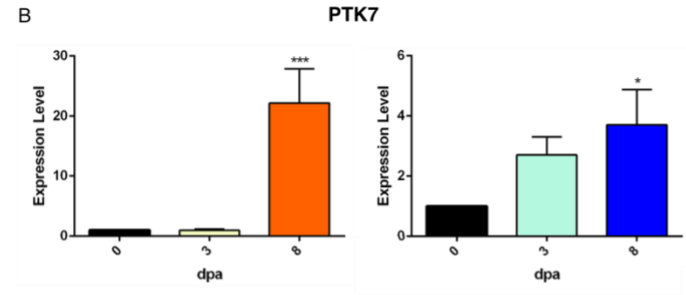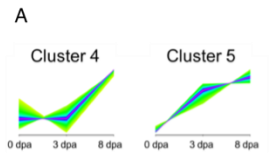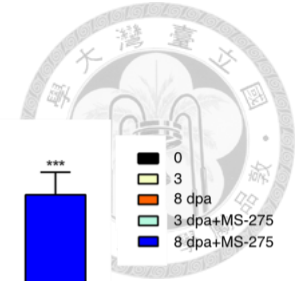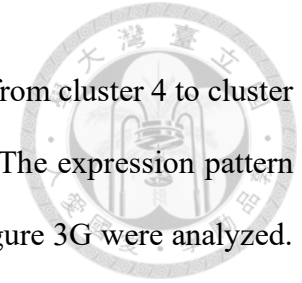
Figure 3.7 Validation of Enriched Transcripts in Cluster Transition Using Q-PCR. (A) The expression pattern trends from cluster 4 to cluster 5 were assessed at 0, 3, and 8 dpa. (B-C) The expression levels of genes highlighted in Figure 3G were examined. (D) The expression pattern trends from cluster 4 to cluster 6 were evaluated at 0, 3, and 8 dpa. (E-I) The expression levels of genes highlighted in Figure 3G were analyzed. The data are presented as means ± SEMs, with n = 3 per group. Statistical significance (*$P < 0.05$) is indicated.
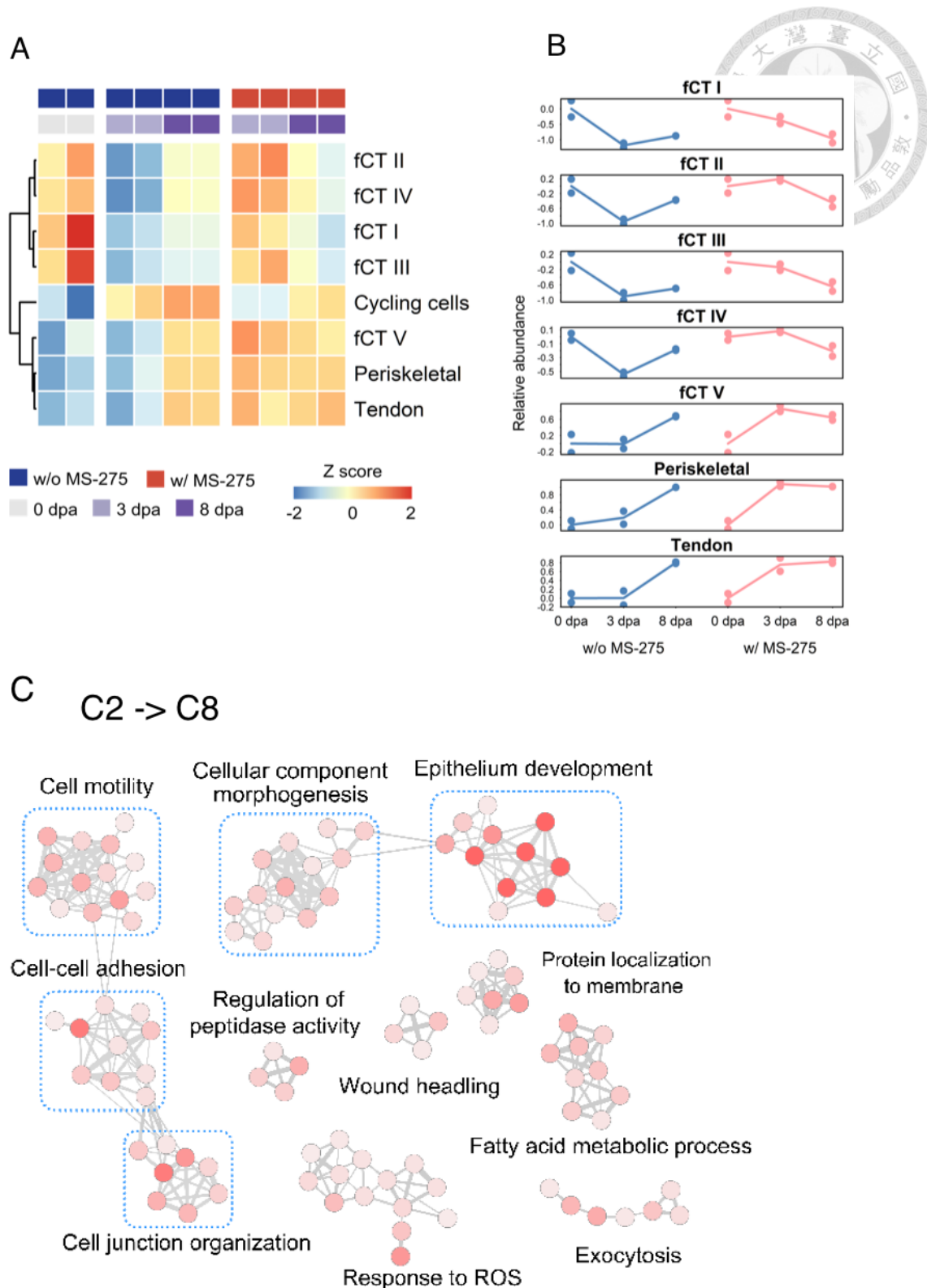
Figure 3.8 The Inferred Changes in Cell Composition Associated with HDAC1 Inhibition, Based on the Expression Patterns of Signature Genes Specific to CT Cell Types in the ST during Early Limb Regeneration. (A) The heatmap illustrates

doi:10.6342/NTU202301772

the predicted relative abundance of various CT cell types, estimated using the abundance of signatures specific to each cell type. The color gradient (red to blue) indicates the predicted abundance, with red representing high abundance and blue representing low abundance. (B) The expression patterns of cell type-specific enriched gene cohorts associated with early regeneration stages were significantly altered by MS-275 treatment. (C) Enrichment maps display the gene sets that were significantly enriched (FDR < 0.05) among genes transitioning from cluster 2 to cluster 8 after exposure to MS-275. These gene sets exhibited similar pattern changes as observed in the representative genes of CT cell types (fCT I, fCT II, fCT III, and fCT IV) shown in (B). The color gradient (red to white) within each GO node represents the statistical significance of enrichment for the corresponding GO term, with red indicating higher significance.
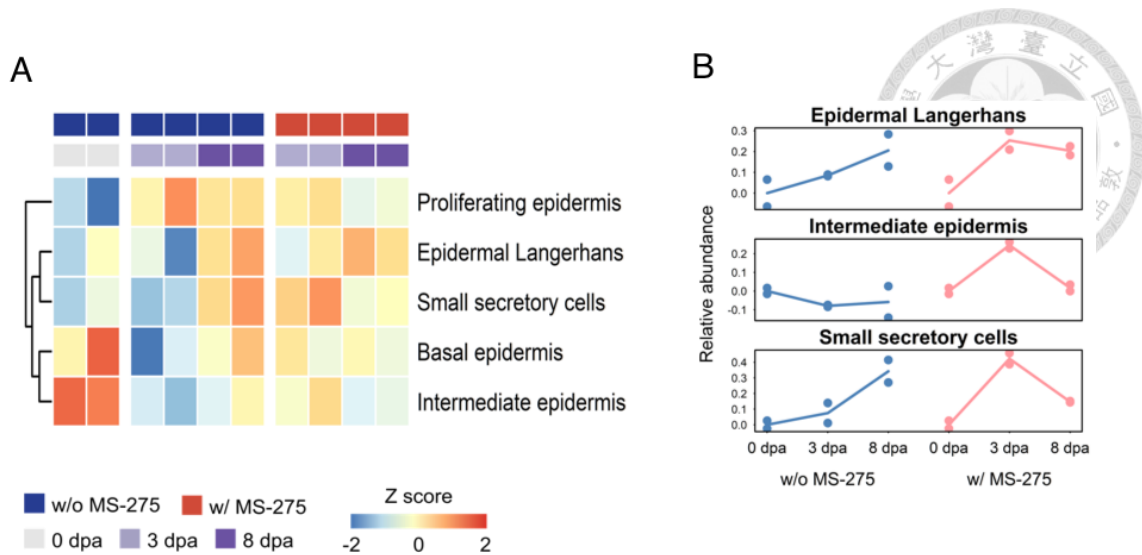
Figure 3.9 The Inferred Shift in Cell Composition within the WE under MS-275 Treatment during the Early Stage of Limb Regeneration. The figure focuses on the putative abundance of different epidermal cell types in WE, comparing samples with and without MS-275 treatment. (A) The heatmap illustrates the predicted relative abundance of various epidermal cell types, estimated using the abundance of signatures specific to each cell type. The color gradient (red to blue) indicates the predicted abundance, with red representing high abundance and blue representing low abundance. (B) The panel on the right demonstrates that under MS-275 treatment, there is a premature enrichment of specific epidermal cell types, including epidermal Langerhans cells, intermediate epidermis cells, and small secretory cell types. These cell types show a higher representation compared to the control samples without MS-275 treatment.
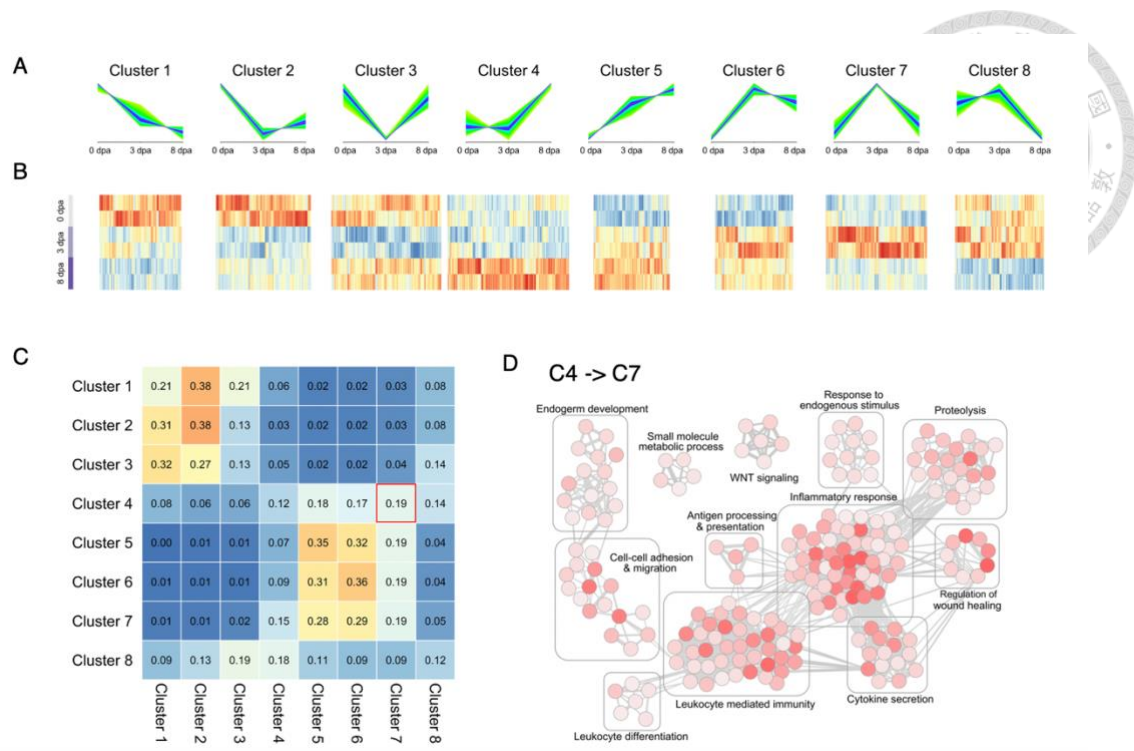
Figure 3.10 Highlighted GO Categories for Genes undergoing Expression-Pattern Transition in Response to MS-275 Treatment in the Epidermis. (A) Unsupervised clustering of transcripts based on the trends in their expression patterns during normal regeneration at 0, 3, and 8 dpa. (B) Heatmap displaying the relative expression levels of transcripts associated with each cluster. Transcript datasets from the epidermis at each stage without MS-275 treatment were included for comparison. (C) Cluster transition matrix indicating the proportion of genes in each cluster (row) that exhibited changes in their expression patterns to other clusters (column) after MS-275 treatment. (D) Enrichment maps showing gene sets significantly enriched (FDR < 0.05) by genes transitioning from cluster 4 to cluster 7 after exposure to MS-275.
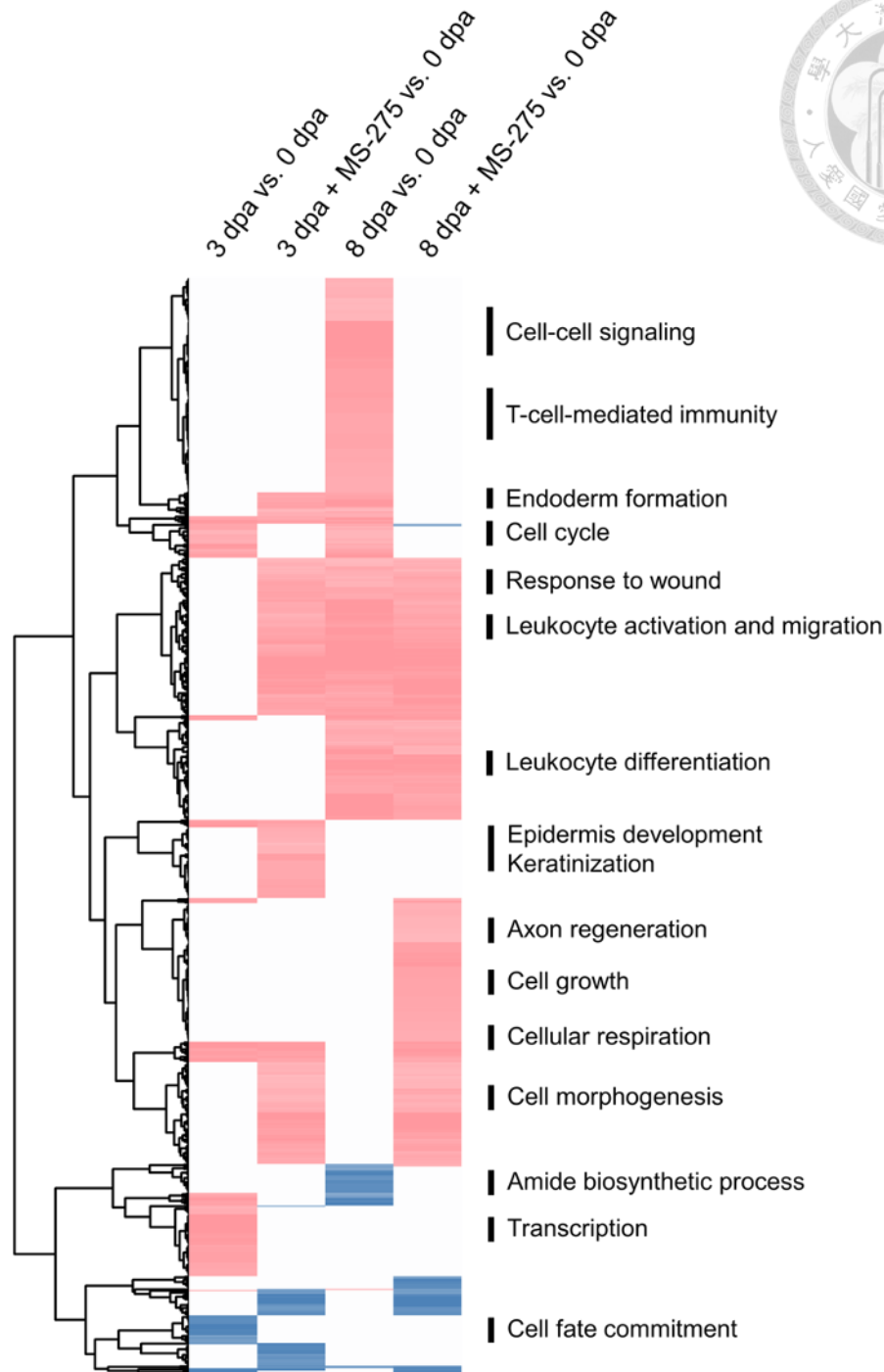
Figure 3.11 Premature or Aberrant Enrichment of Specific GO terms in Epidermal Tissue under MS-275 Treatment. The heatmap illustrates the results of GSEA comparing 3 dpa vs. 0 dpa or 8 dpa vs. 0 dpa, with or without MS-275 treatment, using gene sets defined by GO terms. Red and blue colors indicate gene sets that are significantly positively (red) or negatively (blue) enriched at 3 or 8 dpa (FDR < 0.05). The intensity of the colors is associated with the NES.

Table 3.5 Matrix Depicting the Quantity of Genes Displaying Alterations in Their Gene Expression Trajectories after Treatment with MS-275 (Epidermis).

Epidermis

MS-275 treatment
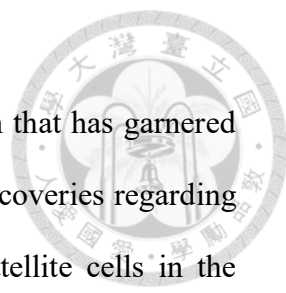
	Cluster 1	Cluster 2	Cluster 3	Cluster 4	Cluster 5	Cluster 6	Cluster 7	Cluster 8
Cluster 1	906	1639	912	245	77	108	118	354
Cluster 2	1540	1912	632	169	100	89	131	401
Cluster 3	1852	1531	714	277	139	138	255	802
Cluster 4	489	354	406	766	1155	1051	1163	887
Cluster 5	15	33	59	303	1445	1307	770	171
Cluster 6	22	25	37	356	1289	1487	791	159
Cluster 7	57	60	130	780	1473	1524	981	286
Cluster 8	427	599	905	863	509	425	425	556

(left margin label: Control)

Chapter 4:

Unraveling the Intricacies of Salamander Limb Regeneration: Insights into Muscle Fiber Reconnection

4.1 Summary

Axolotl limb regeneration has been a captivating phenomenon that has garnered attention for several decades. Dr. Lee's Lab has made significant discoveries regarding axolotl limb regeneration, specifically highlighting the role of satellite cells in the remnant muscles. These satellite cells have been observed to move distally into the blastema, where they regenerate new muscles. During this process, a gap forms between the regenerative muscles and the remnant muscles. Subsequently, the regenerative muscle fibers begin to reconnect with the remnant fibers. This chapter focuses on elucidating the reconnection process at the individual muscle fiber level, aiming to test the hypothesis that this reconnection occurs synchronously among the involved muscles. To achieve this, three pairs of EGFP+ mid bud-stage blastemas were transplanted onto freshly amputated stumps of RFP+ axolotls at the same thigh position. This transplantation resulted in the creation of double fluorescence chimeric regenerative hindlimbs. These regenerative limbs were allowed to develop until a very late stage, well beyond the late differentiation stage. Using fluorescence imaging on cross sections of these limbs, I made a fascinating discovery. The reconnection of muscle fibers occurred at varying rates among the muscles in the proximal remnant part. In the gracilis muscle, which is the major thigh muscle, the reconnection process initiated from the periphery and gradually progressed towards the center. Additionally, I observed that RFP+ muscle fibers contributed to muscle regeneration in the distal regenerative parts. It is worth noting that this contribution was limited to the ventral superficial muscles in the calf region. The utilization of this double fluorescence chimeric limb regeneration model has the potential to provide further insights into the patterning of axolotl limb regeneration during the late stages.

4.2 Introduction

Salamander limb regeneration has been an intriguing biological phenomenon for over two centuries, captivating the scientific community (166). Extensive research efforts have been dedicated to understanding the regenerative capabilities of salamanders, which starkly contrast with the limited regenerative potential observed in humans (167). Lineage tracing techniques and labeling of mature muscle cells in salamanders have provided valuable insights into the contribution of muscle regeneration during this process (32). Surprisingly, fundamental differences have been observed between newts and axolotls, where mature muscles do not contribute to regeneration in axolotls, despite the successful regrowth of limbs. Subsequent investigations involving the labeling of resident satellite cells have confirmed that the resident satellite cells within the remaining muscles play a pivotal role in the regenerative process (80).

Expanding upon these findings, previous research has revealed the migration of satellite cells in axolotls from the remnant muscles, which remain at their original location (168). These Pax7+ satellite cells migrate into the blastema, initiating proliferation. Throughout the limb regeneration process, these satellite cells differentiate into immature muscle fibers within the regenerating area while remaining physically separated from the remnant muscles, even during the late differentiation stage. Notably, a persistent gap between the parental and regenerating muscles has been observed, indicating the dedifferentiation of remnant muscle ends from the bud stages and their subsequent reconnection with the partially differentiated regenerating muscles. The undifferentiated nature of both ends of the remnant and regenerating muscles is believed to facilitate this reconnection, possibly due to the incomplete organization of their sarcomere structures. Additionally, the application of diffusion tensor tractography technique through magnetic resonance imaging (MRI) has confirmed the presence of a

gap between parental and regenerating muscles at 9 weeks post-amputation in adult axolotls, with reconnection occurring from 10 weeks (169). However, recent studies have not provided a comprehensive understanding of the events occurring in individual muscles. Therefore, this study aims to investigate whether the reconnection process synchronously occurs among the involved muscles.

In the present study, blastema transplantation from EGFP-transgenic axolotls onto freshly amputated ends at the thigh portion of RFP-transgenic axolotls was conducted, ensuring the same proximal-distal level and axes. Muscle fibers were distinguished by color, with red representing the remnant origin and green indicating the transplanted blastema. The coexistence of red and green colors in muscle fibers signifies the reconnection between remnant and blastema-derived muscle fibers, enabling a comprehensive examination of muscle fiber reconnection in individual muscles and providing deeper insights into the underlying mechanisms.

4.3 Materials and Methods
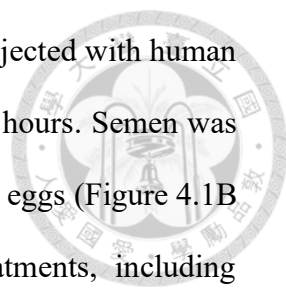
4.3.1 Plasmid Construction and Purification for Genetic Manipulation Studies

This article focuses on the manipulation and purification of plasmids used in genetic studies, particularly for the expression of fluorescent proteins. The EGFP-expression plasmid, pCX-EGFP (170, 171), was graciously provided by Masaru Okabe and Jun-Ichi Miyazaki (Osaka University, Japan). To incorporate an I-SceI recognition sequence flanked by HindIII sequence (5'-AAGCTTTAGGGATAACAGGGTAATAAGCTT-3') into the pCX-EGFP plasmid, it was inserted at the single HindIII restriction site (2996 bp), resulting in the creation of the pCX-EGFP-SceI plasmid. Furthermore, for the development of the pCX-RFP-SceI plasmid, the EGFP sequence flanked by EcoRI sites in the pCX-EGFP-SceI plasmid was replaced with the Texas Red sequence. Plasmid purification was carried out using the Geneaid™ Midi Plasmid Kit (Geneaid, Taiwan), ensuring high-quality samples for downstream experiments.

4.3.2 Husbandry and Ethical Considerations in Axolotl Research

Adult or juvenile axolotls were housed individually in fish tanks within an aquaria system, following established protocols (169, 172). The animal care and experimental procedures were conducted in compliance with the approved guidelines of the Institutional Animal Care and Use Committee of National Taiwan University College of Medicine (Permit number: 20160535). Anesthesia was administered using a 0.1% solution of ethyl 3-aminobenzoate methanesulfonate salt (MS-222, Sigma-Aldrich, St. Louis, MO, USA) prior to surgical procedures.

To precisely control the timing of fertilization for plasmid injection, *in vitro* fertilization (IVF, Figure 4.1) was employed instead of natural mating (Figure 4.2). The IVF and transgenic axolotl generation protocols were adapted from previously

published methods (173-175). Female axolotls were anesthetized, injected with human chorionic gonadotrophin (hCG), and began spawning within 24-30 hours. Semen was gently collected from anesthetized male axolotls and mixed with the eggs (Figure 4.1B and C), which were subsequently subjected to a series of treatments, including dejellying and incubation in specific solutions. The eggs were maintained at 4°C until plasmid microinjection (Figure 4.1D). High-quality eggs were selected and microinjected using a pressure injector under a dissecting microscope. Glass capillary needles filled with the pCX-EGFP-SceI or pCX-RFP-SceI plasmid, along with I-SceI enzyme, were used for microinjection. Following injection, the eggs were incubated and transferred to suitable solutions until the hatching stage (Figure 4.2 E-F). The determination of embryonic developmental stages is based on previous research (176). Strict sterilization procedures, including the use of 0.22 μm filters, were implemented for all solutions involved in microinjection and embryo rearing. The founder (F0) transgenic animals served as progenitors to generate F1 axolotls through IVF (Figure 4.3A).

4.3.3 Blastema Transplantation in Transgenic Axolotls

Three pairs of juvenile transgenic axolotls were utilized: a 9 cm leutic to leutic F0 pair, a 4 cm leutic to wild type F1 pair, and a 7 cm leutic to leutic F1 pair. The recipient axolotls were named F0, F1-1, and F1-2, respectively. The body length of the axolotls was measured from the snout to the tail end. Right thigh amputation was performed on the EGFP-transgenic axolotls at the lower third. Once regeneration reached the mid bud stage, which took 10 days for F0 donor axolotls and 8 days for F1-1 and F1-2 donor axolotls, another pair of RFP-transgenic juvenile axolotls underwent right thigh amputation at the lower third as well. The blastemas from the EGFP-transgenic axolotls were excised and carefully transplanted onto the freshly cut surface

102

of the right thighs of the RFP-transgenic axolotls, aligning them along the same anterior-posterior and dorsal-ventral axes. The blood released from the freshly amputated sites served as an adhesive to secure the transplanted blastemas. The recipient animals were covered with a moist Kimwipe paper on their bodies and placed on ice for 1 hour to ensure firm attachment of the blastemas to the recipients' stumps. Subsequently, they were returned to the aquatic environment for further observation and analysis (Figure 4.3B).

4.3.4 Tissue Processing and Sectioning for Confocal Microscopy Analysis in Transplanted Axolotl Hindlimbs

The right hindlimbs of recipient axolotls were collected at distinct time points after transplantation: 88 dpt for the F0 recipient (reaching a length of 14 cm from snout to tail tip), 55 dpt for the F1-1 recipient (reaching 7 cm), and 100 dpt for the F1-2 recipient (reaching 12 cm, Figure 4.4). The right hindlimbs of RFP-transgenic recipient axolotls were excised from the upper thigh and fixed overnight at 4°C in a 3.7% paraformaldehyde solution. Subsequently, these hindlimbs were vertically embedded in Cryomatrix (Thermo Scientific, Miami, FL, USA) and frozen at -80°C until ready for sectioning. The blocks containing the embedded limbs were then subjected to serial sectioning at a thickness of 8 μm, with sequential numbering commencing from the thigh end. To enable visualization, the sections were directly examined using a confocal microscope, and the nuclei were stained using Hoechst 34580 (Molecular Probes, Eugene, OR, USA) for enhanced contrast.

4.3.5 Imaging Approaches for Gross and Histological Analysis

Fluorescence images were captured using an Olympus SZX7 microscope (Olympus, Tokyo, Japan) equipped with an additional light-emitting diode illumination

device, facilitating the visualization of transgenic fluorescence. Furthermore, for a more detailed investigation of the transgenic fluorescence in the sections, imaging was performed on a ZEISS LSM 880 confocal microscope (Carl Zeiss Microscopy, Thornwood, NY, USA), enabling high-resolution imaging for comprehensive analysis and interpretation.

4.3.6 Discrimination of Muscle Fibers Based on Fluorescence Expression Using Confocal Microscopy

Green and red fluorescence images of the same area were acquired and merged into two layers using Adobe Photoshop CC (Adobe Inc., San Jose, CA, USA). Muscle fibers exhibiting exclusive green or red fluorescence were identified as green (G)-only and red (R)-only fibers, respectively. Fibers displaying both green and red fluorescence were categorized as red plus green (R+G) fibers (Figure 4.5). The quantities of these three types of fibers were determined through visual analysis on the screen, providing valuable insights into the distribution and composition of fluorescently labeled muscle fibers.
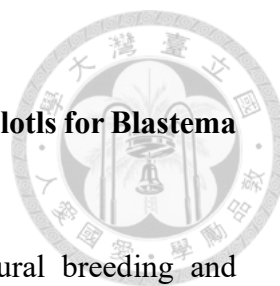
4.4 Results

4.4.1 Generation and Recognition of Fluorescent Transgenic Axolotls for Blastema Transplantation

Because of the unpredictability in achieving successful natural breeding and controlling the timing of egg laying, opting for IVF techniques (Figure 4.1) instead of relying on natural mating (Figure 4.2) can offer advantages. This approach not only reduces waiting time but also enables improved control over the timing of fertilized egg development. The generation of EGFP- and RFP-transgenic axolotls from the F0 and F1 generations, which were raised until the juvenile stage before undergoing blastema transplantation. These transgenic axolotls displayed distinguishable fluorescent colors that were readily discernible even under daylight conditions, facilitating their identification and tracking during experiments (Figure 4.3A).

4.4.2 Development of Green Regenerating Tissue in Red Recipient Axolotl Hindlimbs

The distal parts of the lost hindlimbs gradually regenerated, exhibiting a green coloration, as depicted in Figure 4.4. The speed of regeneration displayed an inverse correlation with body length, with the F0 axolotl reaching the LD stage at 45 dpt, F1-1 at 17 dpt, and F1-2 at 26 dpt. This indicates that regeneration was fastest in F1-1 and slowest in F0. The respective harvesting time and corresponding body length were 88 dpt and 14 cm in F0 (Figure 4.4A), 55 dpt and 7 cm in F1-1 (Figure 4.4B), and 100 dpt and 12 cm in F1-2 (Figure 4.4C). Notably, an intriguing observation in the F1-2 recipient axolotl was the presence of a narrow dorsal muscle with green fluorescence extending from the regenerating tissue all the way up to the pelvis since 88 dpt, as indicated by the green arrowheads in Figure 4.4C.

4.4.3 Fluorescence Imaging and Analysis of Muscle Fiber Types in Transplanted Axolotl Hindlimbs

Figure 4.5 displays the categorization of muscle fibers into three groups: R-only, G-only, and R+G. Based on careful analysis, the R-only fibers are derived from the recipient parental part, while the G-only fibers originate from the transplanted green blastema. The presence of R+G fibers indicates a fusion or connection event between progenitor cells or fibers from both parts.

Figure 4.6 illustrates a series of images showing representative sections of the F0 axolotl. In the proximal parental parts (above the knee), the majority of fibers were classified as R-only (69%-93%, Fig. 4.6B-D and G). A smaller proportion consisted of R+G fibers (0.7%-30%), while G-only fibers were scarce (0-5%). It is noteworthy that during this stage, most of the EGFP+ fibers (including R+G and G-only) were located at the periphery of the major muscle gracilis (GRA, Figure 4.6C and D). Interestingly, a small bundle of muscle fibers in section No. 75 (indicated by an arrow in Figure 4.6D) exhibited characteristics of G-only fibers. Moving to the sections below the knee (Figure 4.6E and F), the ventral muscles also contained RFP+ fibers, with a predominance of R+G (36%) and a few R-only (4%) fibers. Intriguingly, in Figure 4.6F, section No. 124 of the calf revealed that RFP+ fibers were exclusively confined to the ventral superficial muscles, specifically ischioflexorius (ISF), flexor digitorum communis (FDC), and femorofibularis (FMFB), while deep muscles such as interosseus cruris (IOC) did not contain RFP+ fibers. The dorsal muscles, including extensor cruris tibialis (ECT), extensor tarsi tibialis (ETT), extensor digitorum longus (EDL), and extensor cruris et tarsi fibularis (ECTF), did not show any RFP+ fibers. The muscle nomenclature follows established conventions (143, 177).

Figure 4.7 displays a selection of images showing sections at the thigh level from F1-1 and F1-2 axolotls. Firstly, in the F1-2 axolotl depicted in Figure 4.4C, I focused

on the narrow EGFP+ dorsal muscle and identified it as tenuissimus (T) at a very proximal level (No. 47, Figure 4.5A). Upon closer examination (Figure 4.7A1 and A2), it was evident that all the EGFP+ fibers were classified as R+G fibers. Interestingly, the R+G fibers (located to the right of the dashed line) appeared larger in size compared to the R-only fibers (located to the left of the dashed line).

Additionally, I compared the cross sections of F1-1 (Figure 4.7B, No. 57) and F1-2 (Figure 4.7C, No. 107) at approximately similar thigh levels. Both sections exhibited similar structures of pubotibialis (PTB) and GRA muscles. Consistent with the observations in the F0 axolotl at the thigh level (Figure 4.6D), EGFP+ fibers in F1-1 (Figure 4.7B, B1, and B2) were predominantly located at the outer periphery of GRA. These muscle fibers were mostly R-only (60%) with only a few G-only fibers (2%). However, in F1-2, EGFP+ fibers appeared to be evenly distributed within GRA (Figure 4.7C, C1, and C2). These findings suggest that the reconnection of muscle fibers in GRA occurred from the outer periphery towards the inner side. Both animals showed RFP+ staining in the epidermis at this level.

Figure 4.8 displays selected photographs of sections below the knee from F1-1 and F1-2 axolotls. Consistent with the observations in the F0 axolotl, both F1-1 and F1-2 showed a lack of RFP+ fibers in the dorsal muscles ECT, ETT, EDL, and ETCF, as well as in the deep ventral muscle IOC (Figure 4.6A and D). However, the superficial ventral muscles ISF, FDC, and FMFB in F1-1 exhibited RFP+ fibers (Figure 4.8A). The presence of RFP+ fibers extended to the ankle (Figure 4.8B) and the foot (Figure 4.8C) in FDC. The majority of fibers in FDC were classified as R+G (45% to 84%), with a small percentage of R-only (6% to 15%) and G-only fibers (4% to 48%). The section level shown in Figure 4.6D for F1-2 was higher than that in Figure 4.8A for F1-1, and it revealed the presence of RFP+ fibers in the ventral superficial muscles, including

adductor femoris (ADD), PTB, GRA, FMFB, and ISF. Strikingly, FDC in F1-2 did not contain any RFP+ fibers (Figure 4.8D and E).
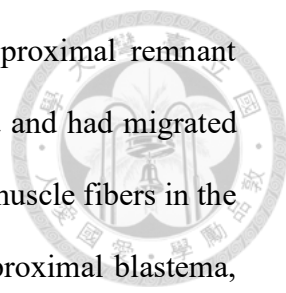
Interestingly, numerous RFP+ chondrocytes were observed at the proximal calf level (Figure 4.8A1), a few at the ankle level (Figure 4.8B1), and none at the foot level (Figure 4.8C1). Curiously, approximately half of the circumference of epidermal cells at the proximal calf (Figure 4.8A), ankle (Figure 4.8B), and foot (Figure 4.8C) exhibited RFP+ staining in F1-1. However, in F1-2, only a very small area of the proximal calf displayed RFP+ staining (Figure 4.8D), and no RFP+ staining was observed at the ankle level (Figure 4.8E).

4.5 Discussion

The previous studies using histology (168) and MRI (169) have demonstrated that during the LD stage of axolotl limb regeneration, the newly formed distal muscles are initially separate from the parental muscles, creating a gap between them. It is only in later stages that the regenerated muscle fibers grow and extend proximally to reconnect with the fibers in the parental muscles. Although MRI imaging confirmed the overall continuity between remnant and regenerative muscle fibers, it lacked the resolution to visualize individual muscles in detail. To address this limitation, we developed a double fluorescence chimeric limb regeneration technique to investigate the reconnection at the level of individual muscle fibers.

Previous studies have employed the transplantation of GFP+ blastemas into wild-type axolotls to investigate the proximo-distal outcome of limb regeneration (154, 178). However, this approach does not allow for differentiation between muscle tissue that is solely derived from the transplanted blastema and muscle tissue that results from fusion between GFP+ and wild-type cells.

Consistent with our previous findings, the chimeric limb regeneration technique used in this study also identified the presence of R+G fibers in the proximal parental muscles (Figures 4.6 and 4.7). The presence of these fibers strongly indicated that a reconnection had taken place between fibers from both sides before tissue harvesting. There were only a few G-only fibers (0 to 5%) observed in these parental muscles. Our hypothesis is that these G-only fibers represent fibers extending from the EGFP+ regenerative part that have not yet encountered the appropriate fibers to establish a connection with in the corresponding remnant muscles. Similar observations of GFP+ muscle fibers in the proximal region have been reported in previous studies involving GFP to wild type transplantation (154, 178). Therefore, it has been suggested that muscle cells exhibit a limitation on distal transformation (179). Nacu et al. also

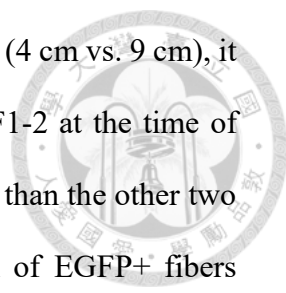,   109

demonstrated the presence of PAX7+GFP+ satellite cells in the proximal remnant muscles, which were likely derived from the transplanted blastema and had migrated proximally (154). As a result, the authors suggested that the GFP+ muscle fibers in the proximal remnant muscles originated from myogenic cells in the proximal blastema, rather than through cell fusion. However, we propose an alternative explanation for the presence of GFP+ muscles in the proximal muscles observed in their studies: these muscles arise from the reconnection between remnant and regenerating muscle fibers. This explanation is biologically more plausible for two reasons. Firstly, it is more challenging for regenerative muscle fibers to grow upwards towards distant sites of origin compared to reconnection. Secondly, the pre-existing fibers still remain in the remnant muscles. Therefore, if the newly formed GFP+ muscle fibers were independent of the remnant muscle fibers, the number of muscle fibers within a muscle would double, which is not observed.

Figure 4.6D displays a small cluster of muscle fibers consisting predominantly of G-only fibers. The exact cause for this observation remains unclear. It is possible that the corresponding parental muscle segment was damaged or retracted upward, potentially due to its different physical elastic properties compared to the other muscles.

The findings from this study indicate that the process of reconnection between muscle fibers was not synchronized, with variations in timing observed among individual muscles. The T muscle exhibited the fastest reconnection in F1-2, but this was not consistent across the other cases.

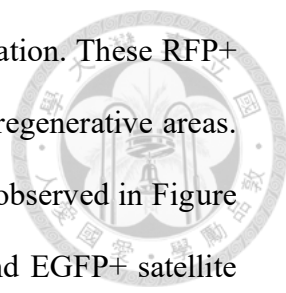Another significant discovery in this study is the observation that the reconnection process appears to initiate from the outer edges of the muscles, as exemplified by the GRA muscle (Figure 4.6C, 4.6D, and 4.7B). Based on this observation, the regenerative stage at the time of tissue collection in F0 (43 days after reaching the LD stage) and F1-1 (38 days after reaching the LD stage) appeared to be

very similar. Since F1-1 was initially smaller in size compared to F0 (4 cm vs. 9 cm), it regenerated at a faster rate. In contrast, the regenerative stage of F1-2 at the time of harvest (74 days after reaching the LD stage) was significantly later than the other two cases. The GRA muscle in F1-2 exhibited a uniform distribution of EGFP+ fibers (Figure 4.7C1). These findings strongly suggest that the reconnection process starts from the outer regions (in F0 and F1-1) before being completed (in F1-2). This pattern of reconnection from the periphery is a rational approach for achieving perfect regeneration. It allows for muscle mass confinement and facilitates the meeting and reconnection of individual interior fibers with their corresponding parental fibers.

The exact mechanism of reconnection between fibers from both parts, whether it occurs end-to-end, end-to-side, or side-to-side, or through fusion mediated by newly proximal green satellite cells, remains unknown (as noted by Nacu et al. (154). However, this reconnection process may result in an increase in the thickness of the reconnected muscle fibers, as depicted in Figure 4.7A2. The molecular and cellular mechanisms responsible for coordinating individual regenerating muscle fibers to accurately locate and connect with their corresponding parental fibers are intriguing and warrant further investigation. Currently, our studies have not determined the exact completion time for this reconnection process.

It is intriguing to note that RFP+ fibers were observed in the calf muscles, which are newly regenerative parts located below the amputation plane (as seen in Figure 4.6F, 4.8A, and 4.8D). Despite being present in small quantities (2% to 4% in F0 and 6% to 15% in F1-1, as shown in Figure 4.6E, 4.6F, and 4.8A-C), R-only fibers were also identified. Previous studies (32, 158, 168) have indicated that satellite cells in the remnant muscles of axolotls migrate distally to contribute to muscle regeneration following limb amputation. Therefore, it is likely that RFP+ satellite cells in the remnant muscles of the freshly amputated thigh migrated across the transplantation

interface into the regenerating part to participate in muscle regeneration. These RFP+ satellite cells subsequently differentiated into muscle fibers in the regenerative areas. The majority of the RFP+ fibers displayed R+G characteristics (as observed in Figure 4.6E and F), indicating the possibility of fusion between RFP+ and EGFP+ satellite cells or connection between differentiated RFP+ and EGFP+ fibers during this stage. The presence of R-only fibers from the upper calf to the foot area (6% to 15%, as shown in Figure 4.8A, B, and C) suggests that these fibers could independently contribute to the regenerative parts.

An intriguing observation is that RFP+ fibers in the calf area were exclusively present in the superficial ventral muscles, namely ISF, FDC, PTB, and FMFB. Figure 4.8C demonstrates that the contribution of RFP+ fibers extended to at least the foot level in FDC. In contrast, the dorsal muscles ECT, ETT, EDL, and ECTF, as well as the deep ventral muscle IOC, did not exhibit any RFP+ fibers. These dorsal muscles originate from femoral epicondyles or tibial condyles, while the ventral muscles (ISF and PTB) originate from the pelvic bone and FMFB originates from the middle femur. It is conceivable that the dorsal muscles are located below the amputation plane and are completely lost during the amputation process, while the superficial ventral muscles pass through the amputation plane and are affected by the cutting during the procedure. The transplanted blastemas already contain early-coming EGFP+ satellite cells; however, after amputation and transplantation, the remnant muscles may give rise to late-coming RFP+ satellite cells that migrate through the amputation plane into the regenerative part. These satellite cells may exhibit a sense of commitment. In the ventral superficial muscles, the late-coming RFP+ satellite cells may possess self-commitment, enabling them to compete with or join the early-coming EGFP+ satellite cells and contribute to the growth of the regenerative parts. However, on the dorsal side, the early-coming EGFP+ satellite cells may dominate the regeneration, resulting in the

failure of the late-coming RFP+ satellite cells to contribute. An intriguing question is: where do the late-coming RFP+ satellite cells on the dorsal side go? This issue remains unknown and warrants further investigation.

Regarding cartilage regeneration, RFP+ chondrocytes were found to contribute to the regenerative parts in the proximal calf but not in the distal region. This suggests that the patterning of distal cartilage had already been determined in the EGFP+ mid bud-stage blastema.

Interestingly, the distribution of RFP+ and EGFP+ epidermis in the regenerative parts differed between F1-1 and F1-2. In F1-1, the epidermis appeared as a mix of RFP+ and EGFP+, while in F1-2, the majority of the epidermis was EGFP+. These findings contradict a previous report, where they observed complete replacement of the grafted GFP+ blastema epidermis by host epidermis (178). The reason for this discrepancy is unknown and may be attributed to technical issues during the transplantation experiment, such as the inclusion of a small portion of EGFP+ stump tissue with the blastema, which could have prevented host RFP+ epidermis replacement.

The use of blastema transplantation between different color transgenic axolotls has led to the discovery of intriguing new findings regarding muscle regeneration in the late stages of limb regeneration, as described above. However, there are still many unknown phenomena that require further investigation.

4.6 Figures

In *vitro* fertilization, plasmid injection, and embryo development
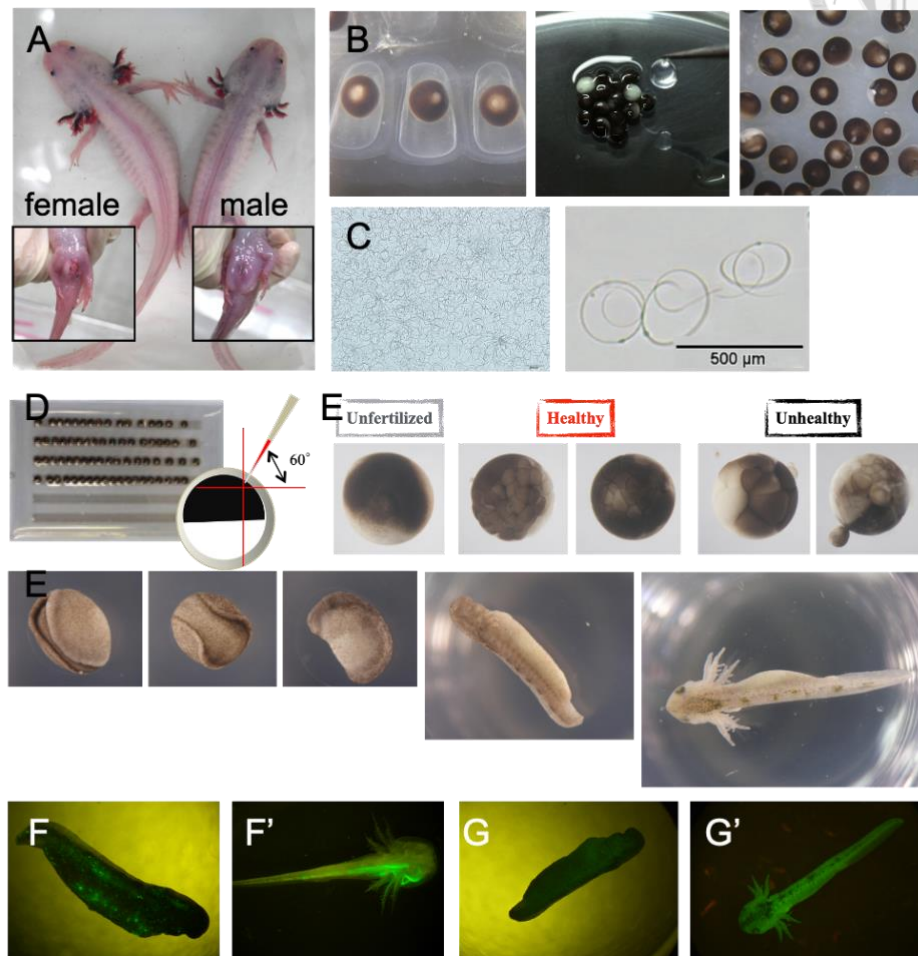
Figure 4.1 Establishment of IVF and Transgenic Techniques in Axolotls. (A) Morphological distinctions between male and female axolotls were readily apparent, primarily in the location of the cloaca. (B) Following hormonal stimulation, eggs were extracted from axolotls. These eggs were enclosed within protective egg shells, which were carefully removed using tweezers. Only healthy eggs were selected for subsequent IVF procedures. (C) Semen was collected from axolotls through abdominal massage. Axolotl sperm could be visualized under a microscope, resembling fine hairs. The right image provides a magnified view. (D) The microinjection technique was employed, where fertilized eggs were placed on an agarose gel platform. An injection needle, filled with a plasmid containing a fluorescent sequence, was used to inject the eggs at a 60°

,   114

angle. (E) Within two to three days after microinjection, microscopic observations revealed unfertilized eggs, healthy embryos, and embryos with developmental abnormalities. As the embryos developed, axolotl embryos underwent a metamorphosis from a spherical shape to a tadpole-like shape, and finally to a fish-like shape. (F) The F0 EGFP-embryo exhibited chimeric fluorescence, indicating the presence of different cell populations with varying fluorescent patterns. (F') Depicts the larval stage. (G) The F1 EGFP-embryo displayed uniform fluorescence throughout its body, indicating the inheritance of the fluorescent gene. (G') Depicts the larval stage.
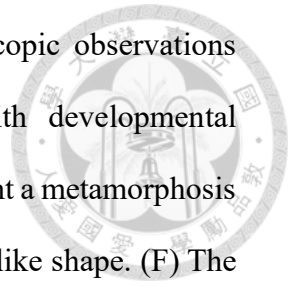
**In *vivo* fertilization
(natural mating)**
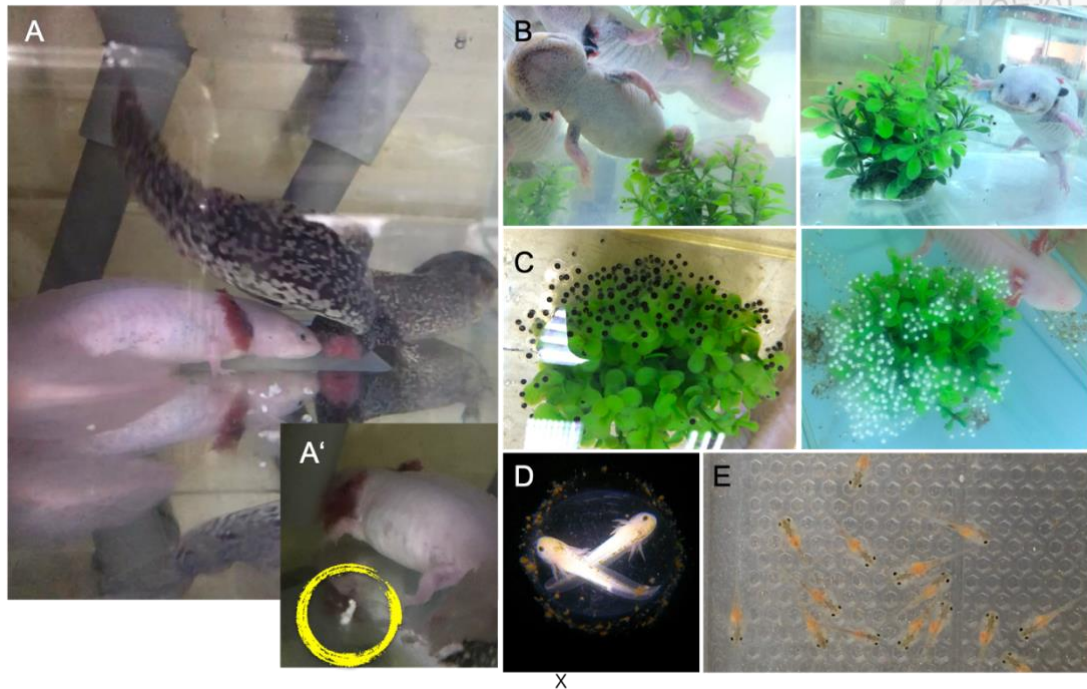
Figure 4.2 The Natural Breeding Process in Axolotls. (A) Spawning was initiated by the male axolotl, which swam around, raised its tail, and displayed vigorous writhing motions. The male occasionally nudged the female's vent and then guided her around the tank. (A') The male then deposited spermatophores, which were packets of sperm attached to the top of jelly cones. Typically, the male placed between 3 and 10 spermatophores around the tank and attempted to lead the female over them. If the female was satisfied with the male's courting dance, she responded by nudging his cloaca to incite him to deposit his spermatophores. During this process, the female picked up the sperm cap from each spermatophore using her cloaca, enabling internal fertilization to occur. She may also have nudged the male's vent, resulting in a prolonged "dance" between the two axolotls around the tank. (B) Between a few hours and two days later, the female commenced spawning, laying eggs on the leaves of plants. (C) There may have been between 100 and over a thousand eggs laid in one spawning. The color of the eggs depended on the female, but as they developed, the axolotl larvae

gently showed their colors. (D) An unhatched embryo (a twin). (E) Hatched axolotl larvae that have eaten brine shrimp.
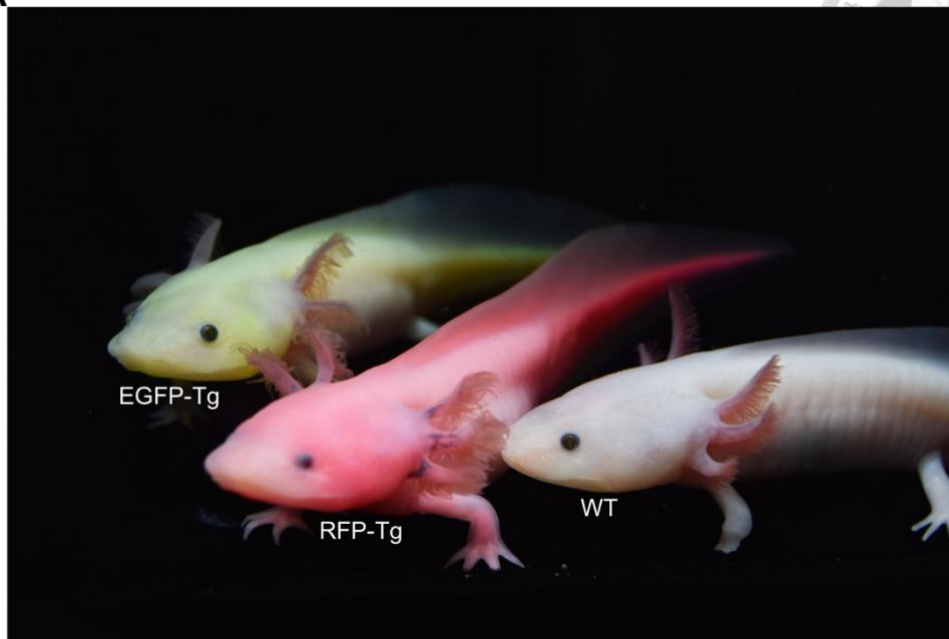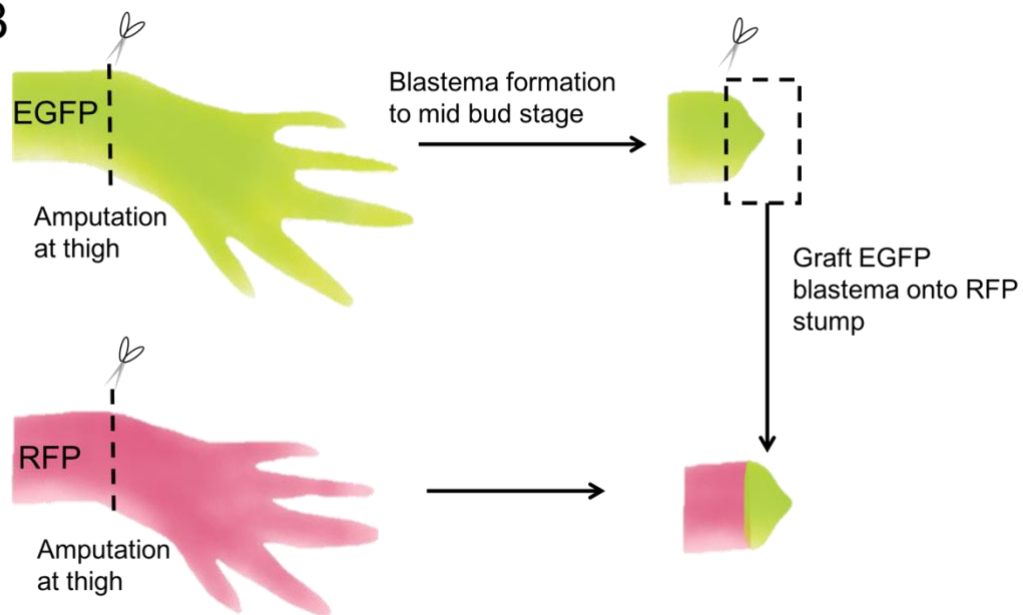
Figure 4.3 Generation of Fluorescence Transgenic Axolotls and Schema of Blastema Transplantation. (A) Fluorescence transgenic axolotls, characterized by their distinct EGFP and RFP fluorescence, were easily distinguishable under daylight conditions. (B) Schematic representation of the blastema transplantation process. A green mid bud-stage blastema, derived from EGFP-transgenic axolotls, was transplanted onto the corresponding red stump of RFP-transgenic axolotls. The

abbreviations used in the schema were as follows: EGFP-Tg = EGFP-transgenic; RFP-

Tg = RFP-transgenic; WT = wild type.
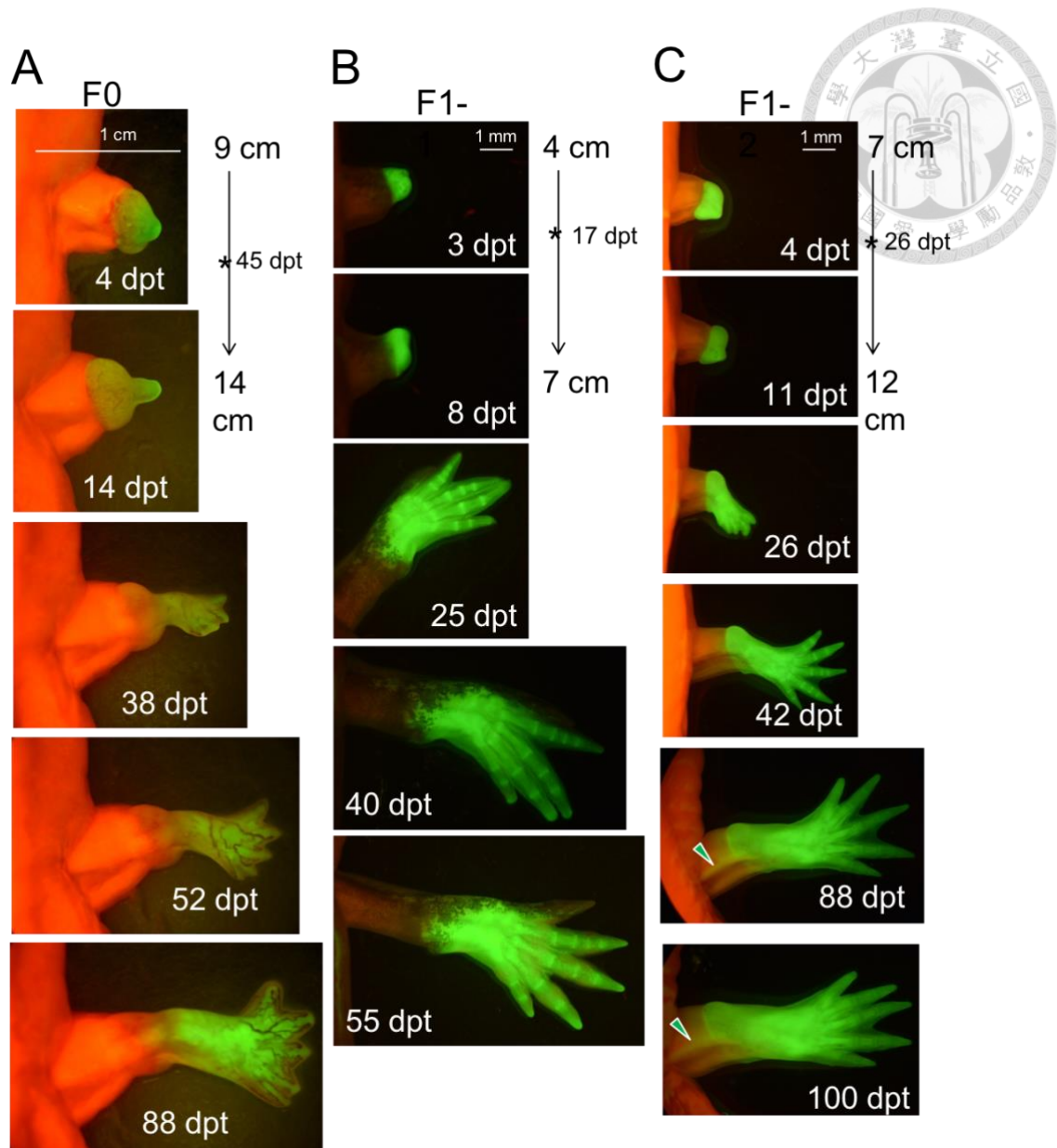
Figure 4.4 Progressive Regeneration and Growth of Double Fluorescence Chimeric Hindlimbs. (A) F0 axolotl: Time-lapse images showcasing the regeneration and growth of the double fluorescence chimeric hindlimb over a series of time points. The dpt are indicated. The corresponding body length of the axolotl from the day of transplantation to the day of limb harvesting is provided. Asterisks (*) highlight the dates when the axolotl reached the late differentiation stage. (B) F1-1 axolotl: Similar progression of regeneration and growth as observed in F0, with corresponding time points, body length measurements, and asterisks (*) indicating the late differentiation

stage. (C) F1-2 axolotl: Continued regeneration and growth of the double fluorescence chimeric hindlimb, with time points, body length measurements, and asterisks (*) representing the attainment of the late differentiation stage. Scale bar in A= 1cm; in B and C = 1 mm
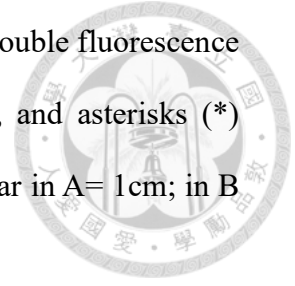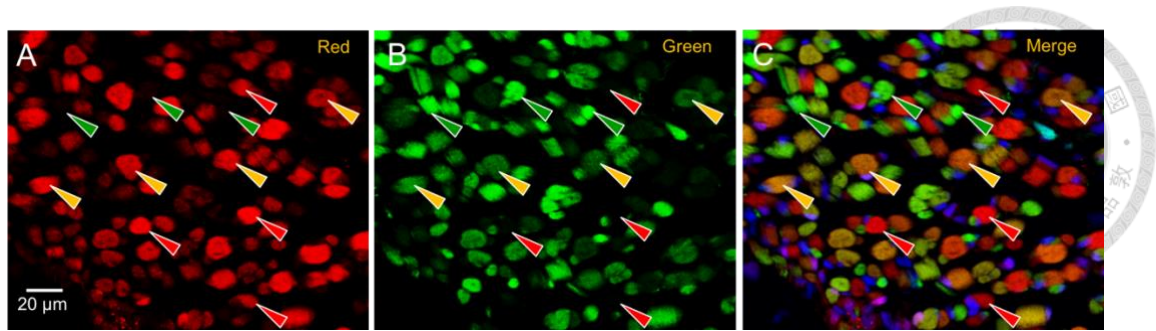
Figure 4.5 The Differentiation of Muscle Fibers Based on Their Fluorescence Expression. This figure illustrates the differentiation of muscle fibers based on their fluorescence expression. Muscle fibers displaying green fluorescence alone are labeled as G-only fibers (indicated by green arrowheads), while those exhibiting red fluorescence alone are identified as R-only fibers (indicated by red arrowheads). Fibers showing both green and red fluorescence are categorized as R+G fibers (indicated by yellow arrowheads).
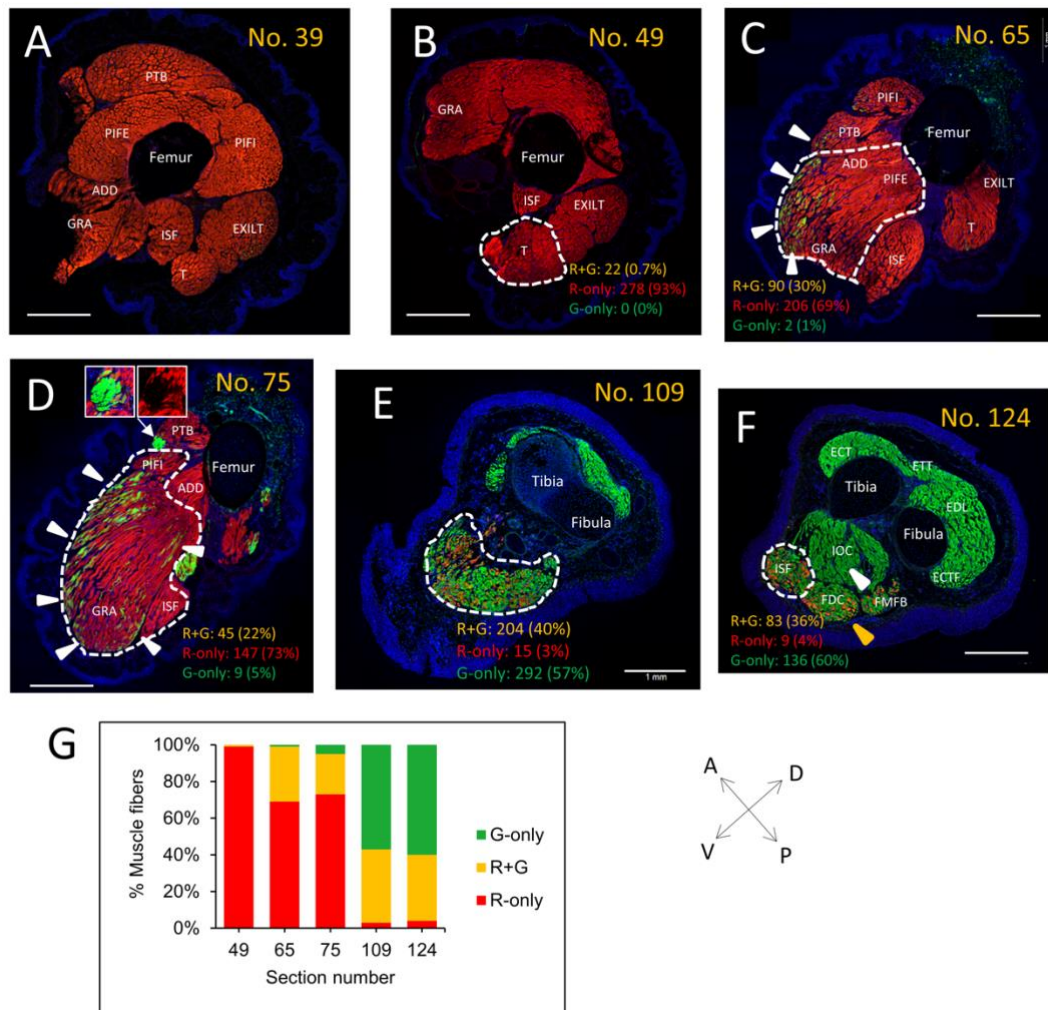
Figure 4.6 Fluorescence Histology of Representative Sections in the F0 Axolotl, as Indicated by Section Numbers. (A) to (F) display selected images corresponding to the indicated sections. The axes are denoted by double arrows, with D representing dorsal, V representing ventral, A representing anterior, and P representing posterior. The femur, tibia, and fibula are labeled in each section. The dash-line circles highlight the regions where muscle fibers were counted for R-only, G-only, and R+G, respectively. In (C) and (D), white arrowheads outline the green-colored muscle fibers, predominantly R+G with a few G-only fibers, which are often located at the periphery of the muscles. A white arrow in (D) indicates an intriguing area containing mostly G-only fibers. The bar chart (G) presents the percentage of R-only, R+G, and G-only muscle fibers in the circled regions of representative sections.
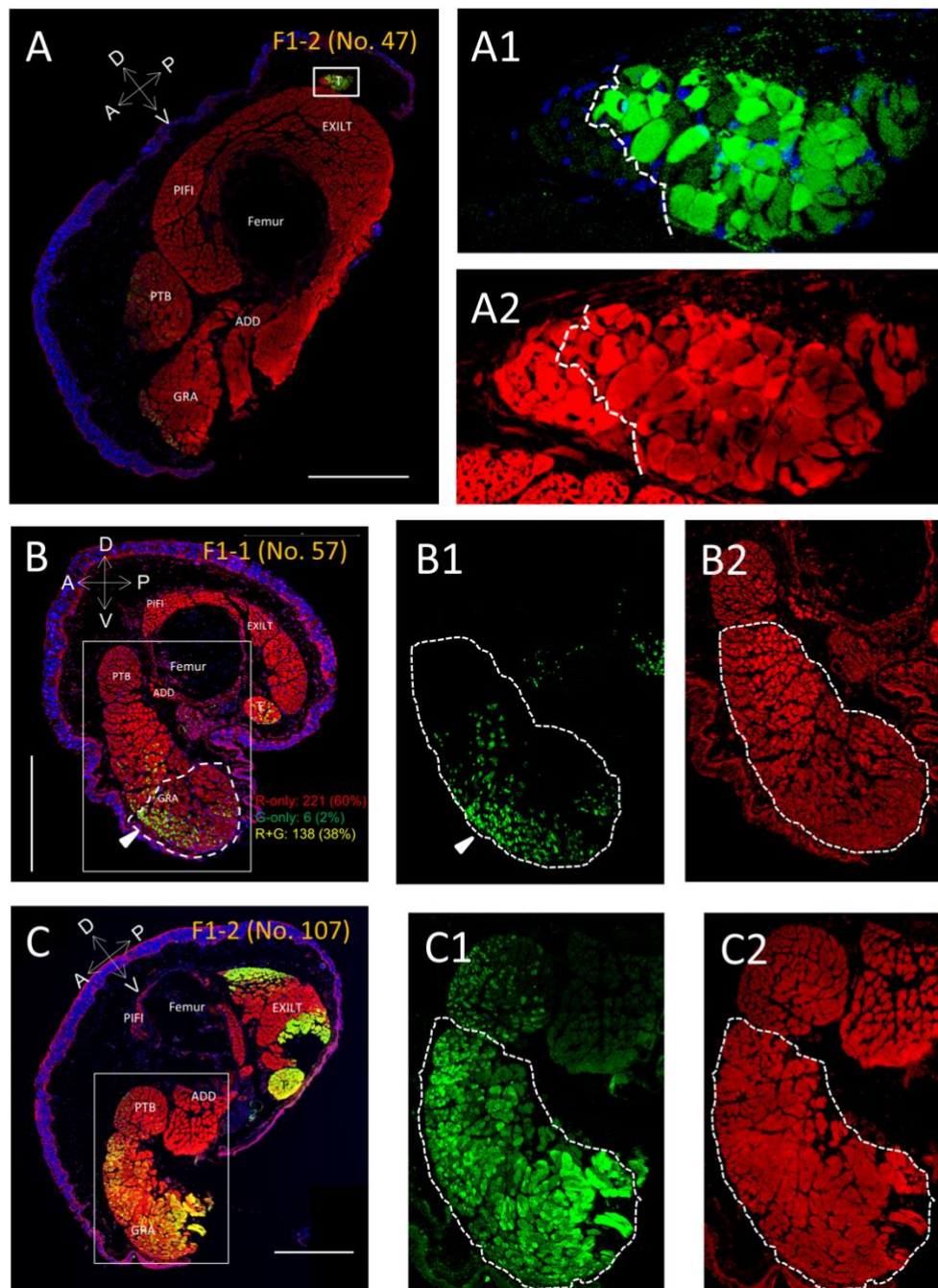
Figure 4.7 Fluorescence Images of the Proximal Thigh in Axolotls F1-1 and F1-2.

This figure displays representative fluorescence images of the proximal thigh in axolotls F1-1 and F1-2. In F1-2, the presence of EGFP+ muscle extending to the proximal dorsal region, as shown in Fig. 2C, was identified as T. Enlarged photos of the boxed area in (A) were presented in green (A1) and red (A2). A dashed line separates

the group of R-only fibers (left) from R+G fibers (right). Images depicting a similar level of the thigh in F1-1 (B) and F1-2 (C) were shown. Boxed areas encompassing the gracilic muscle in (B) and (C) were respectively represented in green (B1 and C1) and red (B2 and C2). White arrowheads on (B) and (B1) indicate the outer periphery where green fluorescence-containing fibers were located. In contrast, the EGFP+ fibers in this area of (C) were uniformly distributed in (C1). The muscle fibers within the circled region in (B) were quantified. Scale bars = 1 mm. Axes were denoted by double arrows.
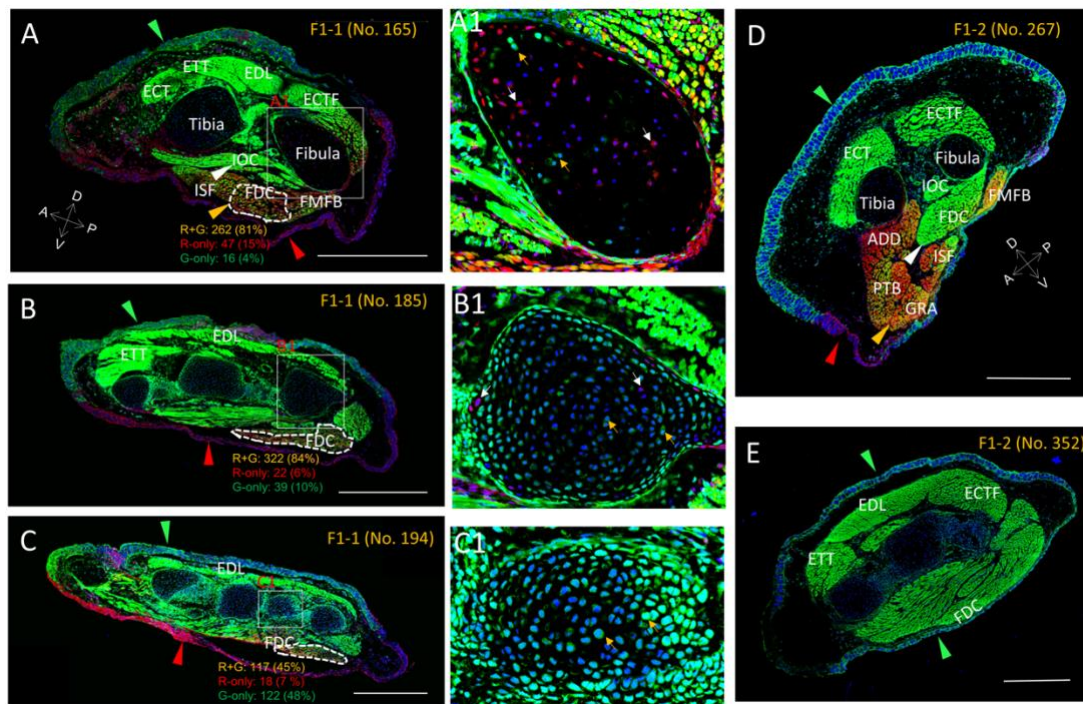
Figure 4.8 Below-Knee Section Images in F1-1 and F1-2. This figure presents representative below-knee section images in F1-1 and F1-2. It includes the upper calf (A), ankle (B), and foot (C) in F1-1, as well as the upper calf (D) and ankle (E) in F1-2. The EGFP-expressing skin is indicated by green arrowheads, while the RFP-expressing skin is indicated by red arrowheads. The calf deep muscle without red fluorescence is marked by white arrowheads, and the calf ventral muscles with red fluorescence are highlighted by yellow arrowheads. The boxed skeletal areas in (A), (B), and (C) are magnified in (A1), (B1), and (C1), respectively. Red chondrocytes are marked by white arrows, and green chondrocytes are denoted by yellow arrows. Muscle fibers within the circled regions in (A), (B), and (C) were quantified. Scale bars = 1 mm, and axes were indicated by double arrows.

Reference

1. Dawn B, Bolli R. Adult bone marrow-derived cells: regenerative potential, plasticity, and tissue commitment. Basic Res Cardiol. 2005;100(6):494-503.

2. Iismaa SE, Kaidonis X, Nicks AM, Bogush N, Kikuchi K, Naqvi N, et al. Comparative regenerative mechanisms across different mammalian tissues. npj Regenerative Medicine. 2018;3(1):6.

3. Patten J, Wang K. Fibronectin in development and wound healing. Adv Drug Deliv Rev. 2021;170:353-68.

4. Wu MY, Hill CS. Tgf-beta superfamily signaling in embryonic development and homeostasis. Dev Cell. 2009;16(3):329-43.

5. Ramirez H, Patel SB, Pastar I. The Role of TGFβ Signaling in Wound Epithelialization. Adv Wound Care (New Rochelle). 2014;3(7):482-91.

6. Penn JW, Grobbelaar AO, Rolfe KJ. The role of the TGF-β family in wound healing, burns and scarring: a review. Int J Burns Trauma. 2012;2(1):18-28.

7. Clevers H. Wnt/beta-catenin signaling in development and disease. Cell. 2006;127(3):469-80.

8. Steinhart Z, Angers S. Wnt signaling in development and tissue homeostasis. Development. 2018;145(11).

9. Whyte JL, Smith AA, Helms JA. Wnt signaling and injury repair. Cold Spring Harb Perspect Biol. 2012;4(8):a008078.

10. Diller RB, Tabor AJ. The Role of the Extracellular Matrix (ECM) in Wound Healing: A Review. Biomimetics (Basel). 2022;7(3).

11. Walma DAC, Yamada KM. The extracellular matrix in development. Development. 2020;147(10).

12. Martin P. Wound healing--aiming for perfect skin regeneration. Science. 1997;276(5309):75-81.

13. Gurtner GC, Werner S, Barrandon Y, Longaker MT. Wound repair and regeneration. Nature. 2008;453(7193):314-21.

14. Raja, Sivamani K, Garcia MS, Isseroff RR. Wound re-epithelialization: modulating keratinocyte migration in wound healing. Front Biosci. 2007;12:2849-68.

15. Chuong CM, Randall VA, Widelitz RB, Wu P, Jiang TX. Physiological regeneration of skin appendages and implications for regenerative medicine. Physiology (Bethesda). 2012;27(2):61-72.

16. Wagner DE, Wang IE, Reddien PW. Clonogenic neoblasts are pluripotent adult stem cells that underlie planarian regeneration. Science. 2011;332(6031):811-6.

17. van Wolfswinkel JC, Wagner DE, Reddien PW. Single-cell analysis reveals functionally distinct classes within the planarian stem cell compartment. Cell Stem

Cell. 2014;15(3):326-39.

18. Wittlieb J, Khalturin K, Lohmann JU, Anton-Erxleben F, Bosch TC. Transgenic Hydra allow in vivo tracking of individual stem cells during morphogenesis. Proc Natl Acad Sci U S A. 2006;103(16):6208-11.

19. Hemmrich G, Khalturin K, Boehm AM, Puchert M, Anton-Erxleben F, Wittlieb J, et al. Molecular signatures of the three stem cell lineages in hydra and the emergence of stem cell function at the base of multicellularity. Mol Biol Evol. 2012;29(11):3267-80.

20. Major RJ, Poss KD. Zebrafish Heart Regeneration as a Model for Cardiac Tissue Repair. Drug Discov Today Dis Models. 2007;4(4):219-25.

21. Pfefferli C, Jaźwińska A. The art of fin regeneration in zebrafish. Regeneration (Oxf). 2015;2(2):72-83.

22. Sehring I, Mohammadi HF, Haffner-Luntzer M, Ignatius A, Huber-Lang M, Weidinger G. Zebrafish fin regeneration involves generic and regeneration-specific osteoblast injury responses. Elife. 2022;11.

23. Flowers GP, Sanor LD, Crews CM. Lineage tracing of genome-edited alleles reveals high fidelity axolotl limb regeneration. Elife. 2017;6.

24. Tu S, Johnson SL. Fate restriction in the growing and regenerating zebrafish fin. Dev Cell. 2011;20(5):725-32.

25. Hou Y, Lee HJ, Chen Y, Ge J, Osman FOI, McAdow AR, et al. Cellular diversity of the regenerating caudal fin. Sci Adv. 2020;6(33):eaba2084.

26. Poss KD, Wilson LG, Keating MT. Heart regeneration in zebrafish. Science. 2002;298(5601):2188-90.

27. Jopling C, Sleep E, Raya M, Martí M, Raya A, Belmonte JCI. Zebrafish heart regeneration occurs by cardiomyocyte dedifferentiation and proliferation. Nature. 2010;464(7288):606-9.

28. Ebert AD, Diecke S, Chen IY, Wu JC. Reprogramming and transdifferentiation for cardiovascular development and regenerative medicine: where do we stand? EMBO Mol Med. 2015;7(9):1090-103.

29. Gargioli C, Slack JM. Cell lineage tracing during Xenopus tail regeneration. Development. 2004;131(11):2669-79.

30. Rodrigues AM, Christen B, Marti M, Izpisua Belmonte JC. Skeletal muscle regeneration in Xenopus tadpoles and zebrafish larvae. BMC Dev Biol. 2012;12:9.

31. Kragl M, Knapp D, Nacu E, Khattak S, Maden M, Epperlein HH, et al. Cells keep a memory of their tissue origin during axolotl limb regeneration. Nature. 2009;460(7251):60-5.

32. Sandoval-Guzman T, Wang H, Khattak S, Schuez M, Roensch K, Nacu E, et al. Fundamental differences in dedifferentiation and stem cell recruitment during skeletal

muscle regeneration in two salamander species. Cell Stem Cell. 2014;14(2):174-87.

33.   Wang H, Loof S, Borg P, Nader GA, Blau HM, Simon A. Turning terminally differentiated skeletal muscle cells into regenerative progenitors. Nat Commun. 2015;6:7916.

34.   Porrello ER, Mahmoud AI, Simpson E, Hill JA, Richardson JA, Olson EN, et al. Transient regenerative potential of the neonatal mouse heart. Science. 2011;331(6020):1078-80.

35.   Storer MA, Miller FD. Cellular and molecular mechanisms that regulate mammalian digit tip regeneration. Open Biol. 2020;10(9):200194.

36.   Dolan CP, Imholt F, Yang TJ, Bokhari R, Gregory J, Yan M, et al. Mouse Digit Tip Regeneration Is Mechanical Load Dependent. J Bone Miner Res. 2022;37(2):312-22.

37.   Yoon JH, Cho K, Garrett TJ, Finch P, Maden M. Comparative Proteomic Analysis in Scar-Free Skin Regeneration in Acomys cahirinus and Scarring Mus musculus. Sci Rep. 2020;10(1):166.

38.   Maden M, Brant JO. Insights into the regeneration of skin from Acomys, the spiny mouse. Exp Dermatol. 2019;28(4):436-41.

39.   Mastellos DC, Deangelis RA, Lambris JD. Inducing and characterizing liver regeneration in mice: Reliable models, essential "readouts" and critical perspectives. Curr Protoc Mouse Biol. 2013;3(3):141-70.

40.   Pibiri M. Liver regeneration in aged mice: new insights. Aging (Albany N Y). 2018;10(8):1801-24.

41.   Dekaney CM, Gulati AS, Garrison AP, Helmrath MA, Henning SJ. Regeneration of intestinal stem/progenitor cells following doxorubicin treatment of mice. Am J Physiol Gastrointest Liver Physiol. 2009;297(3):G461-70.

42.   Slorach EM, Campbell FC, Dorin JR. A mouse model of intestinal stem cell function and regeneration. J Cell Sci. 1999;112 Pt 18:3029-38.

43.   Shieh SJ, Cheng TC. Regeneration and repair of human digits and limbs: fact and fiction. Regeneration (Oxf). 2015;2(4):149-68.

44.   Fernando WA, Leininger E, Simkin J, Li N, Malcom CA, Sathyamoorthi S, et al. Wound healing and blastema formation in regenerating digit tips of adult mice. Dev Biol. 2011;350(2):301-10.

45.   McCusker C, Bryant SV, Gardiner DM. The axolotl limb blastema: cellular and molecular mechanisms driving blastema formation and limb regeneration in tetrapods. Regeneration (Oxf). 2015;2(2):54-71.

46.   Min S, Whited JL. Limb blastema formation: How much do we know at a genetic and epigenetic level? J Biol Chem. 2023;299(2):102858.

47.   Hay ED, Fischman DA. Origin of the blastema in regenerating limbs of the newt

Triturus viridescens. An autoradiographic study using tritiated thymidine to follow cell proliferation and migration. Dev Biol. 1961;3:26-59.

48. Campbell LJ, Crews CM. Wound epidermis formation and function in urodele amphibian limb regeneration. Cell Mol Life Sci. 2008;65(1):73-9.

49. de Both NJ. The developmental potencies of the regeneration blastema of the axolotl limb. Wilhelm Roux Arch Entwickl Mech Org. 1970;165(3):242-76.

50. Muneoka K, Fox WF, Bryant SV. Cellular contribution from dermis and cartilage to the regenerating limb blastema in axolotls. Dev Biol. 1986;116(1):256-60.

51. Endo T, Bryant SV, Gardiner DM. A stepwise model system for limb regeneration. Dev Biol. 2004;270(1):135-45.

52. Satoh A, Gardiner DM, Bryant SV, Endo T. Nerve-induced ectopic limb blastemas in the Axolotl are equivalent to amputation-induced blastemas. Dev Biol. 2007;312(1):231-44.

53. Carlson JD, Maire JJ, Martenson ME, Heinricher MM. Sensitization of pain-modulating neurons in the rostral ventromedial medulla after peripheral nerve injury. J Neurosci. 2007;27(48):13222-31.

54. Kumar A, Godwin JW, Gates PB, Garza-Garcia AA, Brockes JP. Molecular basis for the nerve dependence of limb regeneration in an adult vertebrate. Science. 2007;318(5851):772-7.

55. Makanae A, Mitogawa K, Satoh A. Co-operative Bmp- and Fgf-signaling inputs convert skin wound healing to limb formation in urodele amphibians. Dev Biol. 2014;396(1):57-66.

56. Singer M, Inoue S. The Nerve and the Epidermal Apical Cap in Regeneration of the Forelimb of Adult Triturus. J Exp Zool. 1964;155:105-16.

57. Doi A, Park IH, Wen B, Murakami P, Aryee MJ, Irizarry R, et al. Differential methylation of tissue- and cancer-specific CpG island shores distinguishes human induced pluripotent stem cells, embryonic stem cells and fibroblasts. Nat Genet. 2009;41(12):1350-3.

58. Shi Y, Desponts C, Do JT, Hahm HS, Schöler HR, Ding S. Induction of pluripotent stem cells from mouse embryonic fibroblasts by Oct4 and Klf4 with small-molecule compounds. Cell Stem Cell. 2008;3(5):568-74.

59. Huangfu D, Maehr R, Guo W, Eijkelenboom A, Snitow M, Chen AE, et al. Induction of pluripotent stem cells by defined factors is greatly improved by small-molecule compounds. Nat Biotechnol. 2008;26(7):795-7.

60. Tweedell KS. The urodele limb regeneration blastema: the cell potential. ScientificWorldJournal. 2010;10:954-71.

61. Day RC, Beck CW. Transdifferentiation from cornea to lens in Xenopus laevis depends on BMP signalling and involves upregulation of Wnt signalling. BMC Dev
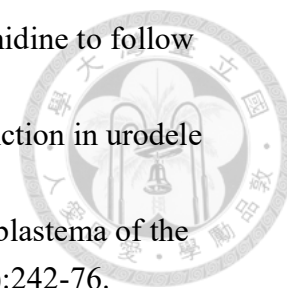
Biol. 2011;11:54.

62. Pearl EJ, Barker D, Day RC, Beck CW. Identification of genes associated with regenerative success of Xenopus laevis hindlimbs. BMC Dev Biol. 2008;8:66.

63. Malloch EL, Perry KJ, Fukui L, Johnson VR, Wever J, Beck CW, et al. Gene expression profiles of lens regeneration and development in Xenopus laevis. Dev Dyn. 2009;238(9):2340-56.

64. Shaw T, Martin P. Epigenetic reprogramming during wound healing: loss of polycomb-mediated silencing may enable upregulation of repair genes. EMBO Rep. 2009;10(8):881-6.

65. Kretsovali A, Hadjimichael C, Charmpilas N. Histone deacetylase inhibitors in cell pluripotency, differentiation, and reprogramming. Stem Cells Int. 2012;2012:184154.

66. Tseng AS, Carneiro K, Lemire JM, Levin M. HDAC activity is required during Xenopus tail regeneration. PLoS One. 2011;6(10):e26382.

67. Mochii M, Taniguchi Y, Shikata I. Tail regeneration in the Xenopus tadpole. Dev Growth Differ. 2007;49(2):155-61.

68. Rouhana L, Tasaki J. Epigenetics and Shared Molecular Processes in the Regeneration of Complex Structures. Stem Cells Int. 2016;2016:6947395.

69. Tassava RA, Mescher AL. The roles of injury, nerves, and the wound epidermis during the initiation of amphibian limb regeneration. Differentiation. 1975;4(1):23-4.

70. Brockes JP, Kumar A. Comparative aspects of animal regeneration. Annu Rev Cell Dev Biol. 2008;24:525-49.

71. Singer M. Trophic functions of the neuron. VI. Other trophic systems. Neurotrophic control of limb regeneration in the newt. Ann N Y Acad Sci. 1974;228(0):308-22.

72. Boilly B, Albert P. In vitro control of blastema cell proliferation by extracts from epidermal cap and mesenchyme of regenerating limbs of axolotls. Rouxs Arch Dev Biol. 1990;198(8):443-7.

73. Singer M, Salpeter MM. The bodies of Eberth and associated structures in the skin of the frog tadpole. J Exp Zool. 1961;147:1-19.

74. Satoh A, Cummings GM, Bryant SV, Gardiner DM. Neurotrophic regulation of fibroblast dedifferentiation during limb skeletal regeneration in the axolotl (Ambystoma mexicanum). Dev Biol. 2010;337(2):444-57.

75. Singer M. The influence of the nerve in regeneration of the amphibian extremity. Q Rev Biol. 1952;27(2):169-200.

76. Goss RJ. Regenerative inhibition following limb amputation and immediate insertion into the body cavity. Anat Rec. 1956;126(1):15-27.

77. Mescher AL. Effects on adult newt limb regeneration of partial and complete

skin flaps over the amputation surface. J Exp Zool. 1976;195(1):117-28.

78. Tassava RA, Garling DJ. Regenerative responses in larval axolotl limbs with skin grafts over the amputation surface. J Exp Zool. 1979;208(1):97-110.

79. Loyd RM, Tassava RA. DNA synthesis and mitosis in adult newt limbs following amputation and insertion into the body cavity. J Exp Zool. 1980;214(1):61-9.

80. Beck CW, Izpisua Belmonte JC, Christen B. Beyond early development: Xenopus as an emerging model for the study of regenerative mechanisms. Dev Dyn. 2009;238(6):1226-48.

81. Haberland M, Montgomery RL, Olson EN. The many roles of histone deacetylases in development and physiology: implications for disease and therapy. Nat Rev Genet. 2009;10(1):32-42.

82. Bolden JE, Peart MJ, Johnstone RW. Anticancer activities of histone deacetylase inhibitors. Nat Rev Drug Discov. 2006;5(9):769-84.

83. Spallotta F, Tardivo S, Nanni S, Rosati JD, Straino S, Mai A, et al. Detrimental effect of class-selective histone deacetylase inhibitors during tissue regeneration following hindlimb ischemia. J Biol Chem. 2013;288(32):22915-29.

84. Hu E, Dul E, Sung CM, Chen Z, Kirkpatrick R, Zhang GF, et al. Identification of novel isoform-selective inhibitors within class I histone deacetylases. J Pharmacol Exp Ther. 2003;307(2):720-8.

85. Hess-Stumpp H, Bracker TU, Henderson D, Politz O. MS-275, a potent orally available inhibitor of histone deacetylases--the development of an anticancer agent. Int J Biochem Cell Biol. 2007;39(7-8):1388-405.

86. Hoxha E, Lambers E, Ramirez V. HDAC1 plays an important role in the differentiation of embryonic stem cells and induced pluripotent stem cells into cardiovascular lineages. Developmental Biology 2011;356(1):221-221.

87. Wu CH, Tsai MH, Ho CC, Chen CY, Lee HS. De novo transcriptome sequencing of axolotl blastema for identification of differentially expressed genes during limb regeneration. BMC Genomics. 2013;14:434.

88. Farkas JE, Freitas PD, Bryant DM, Whited JL, Monaghan JR. Neuregulin-1 signaling is essential for nerve-dependent axolotl limb regeneration. Development. 2016;143(15):2724-31.

89. Farkas JE, Monaghan JR. Housing and maintenance of Ambystoma mexicanum, the Mexican axolotl. Methods Mol Biol. 2015;1290:27-46.

90. Smith JJ, Putta S, Walker JA, Kump DK, Samuels AK, Monaghan JR, et al. Sal-Site: integrating new and existing ambystomatid salamander research and informational resources. BMC Genomics. 2005;6:181.

91. Iten LE, Bryant SV. Forelimb regeneration from different levels of amputation in

the newt,Notophthalmus viridescens: Length, rate, and stages. Wilhelm Roux Arch Entwickl Mech Org. 1973;173(4):263-82.

92. Tank PW, Carlson BM, Connelly TG. A staging system for forelimb regeneration in the axolotl, Ambystoma mexicanum. J Morphol. 1976;150(1):117-28.

93. Yoshida M, Kijima M, Akita M, Beppu T. Potent and specific inhibition of mammalian histone deacetylase both in vivo and in vitro by trichostatin A. J Biol Chem. 1990;265(28):17174-9.

94. Stocum DL. The role of peripheral nerves in urodele limb regeneration. Eur J Neurosci. 2011;34(6):908-16.

95. Suzuki M, Satoh A, Ide H, Tamura K. Nerve-dependent and -independent events in blastema formation during Xenopus froglet limb regeneration. Dev Biol. 2005;286(1):361-75.

96. Gardiner DM, Muneoka K, Bryant SV. The migration of dermal cells during blastema formation in axolotls. Dev Biol. 1986;118(2):488-93.

97. Todd TJ. On the process of reproduction of the members of the aquatic salamander. Quarterly Journal of Science, Literature and the Arts. 1823;16, 84–96.

98. Glozak MA, Seto E. Histone deacetylases and cancer. Oncogene. 2007;26(37):5420-32.

99. Liu T, Kuljaca S, Tee A, Marshall GM. Histone deacetylase inhibitors: multifunctional anticancer agents. Cancer Treat Rev. 2006;32(3):157-65.

100. Wang G, Badylak SF, Heber-Katz E, Braunhut SJ, Gudas LJ. The effects of DNA methyltransferase inhibitors and histone deacetylase inhibitors on digit regeneration in mice. Regen Med. 2010;5(2):201-20.

101. Lv L, Sun Y, Han X, Xu CC, Tang YP, Dong Q. Valproic acid improves outcome after rodent spinal cord injury: potential roles of histone deacetylase inhibition. Brain Res. 2011;1396:60-8.

102. Taylor AJ, Beck CW. Histone deacetylases are required for amphibian tail and limb regeneration but not development. Mech Dev. 2012;129(9-12):208-18.

103. Chou CW, Wu MS, Huang WC, Chen CC. HDAC inhibition decreases the expression of EGFR in colorectal cancer cells. PLoS One. 2011;6(3):e18087.

104. Elder JT, Zhao X. Evidence for local control of gene expression in the epidermal differentiation complex. Exp Dermatol. 2002;11(5):406-12.

105. Markova NG, Karaman-Jurukovska N, Pinkas-Sarafova A, Marekov LN, Simon M. Inhibition of histone deacetylation promotes abnormal epidermal differentiation and specifically suppresses the expression of the late differentiation marker profilaggrin. J Invest Dermatol. 2007;127(5):1126-39.

106. Hughes MW, Jiang TX, Lin SJ, Leung Y, Kobielak K, Widelitz RB, et al. Disrupted ectodermal organ morphogenesis in mice with a conditional histone

deacetylase 1, 2 deletion in the epidermis. J Invest Dermatol. 2014;134(1):24-32.

107. Tang J, Yan Y, Zhao TC, Gong R, Bayliss G, Yan H, et al. Class I HDAC activity is required for renal protection and regeneration after acute kidney injury. Am J Physiol Renal Physiol. 2014;307(3):F303-16.

108. Rosato RR, Almenara JA, Grant S. The histone deacetylase inhibitor MS-275 promotes differentiation or apoptosis in human leukemia cells through a process regulated by generation of reactive oxygen species and induction of p21CIP1/WAF1 1. Cancer Res. 2003;63(13):3637-45.

109. Chen S, Yao X, Li Y, Saifudeen Z, Bachvarov D, El-Dahr SS. Histone deacetylase 1 and 2 regulate Wnt and p53 pathways in the ureteric bud epithelium. Development. 2015;142(6):1180-92.

110. Kiffmeyer WR, Tomusk EV, Mescher AL. Axonal transport and release of transferrin in nerves of regenerating amphibian limbs. Dev Biol. 1991;147(2):392-402.

111. Mescher AL, Connell E, Hsu C, Patel C, Overton B. Transferrin is necessary and sufficient for the neural effect on growth in amphibian limb regeneration blastemas. Dev Growth Differ. 1997;39(6):677-84.

112. Satoh A, makanae A, Hirata A, Satou Y. Blastema induction in aneurogenic state and Prrx-1 regulation by MMPs and FGFs in Ambystoma mexicanum limb regeneration. Dev Biol. 2011;355(2):263-74.

113. Grunstein M. Histone acetylation in chromatin structure and transcription. Nature. 1997;389(6649):349-52.

114. Shahbazian MD, Grunstein M. Functions of site-specific histone acetylation and deacetylation. Annu Rev Biochem. 2007;76:75-100.

115. Ferris DR, Satoh A, Mandefro B, Cummings GM, Gardiner DM, Rugg EL. Ex vivo generation of a functional and regenerative wound epithelium from axolotl (Ambystoma mexicanum) skin. Dev Growth Differ. 2010;52(8):715-24.

116. Tanner K, Ferris DR, Lanzano L, Mandefro B, Mantulin WW, Gardiner DM, et al. Coherent movement of cell layers during wound healing by image correlation spectroscopy. Biophys J. 2009;97(7):2098-106.

117. Currie JD, Kawaguchi A, Traspas RM, Schuez M, Chara O, Tanaka EM. Live Imaging of Axolotl Digit Regeneration Reveals Spatiotemporal Choreography of Diverse Connective Tissue Progenitor Pools. Dev Cell. 2016;39(4):411-23.

118. McCusker CD, Diaz-Castillo C, Sosnik J, A QP, Gardiner DM. Cartilage and bone cells do not participate in skeletal regeneration in Ambystoma mexicanum limbs. Dev Biol. 2016;416(1):26-33.

119. Scheuing MR, Singer M. The effects of microquantitles of beryllium ion on the regenerating forelimb of the adult newt, Triturus. J Exp Zool. 1957;136(2):301-27.

120. Thornton CS. Influence of an eccentric epidermal cap on limb regeneration in Amblystoma larvae. Dev Biol. 1960;2:551-69.

121. Geraudie J, Ferretti P. Gene expression during amphibian limb regeneration. Int Rev Cytol. 1998;180:1-50.

122. Monaghan JR, Epp LG, Putta S, Page RB, Walker JA, Beachy CK, et al. Microarray and cDNA sequence analysis of transcription during nerve-dependent limb regeneration. BMC Biol. 2009;7:1.

123. Monaghan JR, Athippozhy A, Seifert AW, Putta S, Stromberg AJ, Maden M, et al. Gene expression patterns specific to the regenerating limb of the Mexican axolotl. Biol Open. 2012;1(10):937-48.

124. Knapp D, Schulz H, Rascon CA, Volkmer M, Scholz J, Nacu E, et al. Comparative transcriptional profiling of the axolotl limb identifies a tripartite regeneration-specific gene program. PLoS One. 2013;8(5):e61352.

125. Stewart R, Rascon CA, Tian S, Nie J, Barry C, Chu LF, et al. Comparative RNA-seq analysis in the unsequenced axolotl: the oncogene burst highlights early gene expression in the blastema. PLoS Comput Biol. 2013;9(3):e1002936.

126. Campbell LJ, Suarez-Castillo EC, Ortiz-Zuazaga H, Knapp D, Tanaka EM, Crews CM. Gene expression profile of the regeneration epithelium during axolotl limb regeneration. Dev Dyn. 2011;240(7):1826-40.

127. Diaz-Castillo C. Transcriptome dynamics along axolotl regenerative development are consistent with an extensive reduction in gene expression heterogeneity in dedifferentiated cells. PeerJ. 2017;5:e4004.

128. Paksa A, Rajagopal J. The epigenetic basis of cellular plasticity. Curr Opin Cell Biol. 2017;49:116-22.

129. Nowoshilow S, Schloissnig S, Fei JF, Dahl A, Pang AWC, Pippel M, et al. The axolotl genome and the evolution of key tissue formation regulators. Nature. 2018;554(7690):50-5.

130. Hayashi S, Kawaguchi A, Uchiyama I, Kawasumi-Kita A, Kobayashi T, Nishide H, et al. Epigenetic modification maintains intrinsic limb-cell identity in Xenopus limb bud regeneration. Dev Biol. 2015;406(2):271-82.

131. Wang MH, Wu CH, Huang TY, Sung HW, Chiou LL, Lin SP, et al. Nerve-mediated expression of histone deacetylases regulates limb regeneration in axolotls. Dev Biol. 2019;449(2):122-31.

132. Altschul SF, Gish W, Miller W, Myers EW, Lipman DJ. Basic local alignment search tool. J Mol Biol. 1990;215(3):403-10.

133. Durinck S, Moreau Y, Kasprzyk A, Davis S, De Moor B, Brazma A, et al. BioMart and Bioconductor: a powerful link between biological databases and microarray data analysis. Bioinformatics. 2005;21(16):3439-40.

134. Langmead B, Salzberg SL. Fast gapped-read alignment with Bowtie 2. Nat Methods. 2012;9(4):357-9.

135. Li B, Dewey CN. RSEM: accurate transcript quantification from RNA-Seq data with or without a reference genome. BMC Bioinformatics. 2011;12:323.

136. McCarthy DJ, Chen Y, Smyth GK. Differential expression analysis of multifactor RNA-Seq experiments with respect to biological variation. Nucleic Acids Res. 2012;40(10):4288-97.

137. Ritchie ME, Phipson B, Wu D, Hu Y, Law CW, Shi W, et al. limma powers differential expression analyses for RNA-sequencing and microarray studies. Nucleic Acids Res. 2015;43(7):e47.

138. Futschik ME, Carlisle B. Noise-robust soft clustering of gene expression time-course data. J Bioinform Comput Biol. 2005;3(4):965-88.

139. Schwammle V, Jensen ON. A simple and fast method to determine the parameters for fuzzy c-means cluster analysis. Bioinformatics. 2010;26(22):2841-8.

140. Yu G, Wang LG, Han Y, He QY. clusterProfiler: an R package for comparing biological themes among gene clusters. OMICS. 2012;16(5):284-7.

141. Gerber T, Murawala P, Knapp D, Masselink W, Schuez M, Hermann S, et al. Single-cell analysis uncovers convergence of cell identities during axolotl limb regeneration. Science. 2018;362(6413).

142. Leigh ND, Dunlap GS, Johnson K, Mariano R, Oshiro R, Wong AY, et al. Transcriptomic landscape of the blastema niche in regenerating adult axolotl limbs at single-cell resolution. Nat Commun. 2018;9(1):5153.

143. Ashley-Ross MA. The comparative myology of the thigh and crus in the salamanders Ambystoma tigrinum and Dicamptodon tenebrosus. J Morphol. 1992;211(2):147-63.

144. Rivera-Gonzalez GC, Morris SA. Tracing the Origins of Axolotl Limb Regeneration. Dev Cell. 2018;47(6):675-7.

145. Dunis DA, Namenwirth M. The role of grafted skin in the regeneration of x-irradiated axolotl limbs. Dev Biol. 1977;56(1):97-109.

146. Yokoyama H, Maruoka T, Ochi H, Aruga A, Ohgo S, Ogino H, et al. Different requirement for Wnt/beta-catenin signaling in limb regeneration of larval and adult Xenopus. PLoS One. 2011;6(7):e21721.

147. Wischin S, Castaneda-Patlan C, Robles-Flores M, Chimal-Monroy J. Chemical activation of Wnt/beta-catenin signalling inhibits innervation and causes skeletal tissue malformations during axolotl limb regeneration. Mech Dev. 2017;144(Pt B):182-90.

148. Vieira WA, Wells KM, Raymond MJ, De Souza L, Garcia E, McCusker CD. FGF, BMP, and RA signaling are sufficient for the induction of complete limb

regeneration from non-regenerating wounds on Ambystoma mexicanum limbs. Dev Biol. 2019;451(2):146-57.

149. Makanae A, Hirata A, Honjo Y, Mitogawa K, Satoh A. Nerve independent limb induction in axolotls. Dev Biol. 2013;381(1):213-26.

150. Thornton CS. The effect of apical cap removal on limb regeneration in Amblystoma larvae. J Exp Zool. 1957;134(2):357-81.

151. Thornton CS. The inhibition of limb regeneration in urodele larvae by localized irradiation with ultraviolet light. J Exp Zool. 1958;137(1):153-79.

152. Satoh A, Bryant SV, Gardiner DM. Nerve signaling regulates basal keratinocyte proliferation in the blastema apical epithelial cap in the axolotl (Ambystoma mexicanum). Dev Biol. 2012;366(2):374-81.

153. Mescher AL, Neff AW. Regenerative capacity and the developing immune system. Adv Biochem Eng Biotechnol. 2005;93:39-66.

154. Nacu E, Glausch M, Le HQ, Damanik FF, Schuez M, Knapp D, et al. Connective tissue cells, but not muscle cells, are involved in establishing the proximo-distal outcome of limb regeneration in the axolotl. Development. 2013;140(3):513-8.

155. McCusker CD, Gardiner DM. Positional information is reprogrammed in blastema cells of the regenerating limb of the axolotl (Ambystoma mexicanum). PLoS One. 2013;8(9):e77064.

156. Godwin JW, Pinto AR, Rosenthal NA. Macrophages are required for adult salamander limb regeneration. Proc Natl Acad Sci U S A. 2013;110(23):9415-20.

157. Godwin JW, Debuque R, Salimova E, Rosenthal NA. Heart regeneration in the salamander relies on macrophage-mediated control of fibroblast activation and the extracellular landscape. NPJ Regen Med. 2017;2.

158. Fei JF, Schuez M, Knapp D, Taniguchi Y, Drechsel DN, Tanaka EM. Efficient gene knockin in axolotl and its use to test the role of satellite cells in limb regeneration. Proc Natl Acad Sci U S A. 2017;114(47):12501-6.

159. Voss SR, Palumbo A, Nagarajan R, Gardiner DM, Muneoka K, Stromberg AJ, et al. Gene expression during the first 28 days of axolotl limb regeneration I: Experimental design and global analysis of gene expression. Regeneration (Oxf). 2015;2(3):120-36.

160. Erickson JR, Gearhart MD, Honson DD, Reid TA, Gardner MK, Moriarity BS, et al. A novel role for SALL4 during scar-free wound healing in axolotl. NPJ Regen Med. 2016;1:16016-.

161. Kragl M, Roensch K, Nusslein I, Tazaki A, Taniguchi Y, Tarui H, et al. Muscle and connective tissue progenitor populations show distinct Twist1 and Twist3 expression profiles during axolotl limb regeneration. Dev Biol. 2013;373(1):196-204.

162. Zeng L, Kempf H, Murtaugh LC, Sato ME, Lassar AB. Shh establishes an
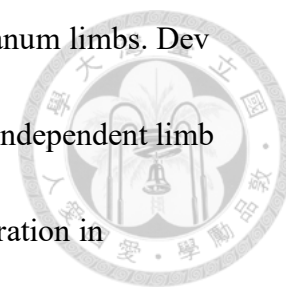
Nkx3.2/Sox9 autoregulatory loop that is maintained by BMP signals to induce somitic chondrogenesis. Genes Dev. 2002;16(15):1990-2005.

163. Rayman JB, Takahashi Y, Indjeian VB, Dannenberg JH, Catchpole S, Watson RJ, et al. E2F mediates cell cycle-dependent transcriptional repression in vivo by recruitment of an HDAC1/mSin3B corepressor complex. Genes Dev. 2002;16(8):933-47.

164. Liang J, Wan M, Zhang Y, Gu P, Xin H, Jung SY, et al. Nanog and Oct4 associate with unique transcriptional repression complexes in embryonic stem cells. Nat Cell Biol. 2008;10(6):731-9.

165. Shi YB. Unliganded thyroid hormone receptor regulates metamorphic timing via the recruitment of histone deacetylase complexes. Curr Top Dev Biol. 2013;105:275-97.

166. Dinsmore CE. Urodele limb and tail regeneration in early biological thought: an essay on scientific controversy and social change. Int J Dev Biol. 1996;40(4):621-7.

167. Tanaka EM. Regeneration: if they can do it, why can't we? Cell. 2003;113(5):559-62.

168. Wu CH, Huang TY, Chen BS, Chiou LL, Lee HS. Long-duration muscle dedifferentiation during limb regeneration in axolotls. PLoS One. 2015;10(2):e0116068.

169. Wu CH, Chen YJ, Wang MH, Chiou LL, Tseng WI, Lee HS. Diffusion tensor tractography reveals muscle reconnection during axolotl limb regeneration. PLoS One. 2017;12(3):e0173425.

170. Niwa H, Yamamura K, Miyazaki J. Efficient selection for high-expression transfectants with a novel eukaryotic vector. Gene. 1991;108(2):193-9.

171. Okabe M, Ikawa M, Kominami K, Nakanishi T, Nishimune Y. 'Green mice' as a source of ubiquitous green cells. FEBS Lett. 1997;407(3):313-9.

172. Huang TY, Chang CC, Cheng NC, Wang MH, Chiou LL, Lee KL, et al. Re-epithelialization of large wound in paedomorphic and metamorphic axolotls. J Morphol. 2017;278(2):228-35.

173. Mansour N, Lahnsteiner F, Patzner RA. Collection of gametes from live axolotl, Ambystoma mexicanum, and standardization of in vitro fertilization. Theriogenology. 2011;75(2):354-61.

174. Casco-Robles MM, Yamada S, Miura T, Nakamura K, Haynes T, Maki N, et al. Expressing exogenous genes in newts by transgenesis. Nat Protoc. 2011;6(5):600-8.

175. Khattak S, Murawala P, Andreas H, Kappert V, Schuez M, Sandoval-Guzman T, et al. Optimized axolotl (Ambystoma mexicanum) husbandry, breeding, metamorphosis, transgenesis and tamoxifen-mediated recombination. Nat Protoc. 2014;9(3):529-40.

176. Schreckenberg GM, Jacobson AG. Normal stages of development of the axolotl. Ambystoma mexicanum. Dev Biol. 1975;42(2):391-400.

177. Diogo R, Murawala P, Tanaka EM. Is salamander hindlimb regeneration similar to that of the forelimb? Anatomical and morphogenetic analysis of hindlimb muscle regeneration in GFP-transgenic axolotls as a basis for regenerative and developmental studies. J Anat. 2014;224(4):459-68.

178. Maden M, Avila D, Roy M, Seifert AW. Tissue specific reactions to positional discontinuities in the regenerating axolotl limb. Regeneration (Oxf). 2015;2(3):137-47.

179. Butler EG. Regeneration of the urodele forelimb after reversal of its proximo-distal axis. J Morphol. 1955;96(2):265-81.

Lists of Publication
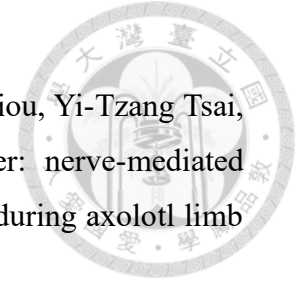
1. <u>Mu-Hui Wang</u>, Chia-Lang Hsu, Cheng-Han Wu, Ling-Ling Chiou, Yi-Tzang Tsai, Hsuan-Shu Lee, Shau-Ping Lin. (2021) Timing does matter: nerve-mediated HDAC1 paces the temporal expression of morphogenic genes during axolotl limb regeneration. Front. Cell Dev. Biol. 9:641987.

2. <u>Mu-Hui Wang</u>, Ting-Yu Huang, Cheng-Han Wu, Ling-Ling Chiou, Hsuan-Shu Lee. (2020) A double fluorescence chimeric limb regeneration model reveals muscle fiber reconnection during axolotl limb regeneration. Int. J. Morphol. 38(5):1485-1495.

3. <u>Mu-Hui Wang</u>, Cheng-Han Wu, Ting-Yu Huang, Hung-Wei Sung, Ling-Ling Chiou, Shau-Ping Lin, Hsuan-Shu Lee. (2019) Nerve-mediated expression of histone deacetylases regulates limb regeneration in axolotls. Dev. Biol. 449(2): 122-131.

4. Cheng-Han Wu, Yu-Jen Chen, <u>Mu-Hui Wang</u>, Ling-Ling Chiou, Wen-Yih Isaac Tseng, Hsuan-Shu Lee. (2017) Diffusion tensor tractography reveals muscle reconnection during axolotl limb regeneration. PLoS One 12(3):e0173425,

5. Ting-Yu Huang, Chun-Che Chang, Nai-Chen Cheng, <u>Mu-Hui Wang</u>, Ling-Ling Chiou, Kuang-Lun Lee, Hsuan-Shu Lee. (2016) Re-epithelialization of large wound in paedomorphic and metamorphic axolotls. J. Morphol. 278(2):228-235.

6. Ting-Yu Huang, Cheng-Han Wu, <u>Mu-Hui Wang</u>, Bo-Sung Chen, Ling-Ling Chiou, and Hsuan-Shu Lee. (2015) Cooperative regulation of substrate stiffness and extracellular matrix proteins in skin wound healing of axolotls. BioMed. Res. Int. 2015:712546.